An X-Ray Diffraction Study of the Reconstructions Induced by Sn and Pb on Ge(111) Surfaces

Pedersen, Jan Skov

Publication date:
1988

Document Version
Publisher's PDF, also known as Version of record

Risø-M-2713

RISØ

Risø-M-2713

An X-Ray Diffraction Study of the Reconstructions Induced by Sn and Pb on Ge(111) Surfaces

Jan Skov Pedersen

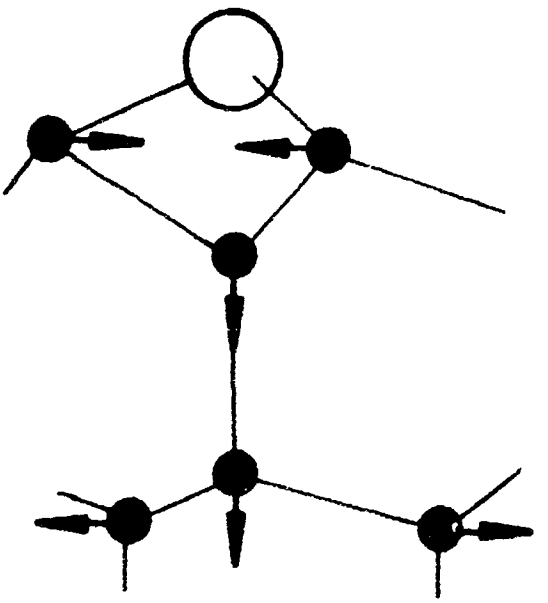

Risø National Laboratory, DK-4000 Roskilde, Denmark
February 1988

AN X-RAY DIFFRACTION STUDY OF THE RECONSTRUCTIONS INDUCED BY Sn AND Pb ON Ge(111) SURFACES

Jan Skov Pedersen

Abstract: This report describes surface x-ray diffraction studies of Ge(111) surfaces covered by submonolayers of Sn and Pb. The report is divided into three parts: The first part is a brief review of the properties of the "clean" Si(111) and Ge(111) surfaces, of the properties of the Sn- and Pb-covered Ge(111) surfaces, and of the surface x-ray scattering technique. Part two of the report concerns x-ray scattering measurements on the α-phase of the Ge(111)$\sqrt{3}\times\sqrt{3}$-Sn and the Ge(111)$\sqrt{3}\times\sqrt{3}$-Pb reconstructions. The structure factor analysis shows a significant relaxation in the Ge substrate induced by the Sn/Pb adatoms. The registry of the adatoms is determined from the analysis of the integer-order reflections. The intensity profiles of the fractional-order Bragg rods display a pronounced variation, which is explained by subsurface relaxation extending four atomic layers into the bulk. Part three of the report describes the structure of the 7×7 and 5×5 reconstructions that are observed after deposition of submonolayers of Sn on the Ge(111) surface and subsequent annealing. The diffraction patterns for both structures show considerable similarity with the pattern for Si(111)7×7, and the analysis shows that the Dimer-Adatom-Stacking-fault (DAS) model also is applicable to the Sn-induced Ge(111)7×7 and Ge(111)5×5 structures. The adatoms are identified to be Sn. The results of the refinement of the atomic coordinates show that the atoms in the upper five atomic layers are displaced from their ideal positions. The displacements around the adatoms are similar to the displacements of the Ge(111)$\sqrt{3}\times\sqrt{3}$-Sn surface. Furthermore, the observed relaxations are in good agreement with the predictions of total-energy calculations. In order to perform a detailed comparison between the experimentally and theoretically determined atomic positions, a series of elastic strain calculations by the Keating model have been carried out. It is demonstrated that this model gives a good description of the atomic relaxations of the Ge(111)$\sqrt{3}\times\sqrt{3}$-Sn (Pb), Ge(111)7×7-Sn, and Ge(111)5×5-Sn surfaces.

February 1988
Risø National Laboratory, DK-4000 Roskilde, Denmark

This is a licentiate (Ph.D.) thesis for a study at Fysisk Centralinstitut, Copenhagen University. The work has been performed at the Physics Department, Risø National Laboratory, and the measurements have been done at Hamburger Synchrotron-Strahlungslabor (HASYLAB) at the storage ring DORIS II, DESY, Hamburg, in collaboration with the Max Planck Institute for Solid State Research, Stuttgart. The study has been supervised by Kim Carneiro and Mourits Nielsen.

Dette er en licentiat-afhandling for et licentiatstudium ved Fysisk Centralinstitut, Københavns Universitet. Arbejdet er udført på Fysikafdelingen, Forskningscenter Risø, og målingerne er udført på Hamburger Synchrotron-Strahlungslabor (HASYLAB) ved lagerringen DORIS II, DESY, Hamborg, i samarbejde med Max-Planck-Institut für Festkörperforschung, Stuttgart. Vejledere har været Kim Carneiro og Mourits Nielsen.

ISBN 87-550-1425-9
ISSN 0418-6435

Grafisk Service, Risø

CONTENTS

		Page
1.	**GENERAL INTRODUCTION**	5
1.1.	Semiconductors and Surface Science	5
1.2.	The Si(111) and Ge(111) Surfaces	7
	1.2.a Surface Reconstruction	7
	1.2.b The Cleaved Si(111)2 × 1 and Ge(111)2 × 1 Surfaces	9
	1.2.c The Si(111)7 × 7 Surface	11
	1.2.d The Ge(111)c(2 × 8) Surface	15
1.3.	Pb- and Sn-covered Ge(111) Surfaces	18
	1.3.a The Ge(111)-Pb Surfaces	18
	1.3.b The Ge(111)-Sn Surfaces	19
1.4.	Grazing Incidence X-ray Diffraction	21
	1.4.a The History of Surface X-ray Diffraction	21
	1.4.b The Basic Theory of Surface X-ray Diffraction	23
2.	**THE STRUCTURE OF THE α-PHASE OF THE Ge(111)$\sqrt{3}\times\sqrt{3}$-Sn AND Ge(111)$\sqrt{3}\times\sqrt{3}$-Pb SURFACES**	35
2.1.	Introduction	35
2.2.	Experimental	36
2.3.	In-plane Projected Structures	39
2.4.	Integer-order Reflections and Registry	42
2.5.	Rodscans and the Structure in the Direction Normal to the Surface	43
2.6.	Elastic Strain Calculations by the Keating Model	46
2.7.	Discussion and Conclusions	49
3.	**THE STRUCTURE OF THE Ge(111)5 × 5-Sn AND Ge(111)7 × 7-Sn SURFACES**	51
3.1.	Introduction	51
3.2.	Experimental	51
3.3.	Analysis	53
3.4.	Comparisons with Atomic Relaxations from Model Calculations	64
3.5.	Surface Stress and Total Energy	70
3.6.	Summary and Conclusions	76
	ACKNOWLEDGMENTS	77
	REFERENCES	78
	APPENDICES	82
	A: The Keating Model	82
	B: Subsurface Relaxation in the Ge(001)2 × 1 Structure by the Keating Model	87
	C: Data: Rodscans of the α-Phase of the Ge(111)$\sqrt{3}\times\sqrt{3}$-Sn and Ge(111)$\sqrt{3}\times\sqrt{3}$-Pb Surfaces	91
	D: Data: In-plane Intensities for the Ge(111)5 × 5-Sn Reconstruction	93
	E: Data: In-plane Intensities for the Ge(111)7 × 7-Sn Reconstruction	95

1. GENERAL INTRODUCTION

1.1. Semiconductors and Surface Science

The electronics industry has gone through a tremendous development during the last thirty years. First, the production changed to transistors and later to integrated circuits. The way of placing many devices on the same semiconductor substrate has made it desirable to make the individual components as small as possible. As the devices have become smaller the boundaries and interfaces more strongly influence the characteristics. Therefore it is not sufficient to understand the physics of bulk semiconductors. An understanding of the physics of the interfaces is also required.

During the last couple of decades the study of surfaces and interfaces has developed into a separate branch of physics: surface science. The topics of interest are of course the electronic and atomic structure of interfaces. Typical examples of the interfaces that are studied are the semiconductor-vacuum, the semiconductor-semiconductor, and the semiconductor-metal interfaces.

Since the early days of solid state physics it has frequently been considered convenient to treat crystals, as if they were infinite periodic repeating structures. This is realized theoretically by periodic boundary conditions. In reality, a crystal will of course always have surfaces. The simplest way of obtaining a surface theoretically is to consider a crystal which is semi-infinite in one direction. This gives an interface to the vacuum. The lower symmetry at the surface will in many cases lead to a relaxation of the atoms close to the surface away from the positions they would occupy in an ideal crystal. In some cases an additional rebonding of the surface atoms takes place resulting in a surface reconstruction.

In order to perform experimental investigations on surfaces several difficulties have to be overcome. The first requirement is that the sample surface should be kept clean for a period long enough for the measurements. Impurities would change the properties of the surface so the sample has to be under ultra-high vacuum (UHV) conditions, which means a pressure better than 10^{-10} mbar. The next problem is that the number of atoms at the surface is typically seven orders of magnitude smaller than the number of atoms with bulk surroundings. The experiment has to have surface sensitivity to avoid the signal from the surface atoms disappearing in the signal from the bulk atoms. A typical example of a probe for a surface experiment is an electron beam. Electrons interact strongly with matter and "see" therefore only the outermost layers of a crystal. Some of the techniques employing electron beams are Low Energy Electron Diffraction (LEED), Reflecting High Energy Electron Diffraction (RHEED), and Auger Electron Spectroscopy (AES). The latter gives information on the chemical composition of the surface, whereas LEED and RHEED give information on the periodicity of the surface, and to some extent also on the

structure. However, due to the strong interaction, the diffraction is dynamical, and the interpretation of the diffraction patterns requires extensive computer calculations with complex electron scattering models (Kahn (1983)). This excludes the application of the Fourier methods of standard crystallography, which can only be used for kinematical scattering.

The complicated data analysis of LEED has resulted in a search for other structural techniques. In 1979 x-ray scattering at grazing incidence was introduced by Marra et al. (Section I.4.). The great advantage of this technique is that the interaction between x-rays and matter is so weak that the scattering can be described by kinematical theory. In order to enhance the diffraction signal from the surface relative to the signal from the bulk, the angle of incidence of the x-rays is chosen close to the critical angle for total external reflection. To obtain reasonable counting rates intense x-ray sources are needed and the experiments are usually performed with synchrotron radiation.

The electronic structure of surfaces can be studied experimentally by photoelectron spectroscopy (PES). In an angle-integrated PES experiment atoms with different surroundings can be identified by measuring the electronic binding energies of the core electrons. By applying an angle-resolved method the electronic band structure of the surface (and the bulk) can be determined. The actual band structure of a surface is closely interrelated with the surface atomic geometry.

The theoretical understanding of surface reconstructions is mainly based on total-energy calculations. When structural models are proposed, a comparison of their total energy can be used to find the most favourable. In ab-initio total-energy calculations the Schrödinger equation for the electrons is solved without requiring any experimental determined parameters. The only input is the structural model. However, in order to solve the Schrödinger equation some approximations have to be employed. An often used technique is based on pseudopotentials within a local-density approximation. The calculations are extremely expensive in computer time, and therefore only reconstructions with a small number of atoms can be treated. In addition to obtaining the total energy of a surface, the dispersion of the electronic surface bands are usually calculated. The dispersion can be compared to the experimental results from angle-resolved photoemission. Further structural information on the atomic geometry of a proposed model can be obtained from minimizing the total energy with respect to the position of the surface atoms.

Semi-empirical total energy calculations for covalent crystals are often based on tight-binding approximations, in which only a limited number of atomic orbitals is included. The calculations need the value of some parameters from experiments or from more advanced calculations. The great advantage of the tight-binding approach is that large surface reconstructions can be treated without large amounts of computer time. Beside of giving the total energy of a model, the calculations can also be used to obtain the optimized atomic positions.

An alternative way of determining the atomic positions is to apply an elastic strain calculation. In this approach the electronic structure is not taken into account, and the interactions between atoms are taken as purely classical. For covalently bonded crystals a good description of the strain energy is obtained by including only two terms: one describing the energy cost of bond stretching and another describing bond bending. The calculations require only few parameters, which can be determined from the bulk elastic properties. For a given model one has to specify which atoms are bonded to each other. The atomic coordinates are determined from a minimization of the elastic strain energy with respect to the atomic coordinates.

This thesis concerns x-ray scattering investigations of surface reconstructions on germanium surfaces induced by submonolayer coverages of tin and lead. The atomic coordinates of the atoms in the reconstructions are determined in the data analysis. Some theoretical information on the structures are available from ab-initio and tight-binding calculations. However, in order to perform a detailed comparison between the experimentally and theoretically determined atomic positions a series of elastic strain calculations have been carried out.

1.2. The Si(111) and Ge(111) Surfaces

In this section a brief review of the current state of understanding of the reconstructions on the (111) surface of Silicon and Germanium is given. It is not intended to give a complete overview, but to present some information that will make it easier to relate the new results, presented in chapter 2 and 3, to previous work. More extensive reviews have been given by Kahn (1983), van der Veen (1985), Olmstead (1987), and Haneman (1987).

1.2.a Surface Reconstruction

Both Silicon and Germanium belong to group IV in the Periodic Table, and the two elements both have the diamond structure (Figure 1.1.a). A crystal with an ideally terminated (111) surface (Figure 1.1.b) consists of bilayers of atoms, stacked in an ...ABCABC... sequence. Viewed along the surface normal the atoms in each bilayer are arranged in hexagons (Figure 1.1.c). The outer atoms of the surface have each an unsaturated bond directed into the vacuum - a "dangling" bond. The energy of these surface atoms is higher than the energy of the bulk atoms since they can lower their energy by bonding to other atoms. This is in analogy with the lower energy of an H_2 molecule relative to the energy of two separated H atoms. The driving mechanism of surface reconstructions is the lowering of the energy due to the reduction of the number of dangling bonds which can be achieved by a rebonding of the surface atoms. The limiting factor is the energy cost of bond configuration deformation away from the ideal tetrahedral bonds. The resulting surface structure will have a surface unit cell which is larger than the unit cell of the ideally terminated crystal (Figure 1.1.c). When

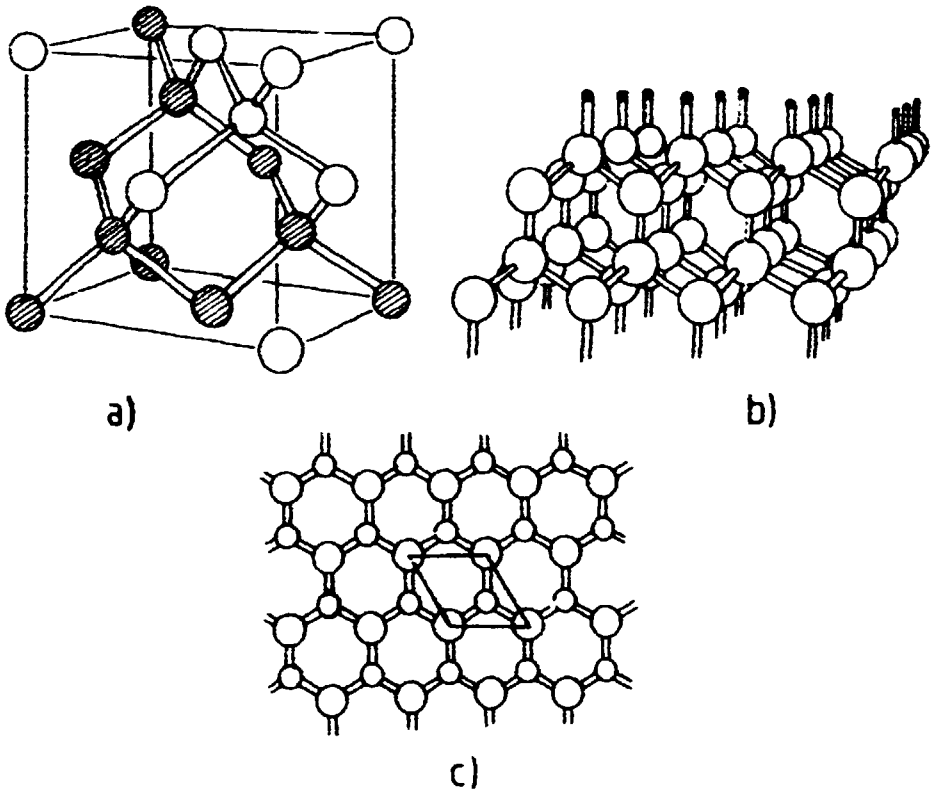

Figure 1.1.: a) The cubic unit cell of the diamond structure. The (111) surface is obtained, when the non-shaded atoms are removed. b) A perspective view of the surface. The "dangling" bonds are indicated by dots. The crystal is made up of bilayers. c) The surface viewed along the surface normal. The unit cell of the surface is shown.

the repeat distance is n times the length of the original unit cell along one axis in the surface coordinate system and m times along the other axis, the structure is referred to as an n × m reconstruction.

In the electronic band structure the dangling bond gives rise to a defect state in the gap between the conduction and the valence band (Harrison (1980) and McKinley et al. (1981)). The dangling bonds are localized states, and therefore the corresponding (half-filled) band has a relatively narrow band width. A reconstruction of the surface can split the occupied and unoccupied states, and a lowering of the electronic energy can occur if the occupied states are shifted to lower energies. Another effect which contributes to an energy reduction is a delocalization of the surface electrons (i.e. an increase of the band width). This is the case for the reconstructions that are presented in the next section.

1.2.b The Cleaved Si(111)2 × 1 and Ge(111)2 × 1 Surfaces

The first LEED observations of 2×1 reconstructions on Si(111) and Ge(111) surfaces, created by cleavage at room temperature, were made by Lander et al. in 1963. These reconstructions are metastable and can be converted by annealing to other stable structures. For Si, annealing to temperatures higher than 400°C, gives a stable 7×7 reconstruction (Lander et al. (1963)) and for Ge a c(2×8) structure is observed after annealing above 200°C. The same stable reconstructions are found on cut and polished (111) surfaces after cleaning by ion bombardment and annealing (Farnsworth et al. (1959) and Palmberg and Peria (1967)).

Several models have been suggested for the 2×1 structure. However, the generally accepted model for Si as well as for Ge is now the π-bonded chain model proposed by Pandey in 1981. All the experimental data for the 2×1 reconstructions seem to be well described by this model. Figure 1.2. shows a perspective drawing of the model. It involves a considerable rearrangement of the atoms, and it appeared unlikely that the energy required for such a rebonding could be made available during cleavage at room temperature. This objection to the model was removed by the total-energy calculations by Northrup and Cohen (1982a). They showed that for Si, the energy barrier between the ideally terminated surface and the π-bonded chain geometry is less than 30meV, which is the same as the thermal energy. Another important result of the total-energy calculations for Si is the very low energy of this model. Relative to the ideally terminated 1×1 surface, the energy is 0.37-0.47 eV lower per surface atom (Northrup and Cohen (1982a), Nielsen et al. (1983) and Vanderbilt (1987a)). Also for Ge the model has a lower energy than other proposed geometries (Northrup and Cohen (1983)).

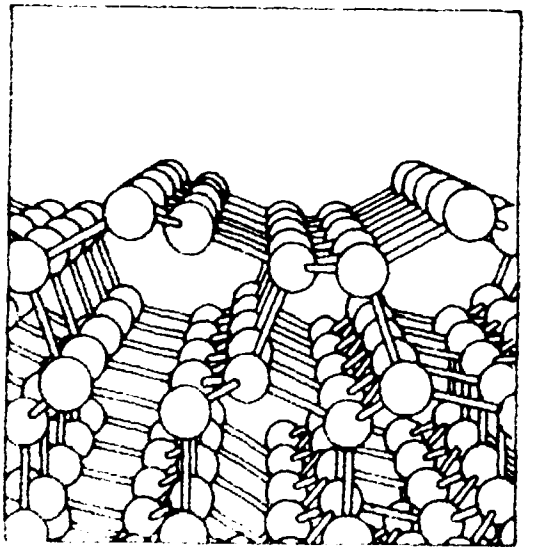

Figure 1.2. The π-bonded chain model of Pandey (1981), shown in perspective view (after Northrup and Cohen (1983)). The tilting of the outer atoms, found theoretically for Ge (Northrup and Cohen (1983)) and experimentally from ion scattering and LEED experiments for Si, is included.

The dispersion of the surface bands of the π-bonded chain model is very anisotropic (Figure 1.3.). Along the chains (close to the view direction in Figure 1.2.) the electrons are delocalized, and the bands are broad. Perpendicular to the chains, the electrons are more localized, which results in narrow bands. Theory and experiment show a good agreement for Si (Northrup and Cohen (1982a), Uhrberg et al. (1982), and Perfetti et al. (1987)) as well as for Ge (Northrup and Cohen (1983) and Nicholls et al. (1985a)). However, the theoretical dispersions have too small band gaps due to the methods used for the calculations.

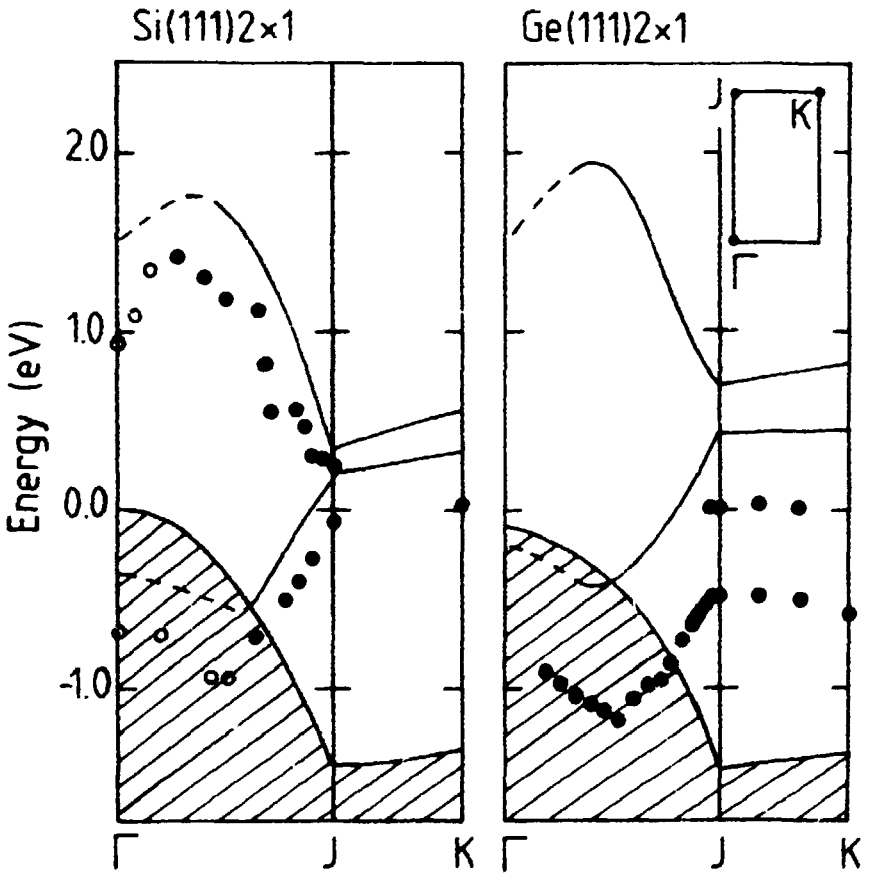

Figure 1.3. The dispersion of the surface state for Si and Ge. The hatched area indicates the projection of the bulk bands. Experimental results are shown as points (Uhrberg et al. (1982), Nicholls et al. (1985a), and Perfetti et al. (1987)). The dispersions found from total energy calculations are displayed as full and broken lines (Northrup and Cohen (1982a,1983)).

Strong indications for the π-bonded chain model were found by Tromp et al. (1983) by Rutherford backscattering (RBS) on Si. The experiments showed that more atoms were visible to the ion beam than for an ideal 1 × 1 surface. This is expected for the model which

has large atomic displacements. Good agreement with the model was obtained by Monte Carlo simulations, when subsurface relaxations and a small tilting of the chain normal to the chain direction were included.

Recent LEED studies give some support for a π-bonded chain model, which includes subsurface relaxations and a chain tilting (Himpsel et al. (1984), Batra et al. (1985), and Sakama (1986)). However, some discrepancies between calculated and measured intensities are present. The agreement is worse than what is considered to be conclusive by LEED standards.

Although more information is available for Si than for Ge, we see that the structure of the 2×1 reconstructions of both Si and Ge is well described by the π-bonded chain model. Consequently, it demonstrates the chemical and physical similarity of the cleaved Si and Ge (111) surface, in agreement with the bulk properties (Harrison (1980)). Hence, it is surprising that the stable reconstructions of the (111) surfaces have very different periodicities: 7×7 for Si (Farnsworth et al. (1959)) and $c(2\times8)$ for Ge (Palmberg and Peria (1967)). These stable structures are discussed in the following sections.

The large unit cell of these stable structures makes it impossible to perform a structure determination by LEED. Due to the multiple scattering one can at present only handle structures with a maximum of about ten atoms per unit cell. Hence, other structural methods, like x-ray diffraction, is needed to solve the structure of these large reconstructions.

1.2.c The Si(111)7×7 Surface

The atomic geometry of the Si(111)7×7 reconstruction seems at present well established. The final model is a result of 25 years' scientific detective work with numerous important contributions. The successful completion of the work is outlined below.

An important clue to the structure was given by RBS experiments performed by Culbertson et al. (1980) and Tromp et al. (1982). Measurements with normal incidence of the ion beam indicated a nearly bulk-like surface, whereas off-normal incidence showed that more atoms were visible to the beam. This means that the atomic positions projected on the surface plane are quite near bulk positions and secondly that the positions of the surface atoms projected along the off-normal directions are quite different from bulk positions. This led Bennett et al. (1983) to propose that the surface layers have a stacking fault. McRae (1983) suggested a model in which the hexagonal 7×7 unit cell is divided into two triangles with different stacking sequence in the surface layers. As shown below, a similar arrangement is present in the final model.

The next important results came from Scanning Tunneling Microscopy (STM) experiments by Binnig et al. (1983). In this technique a sharp tip is scanned across the surface close enough to have a tunneling current between the tip and the surface. The height of the tip above the surface is varied to give a constant current as the tip is scanned. A display of the tip height versus tip position shows 12 maxima distributed in a local 2×2 arrangement, as indicated in Figure 1.4. The maxima were interpreted as adatoms.

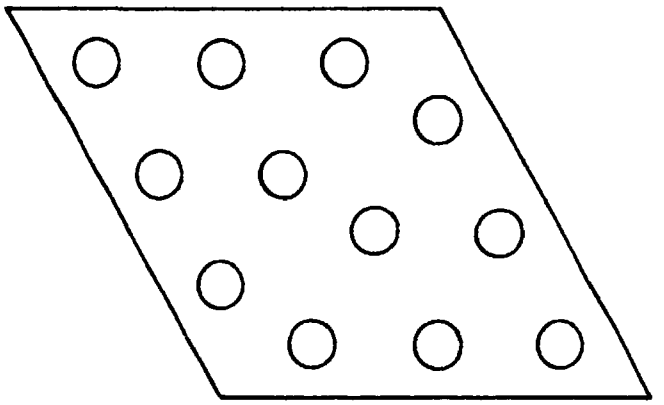

Figure 1.4. Distribution of the 12 maxima, found in a display of the tip height versus the tip position parallel to the surface, for the STM experiment by Binnig et al. (1983).

The final model for the 7×7 reconstruction was determined by Takayanagi (1984) and Takayanagi et al. (1985a,b) after a detailed Transmission Electron Diffraction (TED) study. The model is shown in Figure 1.5.-6., and contains dimers in addition to the previously mentioned ingredients: Adatoms and a stacking fault. Hence, the model proposed by Takayanagi is called the Dimer-Adatom-Stacking-fault (DAS) model. In Figure 1.5. the triangle above the short diagonal has a stacking fault in the outer double layer, whereas the lower triangle has regular stacking. The faulted and regular parts of the surface are connected by rows of dimirized atoms. At the corners of the unit cell, where the rows of dimers meet, they give rise to large corner holes (Figure 1.6.). The adatoms are distributed as suggested by the STM experiments. They are bonded to three atoms from the first layer and sit on top of a second layer atom. This adatom site is called a T_4 site due to the top position with four adjacent atoms. A notable feature of the model is the extra mirror line along the short diagonal of the unit cell which is present for the adatoms and the first double layer. This line is not a mirror line for the deeper atoms, as can be seen in the lower part of Figure 1.5. This means that the top layers have 6 mm symmetry in contrast to the 3 m symmetry of the bulk layers.

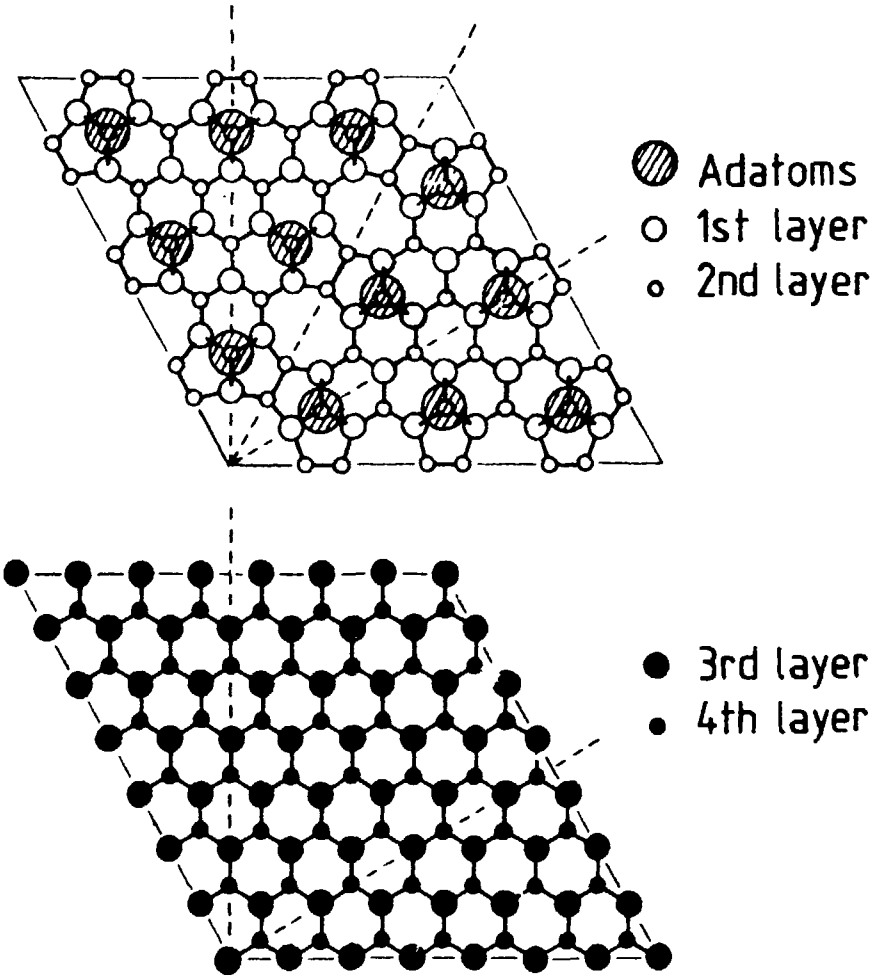

Figure 1.5. The top layers of the DAS model. The mirror lines are shown by broken lines. The first double layer and the adatoms have 6 mm symmetry. The deeper layers have 3 m symmetry.

The great advantage of the TED experiments, compared to LEED and RHEED, is that kinematical theory can be applied (Spence (1983)). In the TED experiment the incoming electron beam is directed along the surface normal. The sample has been chemically thinned, and the diffraction is observed after the beam has passed through the sample. In this geometry the scattering vectors are nearly parallel to the surface plane, and therefore the TED experiment gives information about the in-plane projected structure.

Takayanagi et al. (1985a,b) recorded the diffraction pattern by photographic films and measured the intensities by photometry. The intensities were used to construct a contour plot of the Patterson (pair-correlation) function (see Section 1.4.b for details). Peaks in the Patterson function correspond to interatomic vectors in the unit cell, and from a careful analysis Takayanagi et al. were able to deduce the DAS model. A detailed refinement of

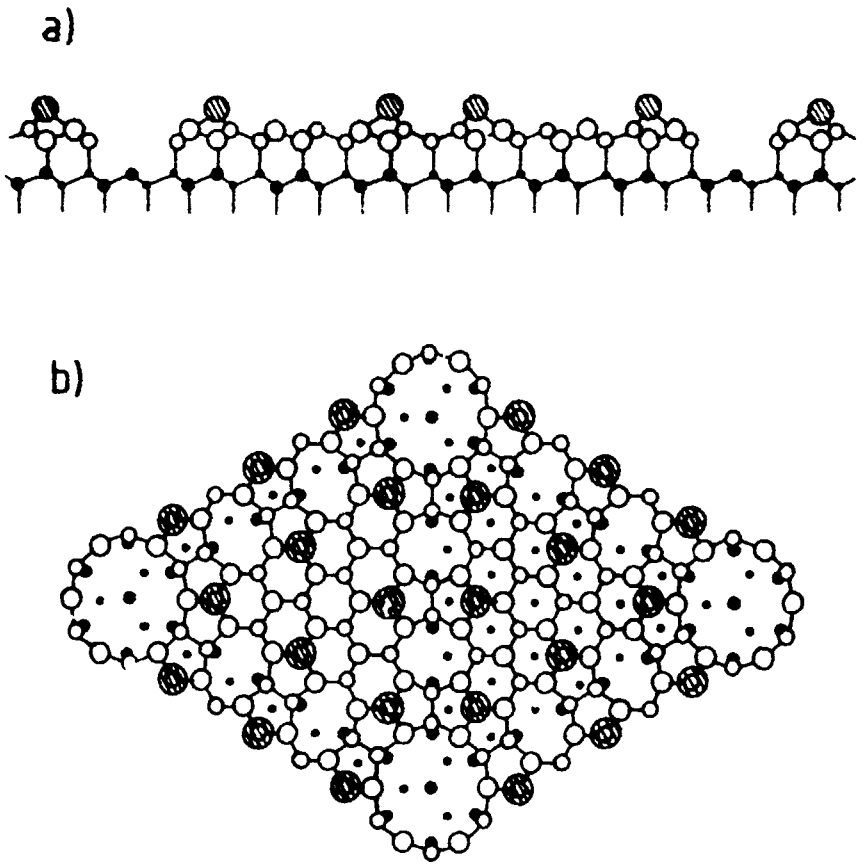

Figure 1.6. The DAS model. a): side view b): top view. Adatoms are shaded, first and second layer atoms are indicated by open circles and third and fourth layer atoms are shown as filled circles.

the atomic positions was not performed. However, a comparison between experimental intensities and the intensities calculated for the DAS model and other proposed models strongly favoured the DAS model.

A lot of experimental support for the DAS model has followed the work of Takayanagi et al.. Tromp and van Loenen (1985) obtained good agreement between results from RBS and Monte Carlo simulations for a DAS model in which atomic relaxations were taken into account. Detailed STM studies by Hamers et al. (1987) have shown that by varying the voltage between the tip and the sample it is possible to have tunneling into different surface states. For the 7×7 reconstruction the predicted electronic states of the DAS model were identified, giving further evidence for the model.

The first x-ray diffraction results for the surface were presented by Robinson in 1986 (a). A contour plot of the Patterson function and the intensity distribution of the superstructure reflections were strikingly similar to the results found by TED (Takayanagi et al. (1985a,b)). Further analysis by a special data-filtering technique and an electron density

difference analysis gave a clear confirmation of the DAS model (Robinson et al. (1986)). Recently, the study has been extended, and a large number of reflections has been measured (Robinson et al. (1988)). This allowed a least-square refinement of the in-plane projected atomic coordinates for all atoms in a D..S model with 6 mm symmetry. The experimental atomic relaxations show excellent agreement with those found by a semi-empirical tight-binding calculation (Qian and Chadi 1987a). The results of the x-ray experiment is discussed further in Chapter 3.

The calculation by Qian and Chadi (1987a) gave an estimate of the total energy of the DAS model. It is found to be 0.40 eV per 1×1 unit cell lower than the ideal unrelaxed surface. This is close to the energy of the π-bonded chain model (Northrup and Cohen (1982)), which shows that the DAS structure is an energetic favourable reconstruction. Previous studies of the total energy, with similar results, have been performed by simply adding up elastic and electronic contributions (Qian and Chadi (1986,87b)).

In summary, the structure of the Si(111)7×7 surface is well described by the dimer-adatom-stacking-fault model. The experimental evidence is large, and theoretical calculations support the model.

1.2.d The Ge(111)c(2×8) Surface

The situation for the Ge(111)c(2×8) surface is less conclusive than for the Si(111)7×7 surface. However, the general tendency, during the last few years, has been in favour of a Simple Adatom (SA) model, like the one shown in Figure 1.7. The symmetry c(2×8) of the unit cell was determined by applying extinction rules to the observed LEED patterns (Chadi and Chiang (1981), Yang and Jona (1984)). There is some disagreement about the possible influence of multiple scattering, but it has been established that the vector, shown as an arrow in Figure 1.7., is at least an approximate translational vector in the unit cell. This means that half of the atomic positions can be generated by a translation with this vector. This conclusion is supported by the STM study by Becker et al. (1985). The graphs of tip height versus tip position parallel to the surface show a distribution of maxima, interpreted as adatoms, in the same arrangement as shown in Figure 1.7.

A recent RBS study by Mareé et al. (1987) gave low backscattering yields, suggesting that the surface does not have a stacking fault like the Si(111)7×7 surface. The experimental results agree with computer simulations for a simple adatom model, in which atomic relaxations are included. However, the position of the adatoms relative to the surface could not be determined. The three high symmetry sites for the adatoms are shown in Figure 1.8. The T_1 site, on top of the first layer atoms, is usually disregarded. On this site, the adatom saturates only one dangling bond of the first layer. For the T_4 site, on top of the second layer atoms, and for the H_3 site, the hollow site, the adatoms saturate three dangling bonds. In the RBS study the T_4 and H_3 site were tested, but it was not possible to distinguish between them. It should be mentioned that an ion-scattering work by Culbertson et al. (1986) disagree with the conclusions above and was more in favour of a stacking fault.

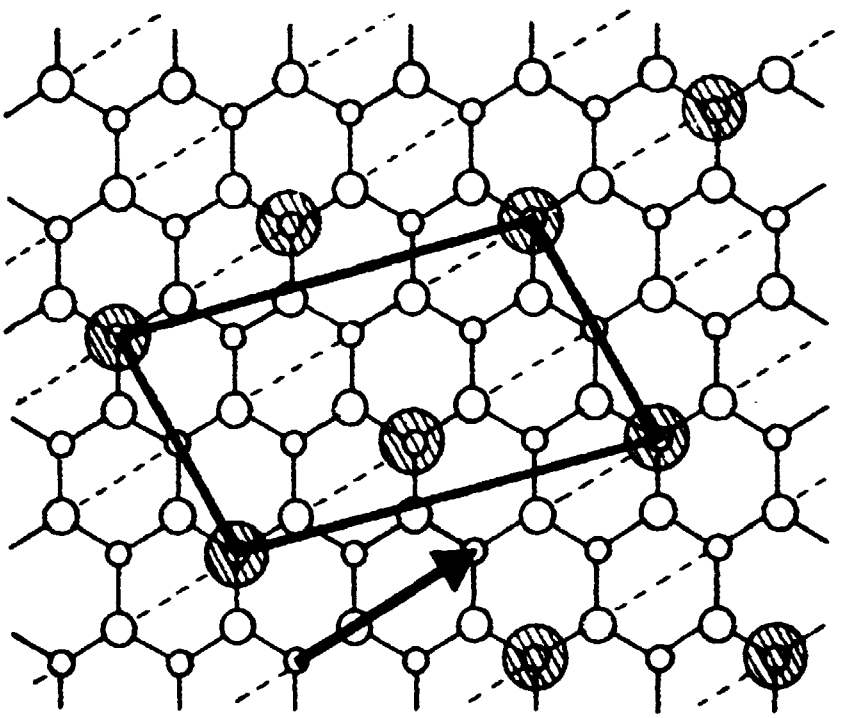

Figure 1.7. The primitive cell of the simple adatom model for the Ge(111)c(2 × 8) reconstruction. The adatoms, shown as large shaded circles, are at T_4 sites. The translational vector of the unit cell is shown as an arrow. The mirror lines in the unit cell are shown as broken lines.

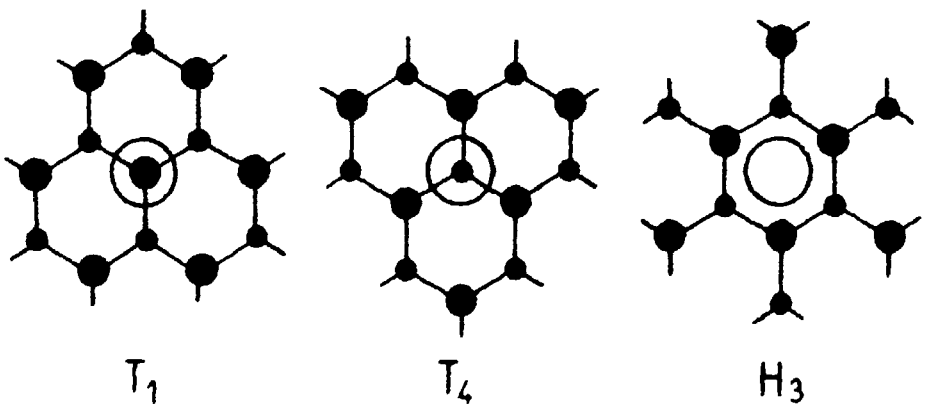

Figure 1.8. The three sites for the adatoms. Large open circles are adatoms, large and small filled circles are first and second layer atoms, respectively. T_1: on top of the first layer atoms with one close neighbour. T_4: on top of the second layer atoms with four close neighbours, i.e. the three first layer atoms and the atom just below. H_3: in the hollow site with three close neighbours.

Angle-integrated photo-emission measurements by DiCenzo et al. (1985) showed that approximately ¼ of a monolayer of atoms have an increased electronic binding energy. These atoms were interpreted as adatoms and their coverage agrees with the STM observations (Becker et al. (1985)). Angle-resolved photo-emission measurements by different authors (Yokotsuka et al. (1984), Bringans et al. (1986), Nicholls et al. (1986), and Aarts et al. (1987)) are in good agreement, as shown by Aarts et al.. The dispersions of the electronic surface states indicate a local bonding geometry similar to the Si(111)7×7 surface and the Al and In-induced $\sqrt{3}\times\sqrt{3}$ reconstructions on the Si(111) surface (Uhrberg et al. (1985) and Nicholls et al. (1985b)). The $\sqrt{3}\times\sqrt{3}$R30° unit cell for 1/3 monolayers of atom is shown in Figure 1.9.. This is the most dense arrangement of adatoms, when each adatom saturates three dangling bonds. The adatoms, shown in the figure, are at the same site (T_4) as the adatoms in the DAS model.

In order to be a plausible model for the Ge(111)c(2×8) reconstruction, the simple adatom model has to have a low total energy. Vanderbilt (1987b,c) has recently made model calculations which show that slightly different parameters can give either the 7×7 DAS model or the c(2×8) simple adatom model. The unit cell of these two structures is too large to allow ab-initio total-energy calculations, however, the c(2×8) simple adatom model is obtained after a small modification of a 2×2 adatom model, and this unit cell can be handled. For the Si(111)2×2-Si (T_4) structure Vanderbilt (1987a) has calculated the energy -0.28 eV per 1×1 unit cell, (i.e. 0.28 eV lower than the ideally terminated surface). Northrup (1987) has found the energy -0.24 eV per 1×1 unit for both the H_3 and the T_4 chemisorption site. This is quite surprising, because all previous calculations for $\sqrt{3}\times\sqrt{3}$ adatom-induced structures have strongly favoured the T_4 site (Northrup (1984, 1986), Nicholls et al. (1985b, 1987), and Zhang et al. (1985)). The two independent calculations by Vanderbilt and by Northrup for the 2×2 (T_4) structure are in good agreement. However, the energy is too high relative to the π-bonded chain model to give convincing support for the c(2×8) simple adatom model.

Experimental evidence for the energetic proximity of the c(2×8) and 7×7 reconstructions has been given by Gossmann et al. (1985). Epitaxially grown Ge films on Si(111) substrates were studied. Due to the different lattice constants of Ge and Si, the Ge film is laterally compressed. By varying the film thickness, the compression can be controlled. For increasing film thickness a change for a 7×7 to a c(2×8) periodicity was observed. The LEED patterns and the STM studies by Becker et al. (1985) demonstrated that the 7×7 structure is very similar to the Si(111)7×7 structure.

Deposition of submonolayer coverages of Sn on a Ge(111) surface can also give a 7×7 reconstruction (Ichikawa and Ino (1978)). A comparison of the RHEED patterns of this surface and of the Si(111)7×7 suggests a strong similarity. A detailed x-ray study of the Sn-induced 7×7 reconstruction and the related 5×5 structure is described in Chapter 3.

1.3. Pb- and Sn-covered Ge(111) Surfaces

Ultrathin overlayers, chemisorbed on semiconductor surfaces, form a variety of different reconstructions, which can be quite different from the structures observed on the "clean" surfaces. In some cases, the deposited atoms are believed to form simple regular adatom patterns, like the $\sqrt{3}\times\sqrt{3}$ structure briefly described in the previous section. Adatoms are recognized as being part of both the Si(111)7×7 and Ge(111)c(2×8) structure, and therefore studies of the most simple adatom structures are useful, when trying to understand more complicated structures.

1.3.a The Ge(111)-Pb Surfaces

For Pb adsorbed on a Ge(111) surface only $\sqrt{3}\times\sqrt{3}$ LEED and RHEED patterns are observed for coverages lower than 1.0-1.3 monolayers (ML). (Le Lay and Métois (1983, 1984), Métois and Le Lay (1983), and Ichikawa (1983)). For higher coverages the additional Pb accumulates in epitaxially oriented crystallites. In the electron diffraction experiments two different $\sqrt{3}$-structures were observed. For coverage 0-0.3 ML a structure known as the α-phase, apparently with only one Pb atom per unit cell, was observed. In the diffraction pattern it is characterized by comparable intensity of the two superstructure reflections that are labelled (1/3, 1/3) and (2/3, 2/3) with respect to the reciprocal basis vectors of an unreconstructed surface. For coverages of 0.3-1.3 ML the α-phase coexists with another phase, the β-phase. At about 1.0-1.3 ML only the β-phase is present, and it is characterized by considerably weaker intensity of the (1/3, 1/3) reflection relative to the (2/3,2/3) reflection. Métois and Le Lay estimated the coverage of the β-phase to be 1.0 ML, whereas Ichikawa got the value 1.3 ML. This discrepancy led the authors to propose quite different models for the β-phase.

The structure of the two phases has been determined by surface x-ray diffraction (Feidenhans'l et al. (1986)). The structural models are displayed in Figure 1.9. The α-phase has only one Pb atom per unit cell, whereas the β-phase has four. Hence, the coverages are 1/3 ML and 4/3 ML for the α- and β-phases, respectively. For intermediate coverages the two phases were found to coexist. The registry of the overlayers was determined from the interference of the scattering from the Ge substrate and the overlayer at integer-order reflections (see Section 2.4. for more information). The β-phase was found to have the Pb atoms at the corners of the unit cell (Figure 1.9.) at the hollow sites (H_3). The analysis for the α-phase suggested that the Pb atoms are situated on top of the second layer of Ge atoms (T_4 site). This is in agreement with the total-energy calculations for the Si(111)$\sqrt{3}\times\sqrt{3}$-M (M = Al, Ga, In, Ge) surfaces (Nicholls et al. (1987) and Zhang et al. (1985)) which show that the T_4 site has a lower energy than the H_3 site.

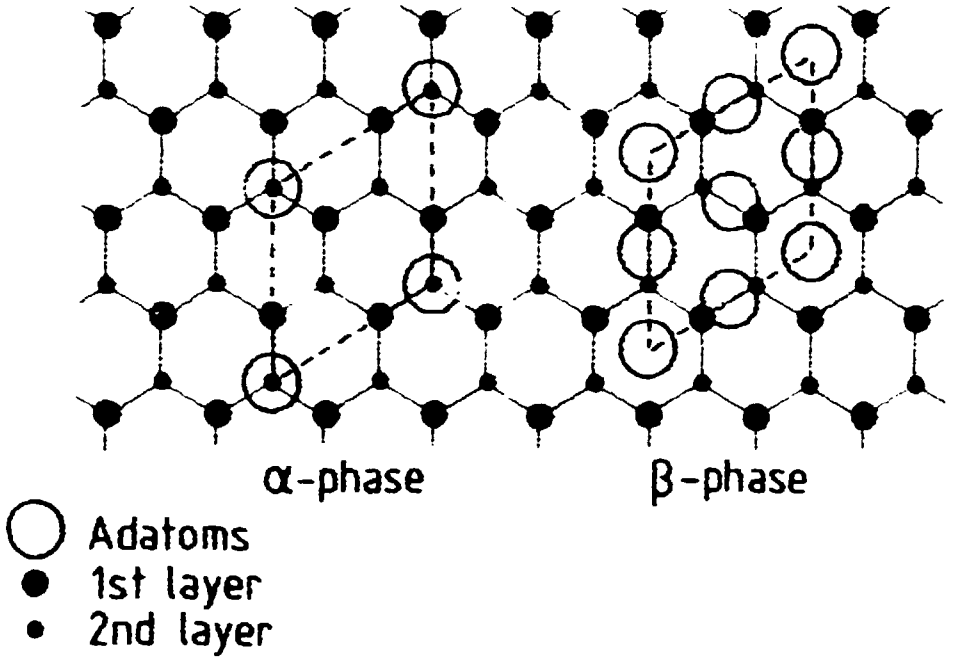

Figure 1.9. The structure of the α- and β-phases of the Ge(111)$\sqrt{3}\times\sqrt{3}$-Pb surface. The Pb atoms are at T_4 sites for the α-phase, and for the β-phase, the atoms, at the corners of the unit cell, are at H_3 site.

A recent angle-resolved photo-emission study of the β-phase by Tonner et al. (1987) revealed two sets of surface bands. A comparison with the experimental results for the Ge(111)c(2×8) surface (Bringans and Höchst (1982)) and with the band structure calculation for the Si(111)$\sqrt{3}\times\sqrt{3}$-M surfaces (Nicholls et al. (1987) and Northrup (1986)) indicated that one Pb atom per unit cell occupies a three-fold coordinated site. A surface state, which was not accounted for by this atom was ascribed to an inequivalent Pb atom at a different height above the surface. These interpretations are in agreement with the structure determined by x-ray diffraction.

1.3.b The Ge(111)-Sn Surfaces

The Sn-covered Ge(111) surfaces exhibit a considerable more complex set of reconstructions in the monolayer coverage regime (Ichikawa and Ino (1978, 1981)). Figure 1.10. shows the structures that have been observed by RHEED, during the initial heating of a sample, when the Sn-coverage θ has been deposited at room temperature. For T < 160°C a disordered c(2×8) pattern was observed, and for θ < 0.3 ML diffuse scattering was seen in the temperature range that has been investigated. For θ > 0.3 moderate temperatures (T < 300°C) result in a $\sqrt{3}\times\sqrt{3}$ structure. If the temperature exceeds 300°C, this reconstruction converts irreversibly to a 7×7 structure (0.3-0.5 ML), a 5×5 structure (0.7-0.9 ML) or a mixture of these two (0.5-0.7 ML). These structures have furthermore reversible

transitions to a 1×1 structure around 500°C. From a comparison of the RHEED patterns of the Ge(111)7×7-Sn and Si(111)7×7 reconstructions Ichikawa and Ino (1978) concluded that these two surfaces have similar atomic arrangements. Also the intensity distributions for the Ge(111)7×7-Sn and Ge(111)5×5-Sn surfaces have resemblance (Ichikawa and Ino (1981)). This indicates that the structures have some similarities.

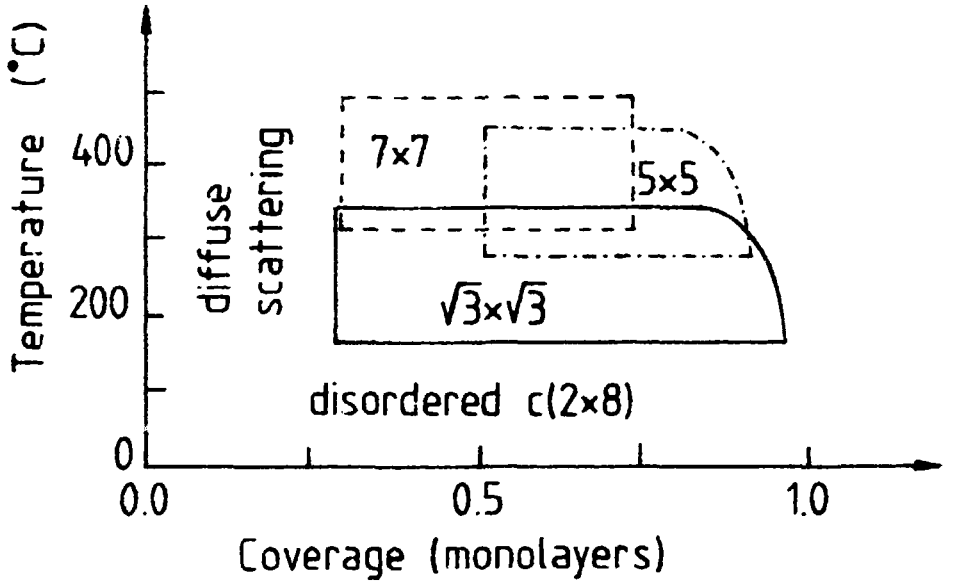

Figure 1.10. The structures observed by RHEED during the initial annealing of a sample, on which the Sn has been deposited at room temperature (Ichikawa and Ino (1981)).

Angle-resolved photo-emission studies by Yokotsuka et al. (1983) of the Ge(111)7×7-Sn and Si(111)7×7 surfaces show that the electronic structure is very similar. DiCenzo et al. (1985) have performed angle-integrated photo-emission experiments on the stable structures of the Ge(111)-Sn surface for coverages up to 1.3 ML. Measurements of the electronic binding energies of the Sn atoms revealed two inequivalent atoms. The intensity of one of the components saturates at about 0.3 ML, whereas the intensity of the other component continues to increase at least up to a coverage of 1.3 ML.

Impact collision ion-scattering spectroscopy by Sato et al. (1985) showed that the Sn atoms are not shadowed by other atoms and hence mainly occupy positions in the outermost layer of the surface. This conclusion was made for all three reconstructions: $\sqrt{3}\times\sqrt{3}$, 5×5, and 7×7.

As mentioned above, the Ge(111)-Sn system has the structural transformations: c(2×8) →7×7→ 5×5 for increasing Sn coverage. That means that the Sn atoms have a crucial influence on the structure of the surface. If the role of the Sn atoms can be revealed by an

experimental determination of the structures, it can help to increase the understanding of the mechanisms and principles that lead to the different reconstructions. Hopefully, it can also give a better understanding of the reconstructions of the "clean" Si(111) and Ge(111) surfaces.

1.4. Grazing Incidence X-ray Diffraction

Several excellent reviews concerning the grazing incidence x-ray diffraction technique and its achievements have been given recently (Feidenhans'l (1986), Robinson (1986b), and Fuoss et al. (1986)). Therefore, the next sections are limited to an outline of the early history of surface x-ray scattering and a summary of the basic equations with some emphasis on the (111) surface of the diamond lattice.

1.4.a The History of Surface X-ray Diffraction

Figure 1.11. shows schematically the scattering geometry applied in the grazing incidence technique. The incoming beam with wave vector $\vec{k}_i$ has the angle of incidence α_i relative to the surface plane. Typical values for α_i are between 0.2° and 1°. The diffracted beam with

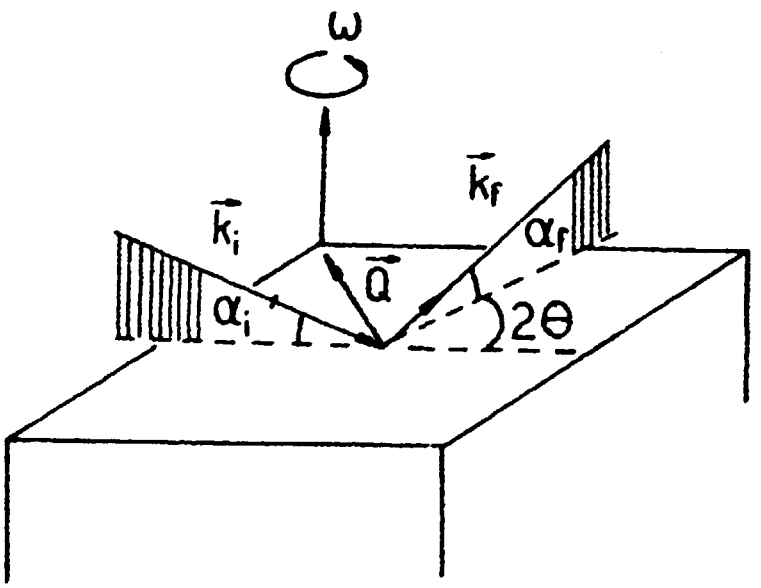

Figure 1.11. The scattering geometry of grazing incidence x-ray scattering. $\vec{k}_i$ and $\vec{k}_f$ are the wave vector of the incoming and detected beams, respectively. α_i is the angle of incidence and 2θ is the in-plane scattering angle. The scattering vector $\vec{Q}$ lies nearly in the surface plane.

wave vector $\vec{k}_f$ is detected just above the surface plane. The scattering angle 2θ is defined to be the angle between the in-plane projections of the incident and detected beam. In this geometry the scattering vector $\vec{Q}$ lies nearly in the surface plane and therefore the technique is primarily sensitive to the in-plane projected structure.

The grazing incidence has two major advantages. Firstly, it gives an enhancement of the surface signal relative to the bulk signal due to purely geometrical reasons: The geometry gives a penetration in the direction normal to the surface which is proportional to $\sin\alpha_i$, neglecting the refraction. Secondly, by using angles of incidence smaller than the critical angle for total external reflection, the electromagnetic waves are exponentially damped in the direction into the crystal. This gives a further enhancement of the signal from the surface relative to the bulk (Vineyard (1982)). The first grazing incidence x-ray scattering experiment by Marra, Eisenberger, and Cho (1979) demonstrated that it was possible experimentally to take advantage of these two points. Marra et al. studied the interface between an epitaxially grown Al film and a GaAs substrate.

The applicability of the technique in surface structure determination was demonstrated by Eisenberger and Marra (1981). A Ge(001)2×1 surface under UHV conditions was studied, and it was shown that the measured intensity of five superstructure reflections were in agreement with a previously proposed model (see Appendix B for additional information).

For a surface reconstruction the structure is not periodic in the direction normal to the surface, and therefore the Bragg condition in this direction is relaxed, which gives rise to Bragg reflections that are rod-like in the direction normal to the surface. For an ideally flat surface reconstruction the only intensity variation along the rods is a smooth decrease for increasing momentum transfer due to Debye-Waller and atomic form factors. When the intensity of the superstructure reflections are measured for a very small momentum transfer normal to the surface, only information on the in-plane projection of the surface structure is obtained. This is sufficient if the surface reconstruction is ideally flat. However, if the reconstruction extends in the direction normal to the surface, it results in a modulation of the intensity along the rods. This is due to the interference of the x-rays scattered from the different layers of the reconstruction. Robinson (1983) used the intensity profiles of the rods to determine the geometry in the direction normal to the surface of the Au(110)2×1 reconstruction. This work also demonstrated, together with the study of the InSb(111)2×2 surface by Bohr et al. (1985) that the Fourier methods of ordinary three-dimensional crystallography can be applied in slightly modified versions to solve the in-plane structure of surface reconstructions.

When atoms are adsorbed on a surface, they can occupy different sites. The possibility of determining the chemisorption site by x-ray scattering was demonstrated by Feidenhans'l et al. (1986) for the Ge(111)$\sqrt{3}\times\sqrt{3}$-Pb surface. The ideally terminated crystal has surface reflections, which arise from the finite extent of the crystal. (See next Section). These

reflections have an intensity which is comparable to the intensity of a single layer of atoms. The $\sqrt{3} \times \sqrt{3}$ arrangement of the Pb atoms has reflections that coincide with the "non-bulk" reflection from the substrate. The two contributions add coherently, and from the measured intensities the chemisorption site can be determined.

The above experiments are fundamental in the history of surface x-ray scattering. Several other experiments have been performed and most are described in the review by Fuoss et al. (1986).

I.4.b The Basic Theory of Surface X-ray Diffraction

The grazing incidence x-ray scattering experiment is a combination of a refraction and a diffraction phenomena (Vineyard (1982)). At the vacuum-surface interface the refractive index changes abruptly, and the critical angle of total external reflection α_c is given by:

$$\cos \alpha_c = n \ , \ n = 1 - \frac{Ne^2}{2\pi mc^2} \ \frac{Z\rho}{A} \lambda^2 \qquad (1\text{-}1)$$

n is the refractive index of the solid, N is Avogadro's number, e and m are the electron charge and mass, respectively, c is the velocity of light, Z and A are the atomic charge and mass number, respectively, ρ is the density, and λ is the wavelength of the x-rays. α_c is typically 0.2°-0.4° for wavelengths around 1.5 Å.

The refraction can be considered as caused by the average dielectric constant of the solid, whereas the diffraction is due to the modulation of the dielectric constant on an atomic length scale. This approach leads to essentially the same results for diffraction as the standard kinematical theory (Warren (1969)).

An important consequence of the refraction is the modification of the diffracted signal in the direction normal to the surface (Dosch et al. (1986), Dosch (1987), and Feidenhans'l (1986)). This effect is most easily explained by the reciprocity theorem elastic of scattering theory (see for instance Schiff (1968)). It states that the scattering is the same, when the direction of propagation for both the incident and scattered waves are reversed. When this is applied to the scattering situation, it means that varying the exit angle α_f, keeping the incidence angle α_i fixed, is simply the same as varying α_i, keeping α_f fixed. In the latter case the intensity of the diffracted beam is proportional to the transmission of the x-rays into the crystal. The transmission can be calculated from Maxwell's equations, and the result can be found in standard text books on optics (see for instance Hecht (1975)):

$$T(\alpha_f) = \begin{cases} 4\left(\frac{\alpha_f}{\alpha_c}\right)^2 \Big/ \left(\left(\frac{\alpha_f}{\alpha_c}\right)^2 + \sqrt{\left(\frac{\alpha_f}{\alpha_c}\right)^2 - 1} \right)^2 & \alpha_f > \alpha_c \\ 4\left(\frac{\alpha_f}{\alpha_c}\right)^2 & \alpha_f \leq \alpha_c \end{cases} \qquad (1\text{-}2)$$

which is valid if α_f and α_c are small. In this expression the absorption has been neglected. The diffraction signals can be calculated by multiplying the results from the kinematical theory with the expression (1-2). Figure 1-12 shows a plot of the transmission $T(\alpha_f)$. The scattering intensity is reduced at small exit angles and enhanced close to the critical angle α_c for total external reflection. For α_f greater than about $2\alpha_c$ the scattering intensity is almost unaffected.

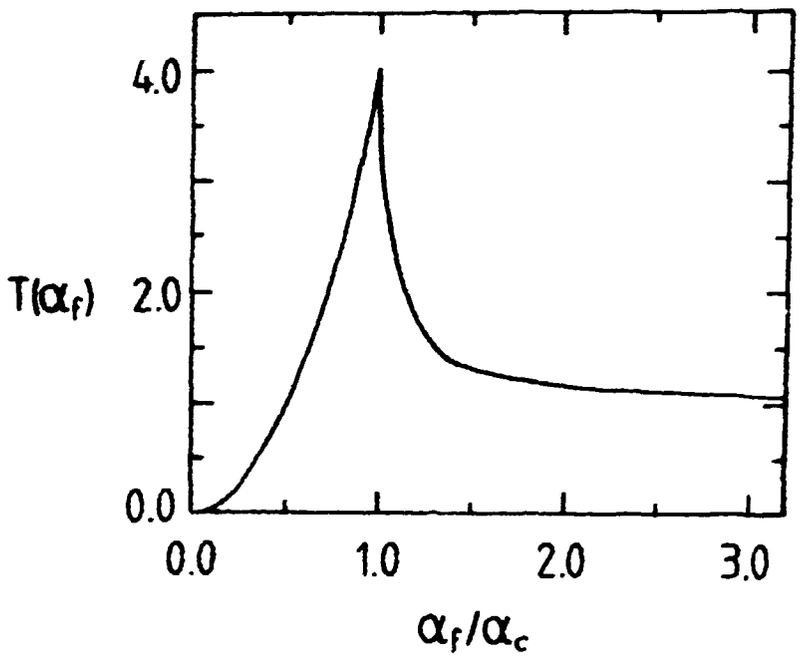

Figure 1.12. The intensity distribution (equation 1-2) by which the diffracted beam is convoluted.

The termination of the bulk crystal by the surface gives rise to some surprising diffraction features. In this section the diffraction pattern from a (111) surface of an ideally terminated crystal with diamond structure is calculated. In order to be able to generate the lattice points on the crystal surface by translations of the basis vectors, two of them have to be chosen in the surface plane. A third basis vector is conveniently chosen in the direction normal to the surface. The in-plane basis vectors for the (111) diamond structure are shown in Figure 1.13.

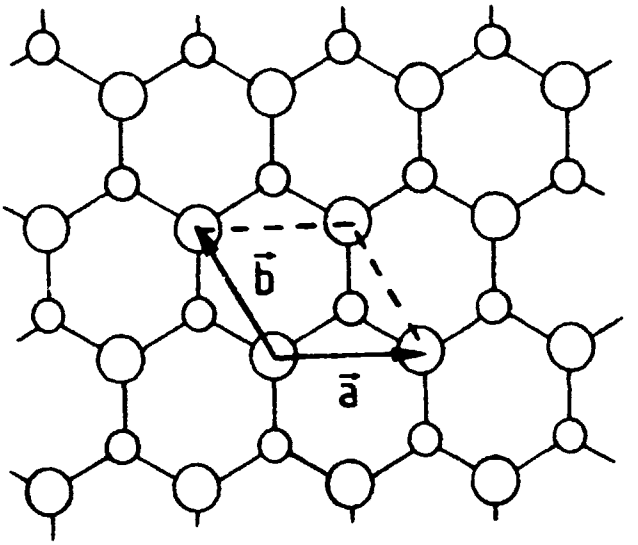

Figure 1.13. The in-plane basis vectors, $\vec{a}$ and $\vec{b}$, of the first bilayer of the diamond structure.

In units of the cubic bulk vectors the three basis vectors are:

$$\vec{a} = \frac{1}{2}[1,0,\bar{1}]_{cubic}$$

$$\vec{b} = \frac{1}{2}[\bar{1},1,0]_{cubic} \qquad (1\text{-}3)$$

$$\vec{c} = \frac{1}{3}[1,1,1]_{cubic}$$

Denoting the cubic lattice constant: a_o, the vectors $\vec{a}$, $\vec{b}$, and $\vec{c}$ fulfil:

$$\sphericalangle(\vec{a},\vec{b}) = 120^o$$

$$a = b = \frac{1}{\sqrt{2}} a_o$$

$$c = \frac{1}{\sqrt{3}} a_o \qquad (1\text{-}4)$$

The corresponding reciprocal unit vectors are:

$$\vec{a}^* = \frac{1}{3}\,[2,2,\bar{4}]_{cubic}$$

$$\vec{b}^* = \frac{1}{3}\,[\bar{2},4,\bar{2}]_{cubic} \qquad (1\text{-}5)$$

$$\vec{c}^* = [1,1,1]_{cubic}$$

which satisfy:

$$\sphericalangle(\vec{a}^*,\vec{b}^*) = 60^o$$

$$a^* = b^* = \frac{2\pi}{a_o}\sqrt{\frac{8}{3}} \qquad (1\text{-}6)$$

$$c^* = \frac{2\pi}{a_o}\sqrt{3}$$

Note that the reciprocal lattice vectors a* and b* are not bulk Bragg reflections. In the direction normal to the surface the translational symmetry is broken at the surface. Therefore, the unit cell is semi-infinite in this direction and l is a continuous variable. The intensity of the diffracted x-rays is given by the geometrical structure factor F_{hkl} of this unit cell. The structure factor G_{hkl} of one bilayer ((h,k,l) is given with respect to the vectors in equation (1-5)):

$$G_{hkl} = f_{hkl}\; e^{-M}\left(1+e^{2\pi i(2/3\cdot h + 1/3\cdot k + 1/4\cdot l)}\right) \qquad (1\text{-}7)$$

where f_{hkl} is the atomic form factor and e^{-M} is the Debye-Waller factor. The ...ABCABC...-stacking of the bilayers gives the phase factor:

$$e^{i\cdot n\cdot \psi_{hkl}} \quad ; \quad \psi_{hkl} = 2\pi(2/3\cdot h + 1/3\cdot k + l) \qquad (1\text{-}8)$$

for the n'th bilayer. Each bilayer scatters a small part of the x-rays giving an attenuation ν of the x-rays per bilayer. Including this and neglecting refraction, the total geometrical structure factor is:

$$F_{hkl} = \sum_{n=0}^{\infty} G_{hkl}\, e^{i \cdot n \cdot \psi_{hkl}}\, e^{-n\nu} = \frac{G_{hkl}}{1 - e^{-\nu}\, e^{i\psi_{hkl}}} \tag{1-9}$$

The intensity is given by the absolute square of F_{hkl}:

$$|F_{hkl}|^2 = f_{hkl}^2\, e^{-2M}\, \frac{2\left(1+\cos\left[2\pi(2/3 \cdot h + 1/3 \cdot k + 1/4 \cdot l)\right]\right)}{1+e^{-2\nu}-2e^{-\nu}\cos\left[2\pi(2/3 \cdot h + 1/3 \cdot k + l)\right]} \tag{1-10}$$

The (h,k,l) values that correspond to bulk Bragg points are obtained, when the denominator is small, i.e. for:

$$2/3 \cdot h + 1/3 \cdot k + l = n \tag{1-11}$$

where n is an integer. Calculating (1-10) for this set of (h,k,l) gives to lowest order in ν:

$$|F_{hkl}|^2 = \begin{cases} 0 & \text{for } l = 4\left(m + \frac{1}{2} - \frac{2}{3}h - \frac{1}{3}k\right) \\ f_{hkl}^2 \cdot e^{-2M} \cdot \frac{4}{\nu 2} & \text{for } l = 4\left(m - \frac{2}{3}h - \frac{1}{3}k\right) \\ f_{hkl}^2 \cdot e^{-2M} \cdot \frac{2}{\nu 2} & \text{for } l = 4\left(m \pm \frac{1}{4} - \frac{2}{3}h - \frac{1}{3}k\right) \end{cases} \tag{1-12}$$

where m is an integer. The reflections that are forbidden in this approach are of course the

same that are forbidden,when calculating the structure factors of the cubic unit cell (Warren (1969)). The attenuation for x-rays is small ($\nu \sim 10^{-4}$), and the intensity of the "allowed" points are orders of magnitude larger than the scattering from a single layer of atoms. This is only an estimate, since close to the bulk Bragg points the diffraction is only correctly described by dynamical theory.

Away from the bulk Bragg reflections the attenuation can be ignored. The in-plane (l = 0) "non-bulk" reflections have the intensity:

$$|F_{hk}|^2 = f_{hk}^2 \cdot e^{-2M} \cdot \frac{1}{3} \tag{1-13}$$

This is comparable to the diffraction intensity from a single layer of atoms. Hence, these reflections, often denoted crystal truncation rods, have importance for surface x-ray diffraction. The expression for the structure factor intensity (1-10) gives rods of intensity in the direction normal to the surface through the in-plane integer-order reflections (Figure 1-14).

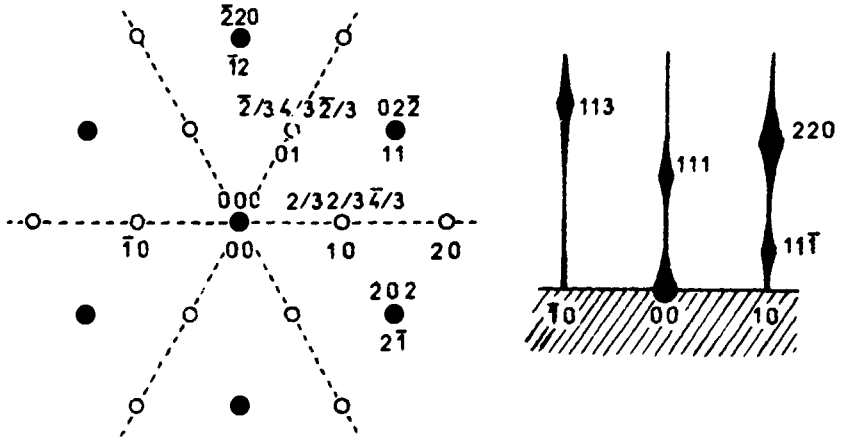

Figure 1.14. The reciprocal lattice of the (111) surface of the diamond structure. Left-hand side: The (111) plane. The filled circles represent bulk Bragg reflections, and the open circles represent the crystal truncation rods. The index of the reflections are given in cubic units above the points and in the surface units below (l = 0). Right-hand side: A cut normal to the surface through (1,0) and ($\bar{1}$,0). The width of the rods schematically indicates the intensity variation. The intensity varies along the rods and increases strongly, as the bulk Bragg reflections are approached. These rods are present due to the termination of the crystal at the surface, and they are usually referred to as truncation rods (Robinson (1986c)).

A surface reconstruction with a surface unit cell, which is n times larger along a and m times larger along b results in reflections of fractional-order with respect to a* and b*: (h,k) = (i/n, j/m), where i and j are integers. As there is no Bragg condition in the direction normal to the surface, l is a continuous variable, and the reflections have a rod character.

In a grazing-angle x-ray scattering experiment, it is usual to measure the integrated intensity of the reflections. This automatically reduces the influence of sample imperfections (e.g. finite width due to domains) and instrumental resolution. The opening of the detector gives a cut-off along the rod when the in-plane values ($l \sim 0$) are measured. If the resolution in the scattering angle 2θ is relaxed sufficiently, the integrated intensities can be obtained by simply rotating the sample around the surface normal in a small range about the reflection. The integrated intensity I_{hk} is related to the geometrical structure factors F_{hk} by:

$$I_{hk} = C \cdot P \cdot \frac{A}{\sin(2\theta)} |F_{hk}|^2 \qquad (1\text{-}14)$$

C is a proportionality constant, P is the polarization factor, A is the active sample area, and $(\sin(2\theta))^{-1}$ is the Lorentz factor (Warren (1969)). In a cross beam technique A is defined by the slits, and it is proportional to $(\sin(2\theta))^{-1}$.

In ordinary three dimensional crystallography the structure factors are defined as the Fourier components of the charge density $\rho(r)$ in the unit cell:

$$F_{hkl} = \int \rho(\vec{r}) e^{i(h\vec{a}^* + k\vec{b}^* + l\vec{c}^*) \cdot \vec{r}} dV \qquad (1\text{-}15)$$

This integral can be split into a sum over the individual atoms in the unit cell:

$$F_{hkl} = \sum_{j=1}^{n} f_j(hkl)\, e^{i2\pi(h \cdot x_j + k \cdot y_j + l \cdot z_j)} \qquad (1\text{-}16)$$

where $f_j(h,k,l)$ is the atomic form factor:

$$f_j(hkl) = \int \rho_j(\vec{r})\, e^{i(h\vec{a}^*+k\vec{b}^*+l\vec{c}^*)\cdot\vec{r}}\, dV \tag{1-17}$$

Expressions for the form factors can be found in "International Tables for X-ray Crystallography", edited by Lonsdale (1962). In equation (1-16) the position of the j'th atom (x_j,y_j,z_j) is given in units of the basis vectors a, b, and c. For finite temperatures the atoms are vibrating around the equilibrium position, and the Debye-Waller factor e^{-M_j} must be included in (1-16). In the following the Debye-Waller factor will be assumed to be isotropic. The parameter M_j is often expressed by the B-factor:

$$M_j = B_j\, Q^2/(4\pi)^2 = \frac{1}{2}\langle(\vec{u}_j\cdot\vec{Q})^2\rangle \tag{1-18}$$

where Q is the scattering vector and $\langle(u_j\cdot Q)^2\rangle$ is the thermal average of the square of the scalar product of Q and the displacement of the j'th atom.

The Fourier transform of (1-15) gives directly the charge density:

$$\rho(x,y,z) = \frac{1}{V}\sum_{hkl} F_{hkl}\, e^{-i2\pi(hx+ky+lz)} \tag{1-19}$$

where V is the unit cell volume.

For a grazing-angle x-ray scattering experiment in which the $l=0$ intensities are measured, it is relevant to consider (1-19) for l equal to zero. The right-hand side becomes:

$$\frac{1}{V}\sum_{hk} F_{hk0}\, e^{-i2\pi(hx+ky)} = \frac{1}{V}\sum_{hkl} F_{hkl}\, e^{-i2\pi(hx+ky)}\,\delta(l)$$

$$= \int_{-\infty}^{\infty} \frac{1}{2\pi V}\sum_{hkl} F_{hkl}\, e^{-i2\pi(hx+ky+lz)}\, dz = \frac{1}{2\pi}\int_{-\infty}^{\infty}\rho(\vec{r})\,dz \tag{1-20}$$

in which the delta function has been expressed by the integral:

$$\delta(l) = \frac{1}{2\pi} \int_{-\infty}^{\infty} e^{-i2\pi l \cdot z} \, dz \qquad (1\text{-}21)$$

Equation (1-20) shows that the electron density projected on the surface is given by the $l=0$ structure factors. With the use of:

$$F_{hk} = |F_{hk}| \, e^{i\alpha_{hk}} \qquad (1\text{-}22)$$

the in-plane projected electron density can be written:

$$\rho(x,y) = \frac{2\pi}{V} \sum_{hk} |F_{hk}| \cos\{2\pi(hx+ky) - \alpha_{hk}\} \qquad (1\text{-}23)$$

In practice, the electron density cannot be calculated by the formula, because only $|F_{hk}|$ can be measured in an experiment. However, the Patterson (pair-correlation) function P(x,y) can be calculated without knowing the phases:

$$P(x,y) = V \int_0^1 \int_0^1 \rho(x',y')\rho(x-x',y-y')dx'dy' \qquad (1\text{-}24)$$

The Patterson function has a peak for (x,y) equal to an interatomic vector. Inserting the expression (1-23) for the electron density gives:

$$P(x,y) = \frac{(2\pi)^2}{V} \sum_{hk} |F_{hk}|^2 \cos\{2\pi(hx+ky)\} \qquad (1\text{-}25)$$

It is, in principle, possible to obtain the interatomic vectors by mapping out the expression (I-25). In order to have a Patterson function which only contains information on the structure of the surface reconstruction the integer-order reflections are usually not included in the sum. This gives negative peaks in the Patterson function for values of (x,y) that correspond to interatomic vectors for the projected bulk structure. The difficulties of interpreting the Patterson function, when all the integer-order reflections are systematically omitted, has recently been discussed by Bohr et al. (1986) and Feidenhans'l (1986). It was shown that the Patterson function can be distorted, but that no false peaks appear.

If the analysis of the Patterson function leads to a model for the structure of the surface reconstruction, the parameters of the model can be optimized by minimizing the expression:

$$\chi^2 = \frac{1}{N-p} \sum_{hk} \frac{(|F_{hk}^{mod}|^2 - |F_{hk}^{exp}|^2)^2}{\sigma_{hk}^2} \qquad (I\text{-}26)$$

where N is the number of reflections, p is the number of parameters that are optimized, σ_{hk} is the standard error in the structure factor intensity $|F_{hk}^{exp}|^2$ from the experiment. $|F_{hk}^{mod}|^2$ is the model structure factor intensity. χ^2 is a statistical measure of the agreement between the model and the experimental results (Bevington (1969)). For the experiments described in Chapter 2 and 3 the absolute values of the structure factor intensities were not measured and therefore a scale factor for the model structure factor intensities was included as a fit parameter in (I-26).

The standard error σ_{hk} is calculated from the reproducibility of symmetry equivalent reflections and the counting statistics. The following procedure is usually applied. The average value of a set of symmetry equivalent reflections is calculated as the weighted sum (Robinson (1986b)):

$$\langle |F_{hk}|^2 \rangle = \sum_i \frac{|F_{hk}|_i^2}{(S_{hk}^i)^2} \cdot \langle S_{hk} \rangle^2$$

$$\frac{1}{\langle S_{hk} \rangle^2} = \sum_i \frac{1}{(S_{hk}^i)^2} \qquad (I\text{-}27)$$

The i-sums are over symmetry equivalent reflections with index h,k, and S_{hk}^i is the error on $|F_{hk}|_i^2$ from counting statistics. The standard error SE_{hk} is:

$$SE_{hk}^2 = \sum_i \left[\frac{|F_{hk}^2|_i^2}{(S_{hk}^i)^2} \cdot \langle S_{hk} \rangle^2 - \langle |F_{hk}|^2 \rangle^2 \right] \tag{1-28}$$

which includes both reproducibility and counting statistics. The average relative standard error is calculated for the reflections that are larger than three times their standard error. This ensures that the contribution to SE_{hk} is mainly from the reproducibility:

$$\varepsilon'' = \frac{1}{M} \sum_{hk} \frac{SE_{hk}}{\langle |F_{hk}|^2 \rangle} \tag{1-29}$$

where M is the number of reflections that are larger than three times SE_{hk}. The contribution to ε'' from the counting statistics is:

$$\varepsilon' = \frac{1}{M} \sum_{hk} \frac{\langle S_{hk} \rangle}{\langle |F_{hk}|^2 \rangle} \tag{1-30}$$

where the sum is over the same reflections as included in (1-29). Finally, the reproducibility is:

$$\varepsilon 2 = (\varepsilon'')2 - (\varepsilon')2 \tag{1-31}$$

and the standard error σ_{hk} can be calculated for all reflections:

$$\sigma_{hk}^2 = \langle S_{hk} \rangle^2 + \varepsilon^2 \langle |F_{hk}|^2 \rangle^2 \tag{1-32}$$

which goes into the expression (1-26) for χ^2 together with $|F_{hk}^{exp}|^2 = \langle|F_{hk}|^2\rangle$. If the optimization of the model gives a value for χ^2 close to one, there is a statistical agreement between model and experiment, and the data analysis is finished. Larger values of χ^2 indicate that the model should be improved. This can either be done by proposing a new model from a reexamination of the Patterson function or by performing an error synthesis. If the model is not too far from the real structure, the phases of the experimental structure factors can be approximated by the phases of the model structure factors. The difference in electron density between the experiment and the model $\Delta\rho(x,y)$ can then be calculated by (1-23) as:

$$\Delta\rho(x,y) = \frac{2\pi}{V} \sum_{hk} \left(|F_{hk}^{exp}| - |F_{hk}^{mod}| \right) \cos\left(2\pi(hx+ky) - \alpha_{hk}^{mod}\right) \qquad (1\text{-}33)$$

Positive peaks in a plot of $\Delta\rho(x,y)$ indicate electron density which is missing in the model, and negative peaks indicate the presence of too much electron density in the model. The model can then be modified accordingly and the new model optimized. In a successful structure determination a repetition of the minimization of χ^2 and the error synthesis will eventually give a value of χ^2 close to unity.

2. THE STRUCTURE OF THE α-PHASE OF THE Ge(111)$\sqrt{3}\times\sqrt{3}$-Sn AND Ge(111)$\sqrt{3}\times\sqrt{3}$-Pb SURFACES

2.1 Introduction

In this Chapter a surface x-ray diffraction study of $\sqrt{3}$-structures of Sn and Pb on Ge(111) surfaces is described. Measurements of the in-plane intensities of fractional-order reflections have been performed on two Sn-covered and two Pb-covered samples. From the data analyses it is concluded that the ordered structures have a coverage of 1/3 monolayer (ML). This is known as the "α-phase" and, with its small unit cell containing only one adsorbed atom, is one of the simplest reconstructions that exists on the Si(111) and Ge(111) surfaces. Similar structures are observed after adsorption of 1/3 ML of Group III or IV elements on Si(111) (Chen et al. (1982), Estrup and Morrison (1964), Hansson et al. (1981), Kinoshita et al. (1986) and Nicholls et al. (1985b)) or on Ge(111) (Ichikawa and Ino (1978) and Métois and Le Lay (1983)). Despite the large effort in recent years, the detailed atomic geometry and chemisorption sites have still not been determined unambigiously (Kinoshito et al. (1985,1986), Nicholls et al. (1985b,1987), Northrup (1984), Hansson et al. (1986) and Saitoh et al. (1985)). However, a previous x-ray diffraction study (Feidenhans'l et al. (1986)) of $\sqrt{3}$-structures of Pb on Ge(111) for coverages of 0.6 - 1.3 ML indicated that the chemisorption site of the α-structure is the T_4 site, i.e. on a three-fold coordinated site on top of the second layer of Ge (Figure 2.1).

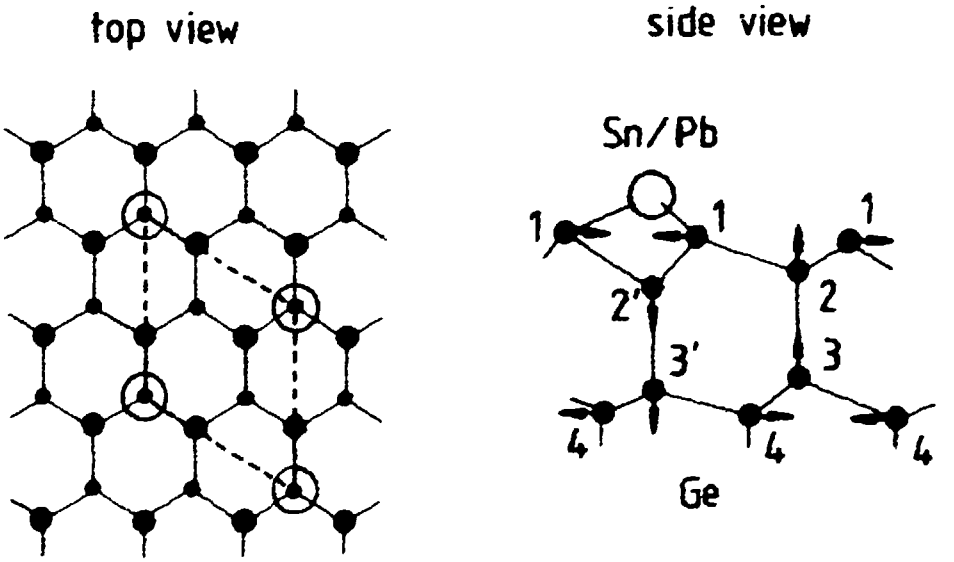

Figure 2.1: Left-hand side: Top view of the α-phase of the $\sqrt{3}\times\sqrt{3}$R30° structure. The large and small filled circles indicate the positions of the atoms in the first bilayer of the substrate. Large open circles are adatoms. The chemisorption site is T_4. Right-hand side: Side view of the T_4 geometry.

A detailed investigation of the α-phase of the Sn- and Pb-induced Ge(111)$\sqrt{3}\times\sqrt{3}$ R30° surface reconstruction by grazing-incidence x-ray scattering is presented below. The data analysis is performed af follows: First, the projection of the structure on the surface plane is determined for all four samples by an analysis of the in-plane intensities of the fractional-order Bragg rods. For one of the Sn-covered and one of Pb-covered samples the in-plane intensities of the integer-order reflections were measured. Also, the intensity profiles of a subset of the fractional-order Bragg rods were measured for these two samples. At the integer-order reflections the scattering from the surface layers and the Ge substrate interfere. The registry of the surface layers relative to the bulk crystal is determined from an analysis of these reflections. The geometry normal to the surface is then deduced from an analysis of the intensity variation along the fractional-order Bragg rods. Finally, the observed atomic relaxations are compared to the results of a simple elastic energy minimization employing a Keating potential (Keating (1966)).

2.2 Experimental

The samples were prepared at the Flipper II photoemission beamline at the Hamburg Synchrotron Radiation Laboratory (HASYLAB). The Ge(111) substrates have been cut from a precisely oriented Ge crystal. The 10 × 10 mm^2 surface were polished to be optically flat. After insertion in the UHV chamber the samples were sputtered with 500 eV Ar ions for half an hour at a substrate temperature of about 400°C and afterwards annealed at ~ 700°C for one hour. They were then cooled slowly to room temperature and characterized by LEED and photoemission. Typically 3-4 cycles produce a sharp c(2 × 8) LEED pattern and a valence band photoemission spectrum characteristic of the clean surface.

The adlayers were deposited from BN effusion cells. The two Sn-covered samples (henceforth referred to as Sn-1 and Sn-2) were kept at 250-300°C during the evaporation, whereas the two Pb-covered samples (Pb-1 and Pb-2) were at room temperature during the evaporation. The latter two were mildly annealed to 300°C after the deposition. The coverages of the four samples were estimated by a quartz crystal thickness monitor and from the relative core level (Ge3d, Sn4d, Pb5d) energy distribution intensities. The estimated coverages are Sn-1: 0.5 ML, Sn-2: 0.7 ML, Pb-1: 0.3 ML and Pb-2: 0.3 ML.

After a sample had been prepared and characterized it was transferred to a small portable UHV cell with a 360° Be-window for x-ray diffraction (Feidenhans'l (1986)). The x-ray cell was mounted on the vertical scattering diffractometer on the 32-pole wiggler beam line W1 in HASYLAB. The synchrotron beam was monochromatized by two Ge(111) crystals and focussed on the sample by a toroidal Au-coated mirror. The mirror also reduces higher-order harmonics in the beam. The beamline and the sample alignment have been described in detail by Feidenhans'l (1986). The sample surface is aligned by means of a position sensitive detector (PSD) and the total-reflected beam. The sample surface is

adjusted until the angle of incidence is independent of the sample azimuthal angle ω, which ensures equal penetration depth for all values of ω.

The in-plane collimation of the beam is given by 2.0 mm slits before and after the sample. The PSD has the counting wire subtending 2.4° normal to the surface and 0.5° parallel to the surface along the scattering angle 2θ. The relaxed 2θ-resolution allows integrated intensities to be measured by performing only ω-scans. Figure 2.2 shows the (2/3,2/3) reflection of sample Sn-1 which is a typical reflection. The upper part of the figure shows the ω-scan and the lower part shows the angle-integrated intensity along the rod. It has a enhanced intensity at the critical angle in accordance with equation (1-2) and Figure 1.12.

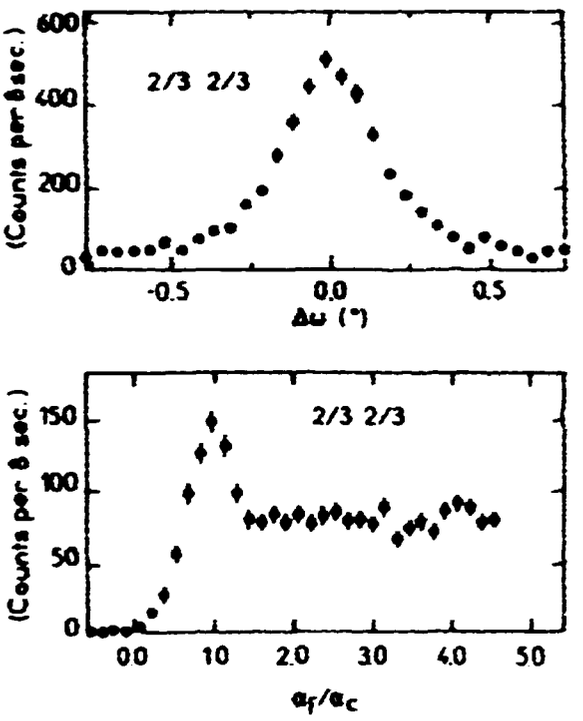

Figure 2.2: Upper part: An ω-scan of the (2/3,2/3) reflection. The integrated intensity is found as the numerical sum of the background-subtracted counts multiplied by the step length. Lower part: The angle-integrated intensity profile along the rod.

The onset peak is smeared due to a slight curvature of the sample surface. The width of the ω-scan is mainly determined by the resolution of the present set-up. For the relaxed resolution along the rod, it takes a finite angular width to scan the Ewald sphere describing the rod through the counter. A typical recording time for a reflection is 5-10 minutes.

The integrated intensities were obtained after subtracting the background and numerically integrating the ω-scan. The structure factor intensities were calculated, as described in section 1.4, by correcting the integrated intensities for the Lorentz factor $(\sin 2\theta)^{-1}$ and active sample area $(\sin 2\theta)^{-1}$. For small angles the cross-beam area exceeds the sample area and the structure factors were also corrected for this effect. For the vertical scattering plane the polarization factor is close to unity and therefore no correction is performed.

The important experimental parameters for the four samples are listed in Table 2.1: estimated coverage θ, angle of incidence α_i, x-ray wavelength λ, reproducibility of symmetry equivalent fractional-order reflections ε, total number of fractional- and integer-order reflections N_F^{Tot} and N_I^{Tot}, respectively, and the corresponding number of independent reflections N_F^{Indp} and N_I^{Indp}.

Table 2.1. Estimated coverage θ, angle of incidence α_i, x-ray wavelength λ, reproducibility of symmetry equivalent fractional-order reflections ε, total number of fractional- and integer-order reflections, N_F^{Tot}, and N_I^{Tot}, respectively, and corresponding number of independent reflections, N_F^{Indep} and N_I^{Indep}.

	Sn-1	Sn-2	Pb-1	Pb-2
θ(ML)	0.5	0.7	0.3	0.3
α_i	0.63°	1.00°	0.42°	0.57°
λ(Å)	1.535	1.345	1.344	1.375
ε	0.061	0.055	0.114	0.170
N_F^{Tot}	36	16	30	20
N_F^{Indep}	13	9	15	9
N_I^{Tot}	14	2	10	6
N_I^{Indep}	5	1	6	3

The extent of the surface reconstructions in the direction normal to the surface gives rise to an intensity variation along the fractional-order rods. The symmetry of the crystal gives the relation $|F_{hk\ell}|^2 = |F_{-k-h\ell}|^2 = |F_{kh-\ell}|^2$ which demonstrates that the reflections (h,k) and (k,h) are only equivalent for $\ell = 0$. In the experiment the reflections are measured with a finite momentum transfer in the ℓ-direction. Due to the slope of the rod intensity for some of the reflections around $\ell = 0$, different intensities are observed for in-plane equivalent reflections. Thus, special attention must be paid to the averaging of in-plane equivalent reflections to ensure that the averaging is done over both reflections that are sloping up and down for increasing perpendicular momentum transfer. The resulting fractional-order structure factor intensities are displayed in Table 2.2 as $|F_{hk}^{exp}|^2$ and the integer-order structure factor intensities of the samples Sn-1 and Pb-1 are shown in Table 2.4. Also displayed in the two tables are the uncertainties calculated from the reproducibility and counting statistics as described in Section 1.4. The results in Table 2.2 demonstrate a good reproducibility of the experiment for both the Sn- and Pb-covered samples.

For the samples Sn-1 and Pb-1 the intensity profiles (ω-integrated) of a subset of the fractional-order reflections were recorded up to a momentum transfer of ~ 1 Å^{-1} in the direction normal to the surface. The upper limit is determined by mechanical constraints in the experimental set-up. The measurements were done by moving the detector out of plane, preserving the grazing angle of incidence and the advantage of a small penetration into the sample. The measured structure factor intensities (rodscans) are displayed in

Table 2.2. Measured fractional-order structure factor intensities $|F_{hk}^{exp}|^2$, uncertainties σ_{hk} and model structure factor intensities $|F_{hk}^{mod}|^2$. The models are described in the text.

	Sn-1			Sn-2			Pb-1			Pb-2		
h k	$\|F_{hk}^{exp}\|^2$	σ_{hk}	$\|F_{hk}^{mod}\|^2$	$\|F_{hk}^{exp}\|^2$	σ_{hk}	$\|F_{hk}^{mod}\|^2$	$\|F_{hk}^{exp}\|^2$	σ_{hk}	$\|F_{hk}^{mod}\|^2$	$\|F_{hk}^{exp}\|^2$	σ_{hk}	$\|F_{hk}^{mod}\|^2$
1/3 1/3	22.1	1.6	22.6	22.1	1.3	23.2	81.7	9.4	88.1	81.7	14.0	76.5
2/3 2/3	8.9	0.6	9.5	9.5	0.5	9.1	56.4	6.5	48.2	45.0	7.7	43.7
4/3 1/3	15.8	0.7	14.9	13.2	2.4	12.8	45.8	5.3	46.2	63.7	11.0	46.9
5/3 2/3	14.1	0.9	13.5	12.5	4.1	14.6	42.0	4.9	40.5	43.6	7.9	54.9
4/3 4/3	13.4	1.1	14.0	17.4	1.2	16.6	37.3	4.3	40.3	62.6	10.5	61.2
5/3 5/3	2.1	0.3	2.3	0.0	1.0	1.5	7.8	1.0	9.0	0.0	12.4	18.0
7/3 1/3	8.3	0.7	7.5	1.8	1.8	5.5	18.7	2.3	17.3	21.0	3.8	24.1
7/3 4/3	10.4	1.0	11.8	12.4	2.9	8.9	14.9	1.7	14.7	28.7	6.8	23.3
7/3 7/3	5.9	0.5	5.8									
8/3 2/3	10.4	0.8	10.5	11.8	3.0	8.9	18.0	2.1	17.3	37.4	6.5	32.5
8/3 5/3	5.4	0.5	4.9				10.8	1.3	9.8			
8/3 8/3							1.3	0.3	1.3			
10/3 1/3	6.6	0.5	6.7				12.3	5.0	15.5			
10/3 4/3							7.4	0.9	6.9			
11/3 2/3	2.3	0.9	2.8				4.2	0.6	3.8			
13/3 1/3							4.4	1.7	7.4			

Figure 2.4. The momentum transfer ℓ normal to the surface is in units of the bulk reciprocal lattice vector (111). The rodscans of the reflections (4/3,1/3), (1/3,4/3), (5/3,2/3) and (2/3,5/3) are shown in pairs next to each other to indicate the symmetry relation: $|F_{hk\ell}|^2 = |F_{kh\text{-}\ell}|^2$. The intensities close to $\ell=0$ are not included due to the influence of refraction around the critical angle. The horizontal and vertical bars in the figure indicates resolution along the rod and experimental uncertainty, respectively. An average value of the in-plane uncertainties has been assigned to all points.

2.3. In-Plane Projected Structures

The first step in the analysis was to make a contour plot of the Patterson function (1-25) that can be constructed from the four data sets. The only strong feature in the plots is the self-correlation peak, which indicates that the dominant feature of the structures are the adatoms arranged in the $\sqrt{3}$-pattern.

First the analysis for sample Sn-1 is discussed. Fitting a model with one Sn atom per unit cell gave the agreement $\chi^2 = 38$ allowing only a scale factor to vary. That means that the

average deviation between model and experimental structure factor intensities is about six times larger than the average experimental uncertainty. An electron density difference plot (EDDP) according to equation (1-33) indicated that six Ge atoms should be included at positions near the corners of a hexagon with the adatom in the center. In the next model the Ge atoms were allowed to relax according to the 3m symmetry of the bulk (Figure 2.3). Two isotropic Debye-Waller (DW) factors were also included: One for the Sn atom and one common for the Ge atoms. A least-square fit of this model gave $\chi^2 = 1.0$ with three Ge

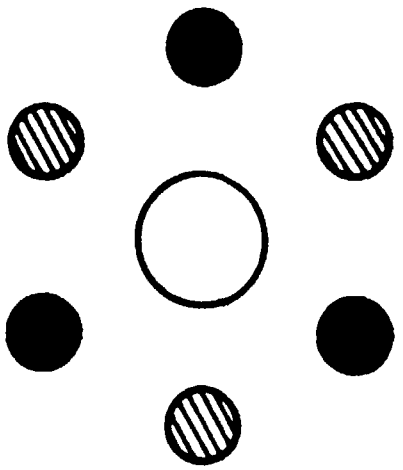

Figure 2.3: The atoms included in the final model. The adatom (open circle) is situated where three mirror lines cross. The hatched circles indicate three equivalent substrate atoms and the filled circles indicate three other equivalent atoms.

atoms displayed away from their ideal bulk position towards the Sn atom and three Ge atoms displaced outwards. The calculated structure factor intensities are displayed as $|F_{hk}{}^{mod}|^2$ in Table 2.2. The displacements and B-factors for this fit are listed in Table 2.3. The displacements are given in units of a = 4.000 Å, the length of the basis vectors of the 1×1 surface unit cell. The parameters a_1 and a_2 are the displacements of the inwards and outwards displaced Ge atoms, respectively. For Sn-1, a_1 is about twice as big as a_2. The model has in total 5 parameters and with only 13 observations, it has to be considered if the model is meaningful in a statistical as well as in a physical sense. A model with only three Ge atoms has a minimum χ^2 of 16, which demonstrates that this model is indequate. The physical relevance of the model is demonstrated by the analysis and discussion that follows.

For the sample Sn-2 the model with only one Sn atom gave $\chi^2 = 21$. Including three Ge atoms led to a significant improvement: $\chi^2 = 2.3$. A model with six Ge atoms and a DW-factor for the adatom gave a slightly better agreement: $\chi^2 = 2.1$ The parameters in Table 2.3 for the best fits for Sn-1 and Sn-2 are identical within the uncertainties.

From the good agreement of the best fits it can be concluded that the ordered area that contributes to the scattering has a coverage of 1/3 ML. The rest of the Sn must be disordered or have a structure, which is different from the $\sqrt{3}$-structure. The observed LEED pattern excludes all structures different from $\sqrt{3} \times \sqrt{3}$ and 1×1.

Table 2.3. The parameters from the best fits. Displayed are χ^2, displacements a_1 and a_2 in units of a = 4.000 Å and B-factors. The sign of a_1 and a_2 is negative for displacements towards the adatom. Uncertainties on the last digits are given in the parenthesis. A star indicates a fixed parameter.

	Sn-1	Sn-2	Pb-1	Pb-2
χ^2	1.0	2.1	0.93	1.2
a_1	-0.051(4)	-0.040(13)	0.039(7)	-0.027(10)
a_2	0.027(3)	0.013(11)	0.018(4)	0.0*
B(Ad)(Å^2)	3.0±0.5	1.8±1.6	3.2±0.6	0.0*
B(Ge)(Å^2)	0.6±0.2	0.0*	0.7±0.5	0.0*

Bulk B-factors: Ge B = 0.586 Å^2 a)
Sn (white) B = 1.07 Å^2 b)
Sn (grey) B = 0.431 Å^2 b)
Pb B = 2.54 Å^2 c)

a) (Batterman and Chipman (1962))

b) Calculated by the Debye temperature from specific heat (de Launay (1956))

c) (Chipman (1960))

In the analysis for the Pb-covered samples similar models as described above were applied. For the Pb-1 sample a model with one Pb atom and a DW-factor gave χ^2 = 9.3 and a model with one Pb atom with a DW-factor and three Ge atoms with a common DW-factor gave χ^2 = 3.4. The final model with one Pb atom, six Ge atoms and two DW-factors gave χ^2 = 0.93. The displacements, listed in Table 2.3, are slightly smaller than for the Sn-covered samples. For sample Pb-2 a model with one Pb-atom gave χ^2 = 3.7 and including three Ge atoms improved the agreement to χ^2 = 1.2. With this low value for χ^2 there was no need for further improvement of the model. The displacement of the inwards displaced Ge atoms for sample Pb-1 and Pb-2 agrees within the uncertainties. As for the Sn-covered samples, it can be concluded from the analysis that the coverage of the ordered areas are 1/3 ML. The analysis shows that the fits for the Sn-covered samples are considerably more sensitive than the Pb-covered samples to the inclusion of the Ge atoms. For the Pb-covered samples the major part of the scattering is from the large Z element Pb, whereas for the Sn-covered samples the Sn and Ge atoms have smaller differences in Z.

The B-factors of the adatoms, the Ge atoms and their bulk counterparts are displayed in Table 2.3. The values for the Sn adatoms are somewhat larger than the bulk values of white and grey tin. For Pb and Ge the values are in agreement with the bulk values.

2.4 Integer-Order Reflections and Registry

The analysis in this section is restricted to the samples Sn-1 and Pb-1. Only for these two samples are the number of measured integer-order (non-bulk) reflections sufficiently large to perform a reliable analysis. The measured in-plane integer-order structure factor intensities $|F_{hk}^{exp}|^2$ are displayed in Table 2.4. These reflections have two contributions: One from the Ge substrate, and another from the surface reconstruction. The substrate contribution F_{hk}^{bulk} is described by the structure factor (1-9) that gives the crystal truncation rods.

Table 2.4. Measured integer-order structure factors intensities $|F_{hk}^{exp}|^2$, uncertainties σ_{hk} and model structure factor intensities $|F_{hk}^{mod}|^2$.

		Ge(111)-Sn : Sn-1				Ge(111)-Pb : Pb-1			
		$\|F_{hk}^{exp}\|^2$	σ_{hk}	$\|F_{hk}^{mod}\|^2$		$\|F_{hk}^{exp}\|^2$	σ_{hk}	$\|F_{hk}^{mod}\|^2$	
h	k			$T_4(0^o)$	$T_4(180^o)$			$T_4(0^o)$	$T_4(180^o)$
1	0	93.7	20.0	63.5	64.9	176.0	40.0	169.6	171.0
2	0	31.5	12.6	35.0	39.0	136.0	30.0	89.6	93.5
2	1	29.5	1.9	24.7	28.7	72.9	8.4	55.9	60.2
3	1	14.0	0.9	11.1	16.3	32.4	3.7	22.4	27.7
4	0	11.3	0.7	11.4	14.6	24.7	6.0	17.8	21.7
3	2					19.0	5.5	11.8	15.9
				χ^2=4.3	5.8			χ^2=3.3	1.2

The surface contribution F_{hk}^{surf} is the structure factor determined by the analysis in the previous section and therefore the layers of the substrate that contain displaced Ge atoms must be included in this contribution. The resulting structure factor intensities $|F_{hk}^{mod}|^2$ are the absolute square of the coherent sum of the two contributions

$$|F_{hk}^{mod}|^2 = |F_{hk}^{surf} + 3.0\, F_{hk}^{bulk}|^2 \qquad (2\text{-}1)$$

The factor of 3.0 is due to the different size of unit cell area used in the calculation of the two parts of the structure factors. When the scale factor and the parameters for the surface layers are taken from the previous section, there are no adjustable parameters in (2-1) and the agreement can simply be found by calculating χ^2. For the registries with the adatoms on top of the Ge atoms of the first layer (T_1 site) or the second layer (T_4 site), two bilayers of the substrate are included in the surface contribution. For the H_3 site, where the adatom is in the center of the hexagon made up of the Ge atoms in the first bilayer of the substrate, only this bilayer is included. Finally, the substrate can be turned 180° with respect to the $\sqrt{3}$-unit cell, giving a total of six possibilities.

In agreement with the conclusions for Ge(111)$\sqrt{3}\times\sqrt{3}$-Pb by Feidenhans'l et al. (1986), it was found that the adatoms are occupying the T_4 sites. However, it was not possible to distinguish between the two orientations relative to the Ge substrate. The calculated structure factor intensities for the T_4 site are displayed in Table 2.4. The agreements for the sample Sn-1 are $\chi^2 = 4.3$ and 5.8 and for the sample Pb-1 $\chi^2 = 1.2$ and 3.3. The other possibilities give χ^2 in excess of 11. That χ^2 is larger than one for the best agreements can be due to the presence of additional systematic errors for these reflections. The surface contribution could be affected by regions with a 1×1 structure, either due to missing adatoms or due to adatoms in a 1×1 pattern. The substrate contribution could be influenced by surface roughness or Sn migration.

2.5 Rodscans and the Structure in the Direction Normal to the Surface

The measured intensity profiles (rodscans) for the samples Sn-1 and Pb-1 are shown in Figure 2.4. and displayed in Appendix C. The rodscans for the two samples display a pronounced and quite similar intensity variation, demonstrating that the atomic geometry is similar for the Sn- and Pb-induced reconstructions. However, the variation is weakest for the Pb- covered sample, because of the dominant contribution from the Pb atoms. The period of the variation is approximately 0.5 times the (111) vector indicating an extent of the reconstruction of about 6.5 Å, i.e. down to the fourth layer of Ge (Figure 2.1).

The first model, that was tried, included only the adatoms and the Ge atoms that were found to be relaxed in the in-plane analysis. The DW-factors and relaxations were fixed at the values found in the in-plane analysis. In the least-square fits only the distances normal to the surface were allowed to vary. The agreements are $\chi^2 = 12.4$ for Sn-1 and $\chi^2 = 1.4$ for Pb-1. The distances normal to the surface from the adatom to the inwards displaced Ge atoms are 2.11 ± 0.13 Å and 1.81 ± 0.23 Å for the Sn-1 and Pb-1 samples, respectively. The distances from inwards to the outwards displaced Ge atoms are 4.7 ± 0.7 Å for both samples. For an ideal unrelaxed Ge(111) surface the distance from the first layer to the fourth layer atoms is 4.08 Å. Therefore, is can be concluded that the inwards displaced Ge atoms belong to the first layer and the outwards displaced Ge atoms to the fourth layer of the substrate.

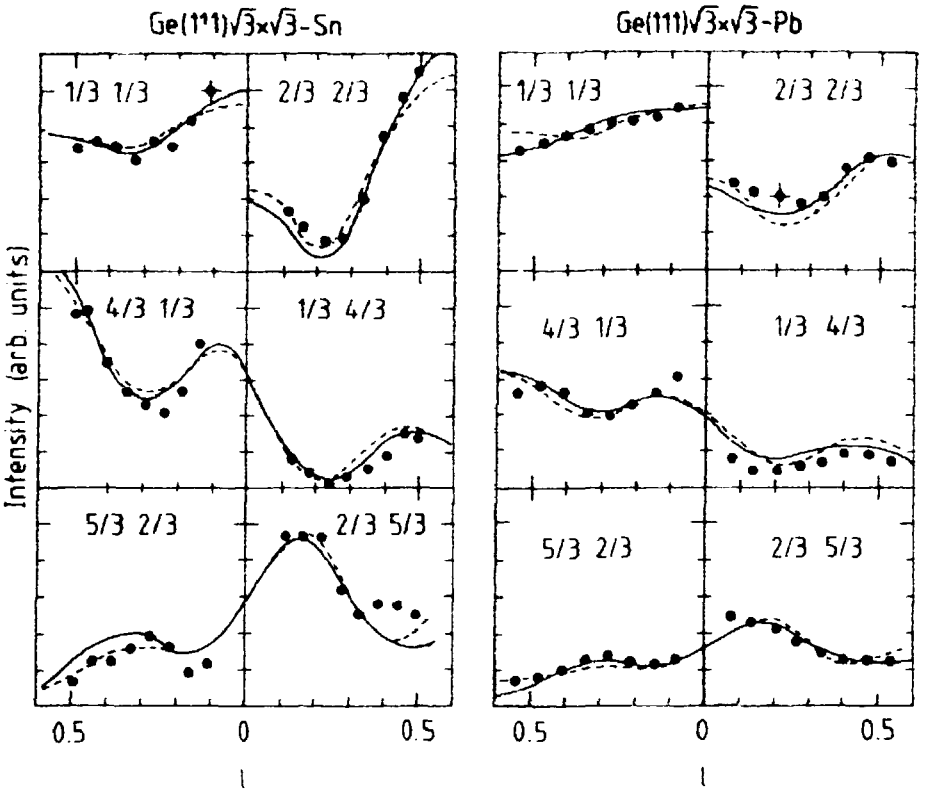

Figure 2.4: Intensity profile of fractional-order reflections. The points indicate the measured intensity and the full curve is the calculated intensity from the data analysis. The broken curve is calculated from the structure found by a Keating model for the elastic strain. l is the momentum transfer in the direction normal to the surface in units of the bulk (111) reciprocal vector.

In the next step the second and third layer of Ge atoms were included, i.e. the model contained all the atoms shown in the right-hand side of Figure 2.1. The first optimization of this model showed that the number of parameters are large compared to the experimental information in the rod scans and that the fits are not very sensitive to the positions of the atoms that are only displaced normal to the surface. To overcome these two problems the distances from the Ge atoms 2' to 3' and 2 to 3 (Figure 2.1) were fixed at the bulk value 2.450 Å. This is a reasonable restriction, considering the elastic properties of Ge (Keating (1966), Martin (1970) and Steif et al. (1987)). The deformation of bond angles costs relatively less energy than deformation of bond length. This point is discussed further in appendix A. The optimized model, having 13 atoms and 5 parameters, gave the agreements $\chi^2 = 4.9$ and 1.3 for the samples Sn-1 and Pb-2, respectively. Finally, the DW-factors were allowed to vary which gave the agreement $\chi^2 = 4.1$ for the Sn-covered sample and $\chi^2 = 0.8$ for the Pb-covered. The relatively large value of χ^2 for the Sn-covered samples is probably due to the introduction of additional systematic errors for the out-of-plane measurements. The calculated rodscans for the model are displayed as full curves in figure 2.4, which shows good agreements between experimental and model structure

factor intensities. That means that the chemisorption sites determined in the previous section are independently confirmed by this analysis. The B-factor for the sample Sn-1 are B(Sn) = 1.4 ± 0.7 Å^2 and B(Ge) = 3.8 ± 1.6 Å^2. Those for Pb-1 are B(Pb) = 4.9 ± 0.7 Å^2 and B(Ge) = 2.0 ± 1.7 Å^2.

The distance from the Sn atom to the Ge atoms in the first layer is d_1 = 2.75 ± 0.08 Å and the distance between the Sn atom and the Ge atom just below it is d_2 = 2.67 ± 0.23 Å. These are slightly larger than the sum of the covalent radii, 2.62 Å (Pauling (1948)). The same distances for the Pb-covered sample are d_1 = 2.72 ± 0.08 and d_2 = 2.59 ± 0.98 Å, compared to the sum of the covalent radii, 2.68 Å. The major part of the uncertainties of the bond lengths is due to the relatively large uncertainties of the distances in the direction normal to the surface. The rest of the bond lengths are for both samples close to the bulk value with relatively large uncertainties. The distances normal to the surface are listed in Table 2.5. The large uncertainties are due to the limited t-range in the present experiments and can be improved by further studies.

Table 2.5. Distances normal to the surface found by the rodscan fits. All distances are in Å and the notation from Figure 2.1 has been used.

Distances between	Ge(111)-Sn	Ge(111)-Pb
Adatom-1	1.72 ±0.13	1.72 ±0.13
Adatom-2'	2.68 ±0.23	2.59 ±0.98
Adatom-3'	5.13 ±0.23	5.04 ±0.98
Adatom-2	2.10 ±0.29	2.44 ±1.20
Adatom-3	4.55 ±0.29	4.89 ±1.20
Adatom 4	6.07 ±0.28	6.37 ±0.42
1-4*)	4.35 ±0.31	4.65 ±0.44

*) Bulk value 4.083 Å

The directions of the relaxations are indicated by arrows in Figure 2.1, and they can be understood as elastic relaxations imposed by the bonding of the adatoms. The Ge atoms of the first layer, labelled 1 in Figure 2.1, are forced inwards by the bonding to the adatom. This forces the atoms 2' and 3' down and the atoms 2 and 3 up. The atoms 3' and 3 push the atoms 4 outwards relative to the atom 3'. The in-plane projected relaxations of the atoms (1) in the first layer are about twice as big as the relaxations of the atoms in the fourth layer (4). The atomic relaxations are elucidated further in the next section by means of model calculations.

2.6 Elastic Strain Calculations by the Keating Model

In 1966 Keating introduced a new model for the elastic energy of a solid in order to explain the bulk elastic properties of covalent crystals. The model has one term describing bond length deformation and another describing mainly bond bending. Later the model has been widely used to investigate atomic relaxations for reconstructions on semiconductor surfaces. In this section a modified version of the Keating model, allowing investigations of structures containing more than one kind of atoms, is introduced. The model is discussed in detail in Appendix A, where the choice of parameters and a comparison with the results from ab-initio total-energy calculations is given. The elastic energy E is described by the expression:

$$E = \alpha \sum_{\substack{\text{all}\\ \text{bonds}}} \left[\vec{x}_{ij}^{\,2} - (b_i + b_j)^2 \right]^2 + \beta \sum_{\substack{\text{all}\\ \text{bond}\\ \text{angles}}} \left[\vec{x}_{ij} \cdot \vec{x}_{ik} + 1/3(b_i + b_j)(b_i + b_k) \right]^2 \qquad (2\text{-}2)$$

where $\vec{x}_{ij}$ is the vector from atom i to atom j, b_i is the covalent radius of atom i and α and β are the parameters which describe the energy cost of bond-length and bond-angle deformation, respectively. The factor 1/3 ensures tetrahedral equilibrium bond angles of 109.47°. The elastic parameters are $\alpha = 0.164$ eV/Å^4 and $\beta/\alpha = 0.10$ for Ge (Steif et al. (1987) and Appendix A). In equation (2-2) these values are used for all bonds and the equilibrium bond angle configurations are assumed to be tetrahedral for all atoms. In Appendix A it is demonstrated that this gives good agreement with total-energy calculations.

The calculations need as input a specific model, i.e. it must be defined which atoms are bonded to each other. Periodic boundary conditions are applied in the direction parallel to the surface. Normal to the surface, a double layer of atoms fixed at bulk positions is used as the boundary between the surface reconstruction and the bulk. To ensure that the boundary has no influence on the relaxation in the surface reconstruction the boundary is moved further and further into the crystal until no significant relaxations are observed in the deepest relaxed layer.

Table 2.6 shows the relaxations for the α-phase of the Ge(111)$\sqrt{3}\times\sqrt{3}$-Sn surface as a function of number of bilayers relaxed. The radial relaxations a_1, a_2 and a_3 of the atoms of the first, fourth and fifth layer, respectively, are displayed. The table also shows the distances d_1 from the adatom to the Ge atoms in the first layer and d_2 from the adatom to the Ge atom just below. All distances are in units of a = 4.000 Å, the length of the basis

vector of the 1 × 1 surface unit cell. The atomic positions that minimize the energy are obtained when three double layers are relaxed. For four double layers the relaxations in the fourth layer are negligible. Therefore only three double layers are relaxed in the rest of the calculations.

Table 2.6. In-plane relaxations for the α-phase of the Ge(111)$\sqrt{3}\times\sqrt{3}$-Sn as a function of n, the number of bilayers relaxed. All distances are in units of a = 4.000 Å. The strain energy E is per 1×1 surface area.

n	E(eV)	a_1	a_2	a_3	d_1	d_2
0	0.786	-	-	-	0.657	0.518
1	0.733	-0.0217	-	-	0.654	0.586
2	0.680	-0.0356	0.0156	-	0.653	0.646
3	0.679	-0.0358	0.0161	0.0051	0.653	0.647
4	0.679	-0.0358	0.0161	0.0052	0.653	0.647

Sum of covalent radii: 0.658

Table 2.7. The in-plane relaxations for the α-phase of the Ge(111)$\sqrt{3}\times\sqrt{3}$-Sn and Ge(111)$\sqrt{3}\times\sqrt{3}$-Pb structures from experiment (sample Sn-1 and Pb-1) and from Keating calculations. The relaxations are in units of a = 4.000 Å.

	Sn		Pb	
	exp.	model	exp.	model
a_1	-0.051(4)	-0.036	-0.040(7)	-0.034
a_2	0.027(3)	0.016	0.017(4)	0.016
a_3		0.005		0.005
a_4		0.004		0.004

Table 2.7 contains the in-plane relaxations for the $\sqrt{3}$-structure of Sn and Pb on Ge(111) from experiment (sample Sn-1 and Pb-1) and from Keating calculations. The sign and magnitude of the observed relaxations are reproduced by the calculation. The calculated relaxations are slightly larger for the Sn-covered surface which is also found experimentally. The relaxations in the fifth a_3 and the sixth layer a_4 cannot be resolved in the experiments.

The distances normal to the surface for the two surfaces are displayed in Table 2.8. The experimental values are those found from the analysis of the rodscans. The table also contains the distances d_1 and d_2 from the adatoms to the nearest neighbours. There is good agreement between experimental and model values and it can be concluded that the Keating calculations can give a reliable prediction of the atomic relaxations for the model.

Table 2.8. Distances normal to the surface from experiment (sample Sn-1 and Pb-1) and from Keating calculations. Also shown are the distances, d_1 and d_2, from the adatom to the nearest neighbours. Distances are in units of $a = 4.000$ Å.

	Sn		Pb	
Distance between	exp.	model	exp.	model
Adatom-1	0.43(3)	0.37	0.43(3)	0.38
Adatom-2'	0.67(6)	0.65	0.65(25)	0.66
Adatom-3'	1.28(6)	1.24	1.26(25)	1.26
Adatom-2	0.53(7)	0.53	0.61(30)	0.55
Adatom-3	1.14(7)	1.15	1.22(30)	1.17
Adatom-4	1.52(8)	1.38	1.59(11)	1.40
1 - 4	1.09(8)	1.01	1.16(11)	1.01
d_1	0.69(2)	0.65	0.69(2)	0.66
d_2	0.67(6)	0.65	0.65(25)	0.67
Sum of co-valent radii	0.66		0.67	

The final comparison between experiment and calculation is done by calculating the rodscans of the optimized structures. The broken curves in Figure 2.4 are obtained by least-square fitting the scale factor and two DW-factors. The agreements are for the Sn-covered sample $\chi^2 = 3.4$ and the Pb-covered $\chi^2 = 1.0$, compared to, respectively, $\chi^2 = 4.1$ and $\chi^2 = 0.8$, which were found for the models in the previous section. The lower value of χ^2 for the Sn- covered sample found for the structure from the Keating calculations is mainly due to the smaller number of fit parameters for this model (equation 1-26).

2.7 Discussion and Conclusions

All ab-initio total-energy calculations on the α-phase of the $\sqrt{3}\times\sqrt{3}$ adatom-induced reconstructions published to date are for the Si(111) surface. The first calculation was for the Al-induced reconstruction (Northrup (1984)). When only the height of the Al atom above the surface is optimized it is found that the H_3 site is 0.34 eV/adatom lower in energy than the T_4 site. However, optimization of the positions of the Si atoms in the first three layers of the substrate favours the T_4 site by 0.29 eV/adatom. This demonstrates clearly the importance of subsurface relaxations. Table 2.9 contains a compilation of the results from total-energy calculations on the Si(111)$\sqrt{3}\times\sqrt{3}$-M reconstruction (M = Al, Ga, In, Si and Ge) (Northrup (1984,1986), Nicholls et al. (1985b,1987), Zhang et al. (1985)). The difference in energy per adatom between the H_3 and T_4 site shows that the T_4 is the most favourable for all the adatoms investigated, when substrate relaxations are allowed. The distances for the T_4 site between the adatom and the Si atoms in the first layer (d_1) and

Table 2.9. $\Delta E = E(H_3) - E(T_4)$ the energy difference per adatom between the H_3 and T_4 chemisorption sites for the Si(111)$\sqrt{3}\times\sqrt{3}$-M surface. For M = Al labelled with a star no substrate relaxations were included. The distance d_1 and d_2 are for the T_4 site. d_1 is the distance from the adatom to the first layer Si atoms, and d_2 is the distance from the adatom to the second layer Si atom just below it. The bond length b is calculated as the sum of the covalent radii.

M:	Al*,[a]	Al[a]	Ga[d]	In[c]	Si[b]	Ge[e]
ΔE(eV)	-0.34	0.29	0.38	0.2	0.64	0.6
d_1(Å)	-	2.50		2.63	2.49	2.50
d_2(Å)	-	2.45		2.59	2.49	2.45
b (Å)	2.43	2.43	2.43	2.61	2.34	2.39

References:
a) Northrup (1984)
b) Northrup (1986)
c) Nicholls et al. (1985b)
d) Nicholls et al. (1987)
e) Zhang et al. (1985)

between the adatom and the second layer Si atom below the adatom (d_2) are also displayed. They are in general slightly larger than the sum of the covalent radii. This agrees with the experimental results for the Sn- and Pb-induced reconstructions on the Ge(111) surface.

The atomic relaxation found by Northrup (1986) for Si(111)$\sqrt{3}\times\sqrt{3}$-Si can be compared to the experimental results. The outer three layers of the Si substrate are relaxed in the calculation and the directions of the relaxations agree with the experimental results for the Sn-and Pb-induced reconstructions on the Ge(111) surface. To make a quantitative comparison easier the relaxations for the Si surface quoted below are given in units of the length of the basis vector of the 1×1 surface unit cell, a = 3.840 Å. For the Si surface the radial displacement of the atoms in the first layer is -0.039 compared to the values -0.051 ± 0.004 for the sample Sn-1 and -0.040 ± 0.007 for the sample Pb-1. The average displacements of the atoms 2' and 3' relative to the atoms 2 and 3 (Figure 2.1), found in the calculation for the Si surface, is 0.104. The experimental values are 0.14 ± 0.09 for the Sn-1 sample and 0.04 ± 0.39 for the Pb-1 sample. The radial displacements agree very well, but the displacements normal to the surface are difficult to evaluate due to the large experimental uncertainties.

Vanderbilt (1987d) has performed a total-energy calculation for a Si(111) surface with Si adatoms at T_4 sites in a 2×2 arrangement. All atoms in a slab with inversion symmetry containing four double layers were relaxed. The bonding geometry near the adatoms are the same for the 2×2 unit cell as for the $\sqrt{3}\times\sqrt{3}$ unit cell. The displacement parallel to the surface of the atoms bonded to the adatoms are -0.027. This forces the second layer atom below the adatom and the third layer atom below this one downwards (see Figure 2.1). As a result the fourth layer atoms bonded to the downwards displaced third layer atom are displaced outwards by 0.012. These displacements and their relative magnitude agree very well with the observed relaxations for the Sn- and Pb-induced Ge(111)$\sqrt{3}\times\sqrt{3}$ structures.

An x-ray photoelectron diffraction study of the Ge(111)$\sqrt{3}\times\sqrt{3}$-Sn surface led Sakurai et al. (1983) to propose a triplet model. However, the agreement between experimental and calculated diffraction pattern was poor and far from the level of agreement found for the Si(111)$\sqrt{3}\times\sqrt{3}$-Ga (Higashima et al. (1986)) and the Si(111)$\sqrt{3}\times\sqrt{3}$-Sn surfaces (Higashima et al. (1987)). The agreement of the triplet model with the x-ray diffraction results presented in this thesis has been tested and led to rejection of the model.

In conclusion, the results of the x-ray study of the α-phase of the Ge(111)$\sqrt{3}\times\sqrt{3}$-Sn and the Ge(111)$\sqrt{3}\times\sqrt{3}$-Pb reconstructions provide unambigious experimental evidence for the T_4 chemisorption site. This should stimulate theoretical work on these structures. The experimentally determined subsurface relaxations are similar to those found in previous theoretical works and from the Keating calculations. The present work demonstrates the great sensitivity of surface x-ray diffraction to small displacements of atoms from bulk positions. The results also demonstrate that information about the atomic geometry normal to the surface can be obtained from the measurements of the intensity variations along Bragg rods.

3. THE STRUCTURE OF THE Ge(111)5 × 5-Sn AND Ge(111)7 × 7-Sn SURFACES

3.1 Introduction

The Ge(111) surface exhibits 5×5 and 7×7 reconstructions after deposition of submonolayer coverages of Sn. The similarity of these structures with the Si(111)7×7 reconstruction was already recognized in 1978 by Ichikawa and Ino, when the Sn-induced structures were observed for the first time. Information on the Sn-induced reconstructions is important in order to gain a complete theoretical understanding of the principles underlying the 5×5, 7×7 and c(2×8) reconstructions on the Si(111) and Ge(111) surfaces. A structural investigation has to reveal the role of the Sn atoms in the reconstructions. This means that Sn atoms must be identified and the positions of all atoms in the surface unit cell have to be determined accurately. X-ray scattering experiments are well-suited for tackling this problem because the stronger scattering of x-rays from Sn atoms than from Ge atoms enables the location of the Sn atoms to be determined uniquely. Since the number of parameters needed to describe the atomic geometry of these structures is quite large the intensity of a considerable number of reflections has to be measured. A reliable least-squares optimization of a model requires that the number of non-equivalent reflections measured is about three to five times larger than the number of parameters to be optimized.

Measurements of the in-plane intensity of the fractional-order reflections have been performed for one sample with a 5×5 reconstruction and three samples with 7×7 reconstructions. The analysis of these data sets are described below. The in-plane projected structures are determined, including the positions of the Sn atoms. The atomic displacements are compared to the results of Keating calculations, tight-binding calculations (Qian and Chadi (1987a,c)) and experiments on the Si(111)7×7 surface (Robinson et al. (1988)). Finally, the total-energy of the surfaces is discussed.

3.2 Experimental

The samples were prepared and characterized at the Flipper II beamline in HASYLAB. The Ge(111) substrates were cleaned, by cycles of sputtering and annealing, as described in Section 2.2. Sn was evaporated onto the Ge substrates at 250-300°C. The coverages were estimated by a quartz crystal thickness monitor and core-level photoemission intensities. The estimated coverages are listed in Table 3.1 together with other important experimental parameters. The three samples with 7×7 reconstructions are labelled no. 1,

no. 3, respectively. After the deposition of the Sn the samples were annealed at 500°C for a few minutes and then cooled slowly to room temperature. The samples were characterized by LEED and photoemission before being transferred to a smaller UHV chamber for the x-ray diffraction experiment.

Table 3.1. Experimental parameters for the Ge(111)5 × 5-Sn and Ge(111)7 × 7-Sn samples. Estimated coverage θ, angle of incidence α_i, x-ray wavelength λ, reproducibility of symmetry-equivalent reflections ε, the total number of reflections measured and number of independent reflections, N^{Tot} and N^{Ind}, respectively.

	5×5	7×7		
		no. 1	no. 2	no. 3
θ(ML)	0.7	0.5	0.4	0.3
α_i	0.275°	0.265°	0.165°	0.270°
λ(Å)	1.344	1.365	1.343	1.343
ε	0.10	0.10	0.11	0.05
N^{Tot}	163	121	260	360
N^{Ind}	115	90	180	269

During the data collection at the diffractometer at the Wiggler beamline W1 a standard reflection was measured regularly to check for possible sample deterioration. Typically data collection lasted for 3-4 days and only in the case of 7 × 7 sample no. 2 was a decrease of the standard reflection observed. The intensity of the (1,3/7) reflection decreased to 60% of the original value during this measurement. The only possible way to correct for this effect is to scale the measured reflections according to the descrease in intensity of the standard reflection. This corresponds to assuming that the decrease in intensity is due to a decrease in the area of the ordered 7 × 7 structure and not due to a change of the structure.

The structure factor intensities are obtained after correcting the measured intensities for the Lorentz factor and for the active sample area. The reproducibility, ε in Table 3.1, is calculated from the symmetry-equivalent reflections as described in Section 1.4 and the uncertainties of the structure factor intensities are calculated from ε and the counting statistics. For the 5 × 5 sample a total of 115 independent reflections with a reproducibility of 0.10 are available. For the best 7 × 7 sample (no. 3), which has a reproducibility of 0.05, 269 independent reflections were recorded. The structure factor intensities $|F_{hk}^{exp}|^2$ and their uncertainties σ_{hk} are listed in Appendix D for the 5 × 5 sample and in Appendix E for the 7 × 7 samples.

3.3 Analysis

The structure factor intensities were used to construct contour maps of the Patterson function (equation I-25) shown in Figure 3.1. Only the positive contours in the irreducible unit have been drawn (see Figure 3.2). The Patterson function of the Si(111)7 × 7 surface is shown for comparison (Robinson et al. (1988)). The plots for the 7 × 7 structures are quite similar with the sharpest peaks for sample no. 3, which has the largest number of reflections. For sample no. 2 the map is noisy and it is somewhat different from the other especially at short distances.

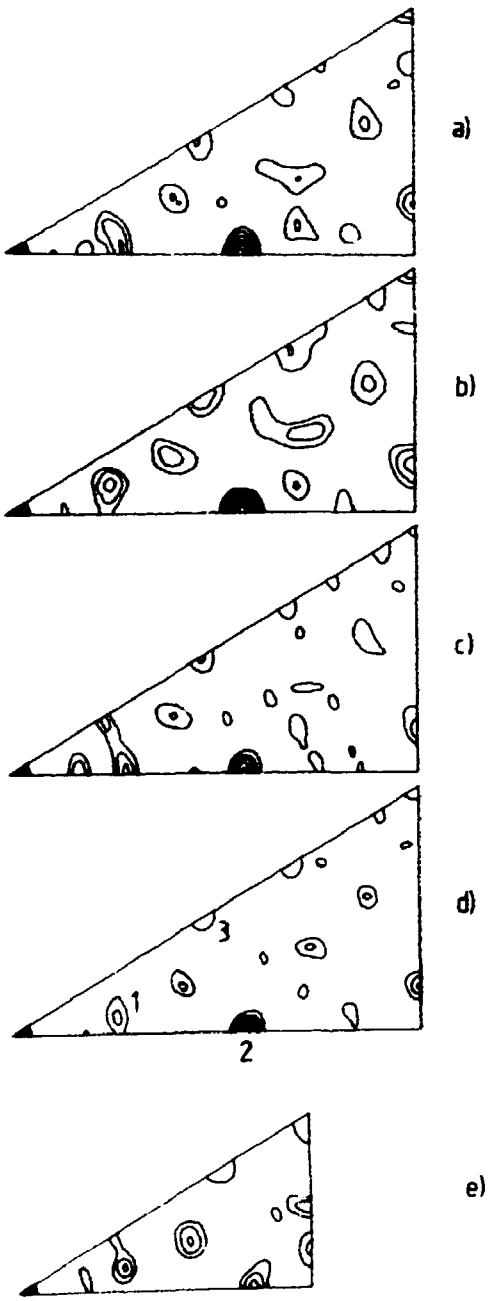

Fig. 3.1: Plots of the positive contours in the irreducible unit of the Patterson functions. a): The Si(111)7 × 7 surface (Robinson et al. (1988)). b, c and d): The Ge(111)7 × 7 – Sn samples no. 1, 2 and 3, respectively. e): The Ge(111)5 × 5-Sn reconstruction.

The strongest peaks are at nearly identical positions in all five maps. The peaks in the Patterson function correspond to inter-atomic vectors in the unit cell and the similarities suggest that the structural models are the same. The similarity of the Patterson functions for the 5 × 5 and 7 × 7 structure shows that the local atomic arrangement are the same. The structure of the Si(111)7 × 7 surface was first solved by Takayanagi et al. (1985a,b) by transmission electron diffraction (TED). By a detailed analysis of the Patterson map the Dimer-Adatom-Stacking-fault (DAS) model shown in Figure 3.2.a was deduced. The Patterson map from the TED experiment is nearly identical to those from x-ray diffraction shown in Figure 3.1. The peak labelled 2 in Figure 3.1.d is the strongest and it correspond to the adatom-adatom separation. The peak labelled 1 is due to the dimers and the peak labelled 3 has contributions from the stacking fault. A detailed analysis of the Patterson function will not be given here and the 7 × 7 DAS model will simply be taken as the starting point for the structure factor analysis. The ingredients of the DAS model can be combined to form reconstructions with $(2n+1) \times (2n+1)$ unit cells. The structure with 5 × 5 and 7 × 7 unit cells are shown in Figure 3.2. The similarities between the plot of the Patterson function for the 5 × 5 and 7 × 7 structure demonstrate that the reconstructions have many interatomic vectors in common. Therefore the 5 × 5 DAS model is chosen as the starting point for the analysis of the Sn-induced 5 × 5 reconstruction.

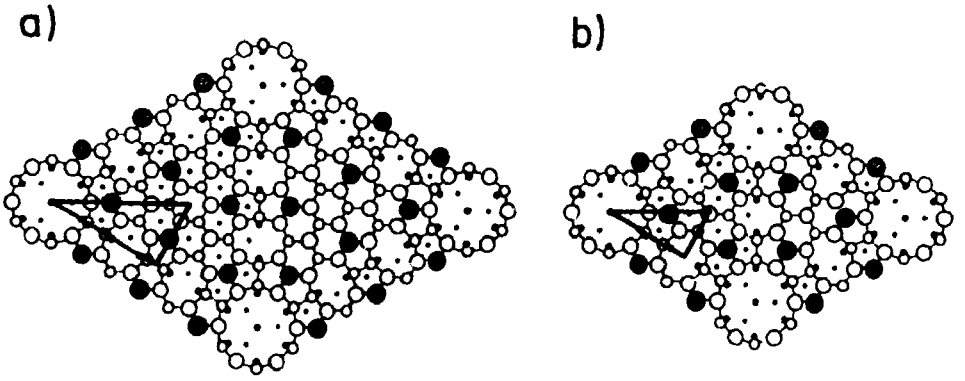

Figure 3.2: The Dimer-Adatom-Stacking-fault (DAS) model. (a): 7 × 7 and (b): 5 × 5. The adatoms are shaded and the irreducible unit of the Patterson function is shown as triangles.

The independent atoms in the top layers of the 7 × 7 and 5 × 5 DAS models are shown in Figure 3.3. The large circles indicate adatoms, medium and small circles indicate first and second layer atoms, respectively. The rest of the atoms in the unit cell can be generated by reflections in the bulk mirror lines shown as broken lines in the figure. The top layers of the DAS models have an extra mirror line indicated by a dashed-dotted line in the figure. The adatoms and the first bilayer of atoms of the ideal model have 6 mm symmetry in contrast to the bulk which has only 3 m symmetry.

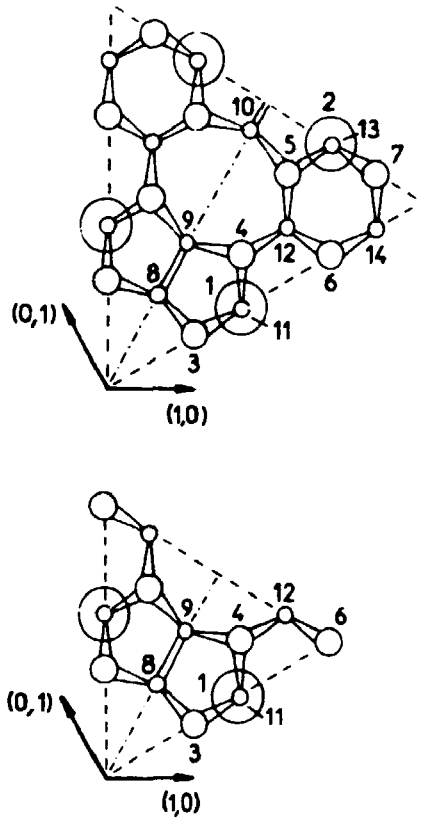

Figure 3.3: The independent atoms in the top layers of the 7×7 (upper part) and 5×5 (lower part) DAS models. The broken lines are mirror lines for the bulk and the dashed-dotted line is an approximate mirror line in the top layers of the DAS model. A labelling of the atoms is shown.

In the least-squares analysis of the Ge(111)-Sn reconstructions the DAS models with 6 mm symmetry were the first models to be tested. All atoms were taken to be Ge with a common isotropic Debye-Waller (DW) factor. Only the positions of the dimer atoms labeled 8, 9 and 10 in Figure 3.3 were allowed to vary and the rest of the atoms were fixed at their ideal positions. For the Ge(111)7×7-Sn data sets no. 1, 2 and 3 the least-squares residuals were, respectively, χ^2 = 7.8, 7.0 and 8.0. The fit for the Ge(111)5×5-Sn data gave χ^2 = 10.7.

After each fit an error synthesis according to equation (1-33) was performed. Figure 3.4 shows plots of the positive contours in the electron density difference $\Delta\rho$ for the 7×7 data set no. 3 and for the 5×5 data set. The figure shows that the model should have more electron density at the positions of the adatoms. The error synthesis for the data set no. 1 was similar. However, for data set no. 2 the contour plot was flat and noisy. Sample no. 2 decayed with time so this data set is somewhat unreliable.

Inspired by the error synthesis the electron density of the adatoms was allowed to vary in the next models. For the 7×7 data set no. 1 and 3 and the 5×5 data set this was done by taken the adatoms to be Sn and multiplying the form factor f_{Sn} by a fitting parameter. The form factors are proportional to the atomic charge Z and have almost the same dependence of the scattering vector Q. Therefore, varying the form-factor of the adatoms corresponds

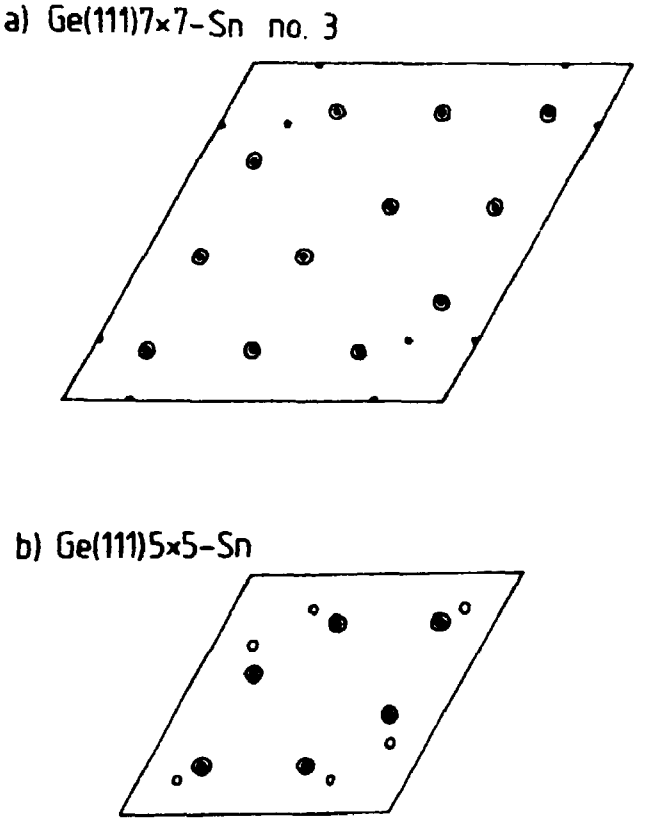

Figure 3.4: Plots of the positive contours of the electron density difference $\Delta\rho$ (Equation 1-33) for the 7×7 data set no. 3 (a) and the 5×5 data set (b).

to fitting the charge of the adatoms. The model had a DW-factor for the adatoms and another for the Ge atoms. The atoms in the model were allowed to relax according to the 6 mm symmetry. For the 7×7 data sets it was not possible to separate the displacements of the adatoms and the atoms just below them. These atoms have nearly coincident in-plane positions and they cannot be distinguished in the fits of the in-plane projected models. Therefore the atoms below the adatoms were fixed at their ideal positions. The results of the fits are displayed in Table 3.2 together with the results for Si(111)7×7 by Robinson et al. (1988). For the 7×7 data set no. 2 the form factor of the adatoms was taken as the form factor of Ge multiplied by a fit parameter. This choice was made due to the lower electron density of the adatoms for this surface, as indicated by the error synthesis. This model had $\chi^2 = 3.7$ for an electronic charge of the adatoms which was only 0.78 ± 0.08 times the charge of the Ge atoms in the deeper layers. An error synthesis showed that the adatom labelled 1 in Figure 3.3 had more electronic charge and therefore the atomic charge of the two adatoms were fitted independently. The results for the fit of this model for the data set no. 2 are displayed in Table 3.2. This model did not give significant improvements for the data sets no. 1 and 3.

Table 3.2. The results from the fits of the 6 mm DAS model. The labels of the atoms refers to Figure 3.3. The absolute displacements are given by multiplying by a = 4.000 Å for the Ge structures and a = 3.840 Å for the Si structure. The results for the Si(111)7×7 surface is from Robinson et al. (1988). The form factors f_{Ad} for the adatoms and the B-factors are also displayed. The numbers in parentheses after the displacements are the uncertainties on the last digits. A star indicates a parameter fixed by symmetry. Two stars indicate parameters that have been fixed in the least-square fit.

			Ge(111)7×7-Sn			
		Ge(111)5×5-Sn	no.1	no.2	no.3	Si(111)7×7
Atom	Displacement vector	χ^2 = 5.1	χ^2 = 2.7	χ^2 = 3.4	χ^2 = 3.6	χ^2 = 1.9
1	1/√3(2,1)	0.031(5)	0.017(5)	0.033(10)	0.020(4)	
11	"	-0.010(10)	0.0**	0.0**	0.0**	-0.007(3)
2	1/√3(1,1̄)	-	0.026(5)	0.048(14)	0.018(4)	
13	"	-	0.0**	0.0**	0.0**	-0.005(3)
3	1/√3(2,1)	0.028(4)	0.025(7)	0.023(5)	0.041(6)	0.031(9)
4	(1,1),1/√3(1,1̄)	-0.023(3),-0.001(1)	-0.029(6), 0.013(5)	-0.023(4),-0.010(3)	-0.025(4),-0.012(4)	-0.029(8), 0.007(12)
5	" " "	-	0.010(4), 0.004(3)	0.020(3) -0.007(3)	0.028(4),-0.002(4)	0.030(7),-0.003(12)
6	1/√3(2,1)	0.0*	-0.041(7)	-0.016(5)	-0.006(6)	-0.016(9)
7	1/√3(1,1)	-	0.005(7)	-0.001(5)	0.000(5)	0.033(9)
8	(1,1)	0.163(4)	0.179(7)	0.168(5)	0.147(5)	0.151(8)
9	(1,1)	-0.180(4)	-0.176(7)	-0.180(5)	-0.172(5)	-0.195(8)
10	(1,1)	-	0.179(7)	0.169(5)	0.175(5)	0.178(8)
12	(1,1),1/√3(1,1̄)	0.0*, -0.004(5)	-0.011(5), 0.001(5)	-0.003(3),-0.012(4)	-0.011(4), 0.004(4)	0.015(6),-0.014(10)
14	1/√3(2,1)	-	-0.035(7)	-0.007(5)	-0.043(6)	-0.007(7)
		B_{Ad}=1.6±0.7 Å^2 B_{Ge}=1.7±0.1 Å^2 f_{Ad}=0.86±0.05 f_{Sn}	B_{Ad}=0.2±0.6 Å^2 B_{Ge}=2.5±0.6 Å^2 f_{Ad}=0.81±0.04 f_{Sn}	B_{Ad}=5.4±1.6 Å^2 B_{Ge}=0.52±0.25 Å^2 $f_{Ad}(1)$=0.84±0.08f_{Sn} $f_{Ad}(2)$=0.53±0.07f_{Sn}	B_{Ad}=2.0±0.3 Å2 B_{Ge}=1.2±0.2 Å^2 f_{Ad}=0.97±0.04 f_{Sn}	B_{Ad}=1.5±0.6 Å^2 B_{3-7}=1.5±0.6Å^2 B_{8-14}=0.0±0.4Å^2

The least-square fits of the models have values of χ^2 which are more than a factor of two lower than that of the starting models. A comparison of the atomic displacements in Table 3.2 shows that the three structures, Ge(111)5×5-Sn, Ge(111)7×7-Sn and Si(111)7×7 have nearly the same atomic displacements. The agreement between the two most reliable data sets no. 1 and 3 for the Ge(111)7×7-Sn reconstruction demonstrates satisfactory reproducibility.

As indicated by the error synthesis performed on the starting models the adatoms are found to have charges that are larger than the charges of the deeper atoms. For the 7×7 data set no. 3 the adatom positions are all occupied by Sn atoms. For the other data sets the charges determined for the adatoms are smaller. However, the analysis does not give the absolute charge, but only the charge relative to the atoms in the deeper layers. The observed reduction of the adatom charge relative to a full occupation of the adatom sites by Sn can be caused by the following effects: 1) Missing adatoms. 2) Some Ge adatoms 3) Sn substitution in the layers below the adatoms. The result for the data set no. 3 can

only occur when no Sn substitution is present in the layers below the adatoms and when all adatom positions are occupied by Sn atoms. For sample no. 2, which decayed during the data collection, the adatom charges are quite small. This could mean that impurities attack the adatoms. The stacking fault and the dimers seems to be unaffected. For the data set no. 1 the adatom charge corresponds to an 81% ± 4% occupation of the adatoms sites by Sn, assuming that the deeper atoms are Ge. However, the B-factor for the adatom is unrealistically small compared with the B-factor of the deeper atoms. This is probably due to the correlation in the model between the adatom charge and the B-factor. A first-order expansion of the Debye-Waller factor gives: $\exp(-BQ^2/(4\pi)^2) = 1 - BQ^2/(4\pi)^2$. The data set no. 1 contains a limited number of reflections with relatively small scattering vectors Q and therefore the adatom charge is correlated with the B-factor. The occupation of 81% ± 4% can be considered as a lower estimate for this sample. The data set for the 5×5 reconstruction gives an adatom charge corresponding to an Sn occupation of 86% ± 5% of the adatom sites, under the assumption that the atoms in the layers below the adatoms are Ge.

Figure 3.5 shows a graphical presentation of the atomic displacements for the Ge(111)7×7-Sn data set no. 3 and the Ge(111)5×5-Sn data set. The displacements are shown as arrows and have been multiplied by ten except for the dimer atoms, which are shown at their actual positions. The main features in the displacement patterns are net inward displace-

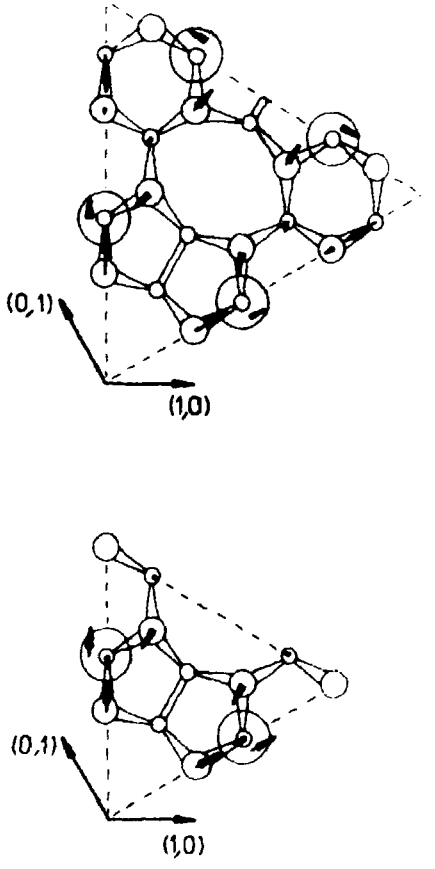

Figure 3.5: The displacements of the atoms in the irreducible unit. The dimer atoms are shown at the actual positions and for the rest of the atoms the arrows show the displacements multiplied by ten. Upper part: Ge(111)7×7-Sn data set no. 3. Lower part: Ge(111)5×5-Sn. The models applied have 6 mm symmetry and the adatom charges have been fitted.

ments of the atoms bonded to the adatoms. For the 7×7 reconstruction it is 0.016 ± 0.005 for the adatom labelled 1 in Figure 2.3 and 0.014 ± 0.005 for the adatom labelled 2. The displacements quoted in this chapter are all in units of the lattice constant of the 1×1 surface: a = 4.000 Å for Ge and a = 3.840 Å for Si. The net inwards displacement for the 5×5 structure of the atoms bonded to the adatoms is 0.021 ± 0.004, which agrees quite well with the displacements for the 7×7 structure. For comparison the Si(111)7×7 structure has a net displacement of 0.029 ± 0.005 around both adatoms (Robinson et al. (1988)) and the Ge(111)$\sqrt{3}\times\sqrt{3}$-Sn structure has a displacement of 0.051 ± 0.004 (Table 2.3).

The projected distance between the two atoms of the dimers are, for the Ge(111)7×7-Sn data set no. 3, 0.678 ± 0.007 (atom 8-9) and 0.650 ± 0.007 (atom 10-10) compared to the bulk bond length of 0.613. For the ideal unrelaxed model the dimer bonds are parallel to the surface. If they are assumed to be parallel to the surface also for the relaxed structures the observed bond lengths correspond to a stretching of 11 ± 1% and 6 ± 1%, respectively, of the two bonds. For the 5×5 structure the dimer bond length is 0.657 ± 0.007 corresponding to a 7 ± 1% stretching. For the Si(111)7×7 structure the average stretching of the dimers is 6 ± 2%. The atomic displacements are discussed further in the next section, where they are compared to the displacements obtained by theoretical calculations.

The agreements of the least-squares fits of the models with the 5×5 data set and the 7×7 data set no. 3 are, χ^2 = 5.1 and 3.6, which still leaves room for improvement. The 5×5 model requires 13 parameters and the 7×7 requires 19, whereas the data sets contain respectively 115 and 269 reflections. In crystallography it is customary, as a rule of thumb, that about five reflections should be available for each parameter to be refined. Even with this quite strict rule the data sets are sufficiently large that more parameters can be included in the models. The obvious way to continue is to allow the atoms to relax according to the lower 3 m symmetry of the bulk. The analysis, which is described below, is restricted to the 5×5 and the 7×7 data set no. 3, because only these two data sets have a sufficiently large number of reflections.

The next model that was fitted to the data included the adatoms and the next two bilayers. The adatoms and the first bilayer were relaxed according to the 6 mm symmetry in order to limit the number of fitting parameters. The choice of 6 mm symmetry for these atoms corresponds to assuming that the displacements in the two parts of the unit cell with regular and faulted stacking are the same. The interaction that gives an energy difference between the two parts of the unit cell is between fourth nearest neighbours atoms and can be expected to have only a small influence on the nearest neighbour bonds at the surface. The energy associated with a stacking fault in the surface layers has been calculated by Vanderbilt (1987a). The ab-initio total-energy calculations showed that, for the relaxed Si(111)1×1 surface, the energy difference between the regular and faulted surface is 60 meV per 1×1 surface unit cell. For the 2×2 adatom model the energy difference is only 20 meV per 1×1 area. These results agree with the energy of the bulk stacking fault in Si of about 30 meV/"1×1" (Chou et al. (1985)) and the energy difference between the cubic and

hexagonal diamond structure of 32 meV per 1×1 surface area for Si and 30 meV/"1×1" for Ge (Yin and Cohen (1982)). The energy estimated for the stacking fault is negligible compared with the energy of a nearest neighbour bond, which is of the order of 3 eV (Northrup (1987)).

The atoms in the second bilayer, which has 3 m symmetry, can be expected to have significant displacements. For Ge(111)$\sqrt{3}\times\sqrt{3}$-M (M = Sn or Pb) with a similar adatom geometry, the displacements in the second bilayer are half as large as the displacements in the first bilayer. In the least-square fits of the model, it is not possible to determine the relaxations of the atoms in the second bilayer that have atoms just above them. Figure 3.6 shows the labelling of the atoms in the models. For the 7×7 model the atoms labelled 18 to 26 were fixed and for the 5×5 the atoms 20, 21, 23 and 24 were fixed. The models have now 40 parameters for the 7×7 and 22 for the 5×5 structure. The least- square fits of these models gave χ^2 = 2.4 and 3.2 for the 7×7 and 5×5 structures, respectively, compared to 3.6 and 5.1 for the previous models including only the adatoms and the first bilayer. The

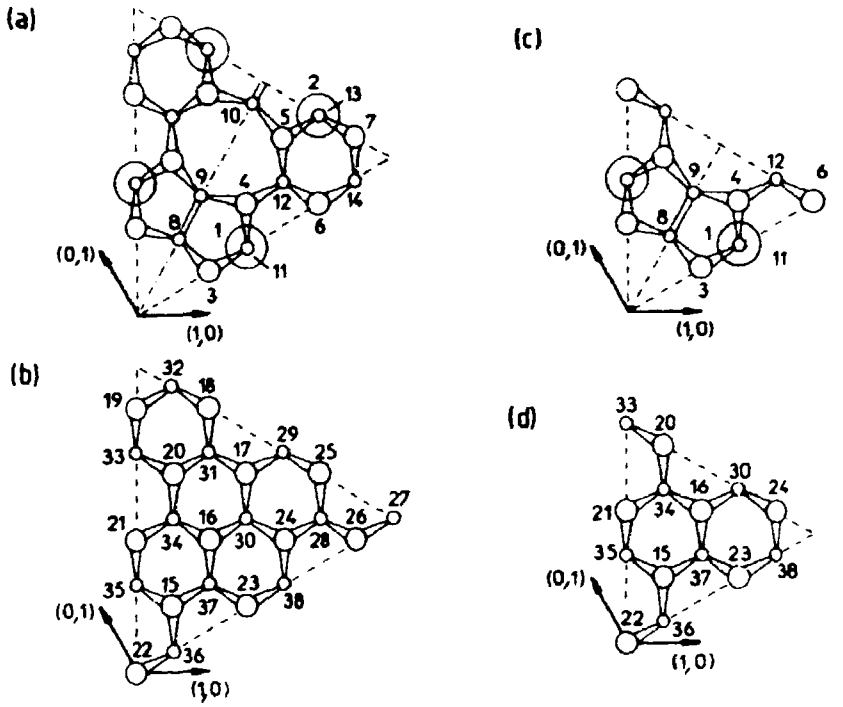

Figure 3.6: The atoms in the first two bilayers of the 7×7 and 5×5 DAS models. (a): First bilayer and adatoms in the 7×7 structure. (b): Second bilayer in the 7×7 structure. (c): First bilayer and adatoms in the 5×5 structure. (d): Second bilayer in the 5×5 structure. In the least-square fits the upper bilayer and the adatoms were allowed to relax in 6 mm symmetry and the lower atoms in 3 m symmetry. For the 7×7 model the atoms labelled 18 to 26 were fixed and for the 5×5 model the atoms 20, 21, 23 and 24 were fixed.

Table 3.3. **Atomic displacements of the atoms in the first two bilayers of the 7×7 and 5×5 DAS models. The atom labelling refers to Figure 3.6. The models that have been used to obtain the experimental displacements are described in the caption of Figure 3.6 and in the text. The parameters marked with a star have been fixed in the least-square fits. The displacements in the other columns (Keating calculation) have been found by a minimization of the elastic strain energy.**

		Ge(111)7×7-Sn		Ge(111)5×5-Sn	
Atom #	Displacement Vectors	Experiment $\chi^2 = 2.4$	Keating calc.	Experiment $\chi^2 = 3.2$	Keating calc.
1	$1/\sqrt{3}(2,1)$	0.016(4)	-0.014	0.030(7)	-0.009
11	"	0.0*	0.003	-0.013(10)	0.007
2	$1/\sqrt{3}(1,\bar{1})$	0.026(5)	-0.005	-	-
13	"	0.0*	0.004	-	-
3	$1/\sqrt{3}(2,1)$	0.036(6)	0.024	0.033(5)	0.028
4	$(1,1),1/\sqrt{3}(1,\bar{1})$	-0.022(8), 0.001(7)	-0.049,-0.016	-0.030(4),-0.007(5)	-0.042,-0.012
5	" "	0.025(5), 0.016(6)	0.040,-0.009	-	-
6	$1/\sqrt{3}(2,1)$	-0.012(7)	0.033	-	-
7	$1/\sqrt{3}(1,\bar{1})$	-0.025(7)	-0.032	-	-
8	$(1,1)$	0.152(5)	0.156	0.161(4)	0.161
9	"	-0.179(5)	0.213	-0.184(4)	-0.207
10	"	0.178(5)	0.187	-	-
12	$(1,1),1/\sqrt{3}(1,\bar{1})$	0.003(5), 0.004(4)	-0.008,-0.036	- ,-0.010(4)	- ,-0.027
14	$1/\sqrt{3}(2,1)$	-0.049(6)	-0.019	-	-
15	$(1,1),1/\sqrt{3}(1,\bar{1})$	-0.021(6), 0.017(10)	0.011, 0.001	-0.007(4),-0.015(9)	0.013, 0.000
16	" "	-0.008(5),-0.005(15)	-0.018,-0.000	-0.012(4),-0.005(13)	-0.016, 0.000
17	" "	0.006(6),-0.011(12)	0.012, 0.001	-	-
18	$1/\sqrt{3}(1,\bar{1})$	0.0*	-0.001	-	-
19	$1/\sqrt{3}(1,2)$	0.0*	-0.005	-	-
20	$(1,1),1/\sqrt{3}(1,\bar{1})$	0.0* , 0.0*	-0.002, 0.006	- , 0.0*	- , 0.004
21	$1/\sqrt{3}(1,2)$	0.0*	0.003	0.0*	0.002
22	-	-	-	-	-
23	$1/\sqrt{3}(2,1)$	0.0*	0.000	0.0*	0.000
24	$(1,1),1/\sqrt{3}(1,\bar{1})$	0.0*,0.0*	-0.002, 0.004	- , 0.0*	- ,-0.005
25	$1/\sqrt{3}(1,\bar{1})$	0.0*	-0.001	-	-
26	$1/\sqrt{3}(2,1)$	0.0*	-0.003	-	-
27	-	-	-	-	-
28	$(1,1),1/\sqrt{3}(1,\bar{1})$	-0.033(8), 0.002(8)	-0.015,-0.004	-	-
29	$1/\sqrt{3}(1,\bar{1})$	-0.053(9)	-0.009	-	-
30	$(1,1),1/\sqrt{3}(1,\bar{1})$	-0.009(8),-0.015(7)	0.004,-0.006	- ,-0.020(8)	,-0.007
31	" "	-0.007(10),0.023(10)	0.007, 0.005	-	-
32	$1/\sqrt{3}(1,\bar{1})$	-0.030(14)	-0.015	-	-
33	$1/\sqrt{3}(1,2)$	-0.036(8)	-0.002	-	-
34	$(1,1),1/\sqrt{3}(1,\bar{1})$	-0.014(15),0.026(14)	0.011, 0.008	0.020(7), 0.000(9)	0.014, 0.007
35	$1/\sqrt{3}(1,2)$	0.046(10)	0.013	0.013(10)	-0.011
36	$1/\sqrt{3}(2,1)$	0.049(11)	0.005	0.044(7)	0.009
37	$(1,1),1/\sqrt{3}(1,\bar{1})$	0.004(7),-0.014(6)	0.001,-0.009	0.006(5), 0.015(5)	0.001,-0.009
38	$1/\sqrt{3}(2,1)$	0.012(10)	0.016	0.021(6)	0.016

atomic displacements are displayed in Table 3.3 and are shown graphically in the left-hand sides of the Figure 3.7 and 3.8. As before, the dimer atoms are shown at the actual positions and for the other atoms the arrows show the displacement multiplied by ten. The shaded atoms have been fixed in the fits.

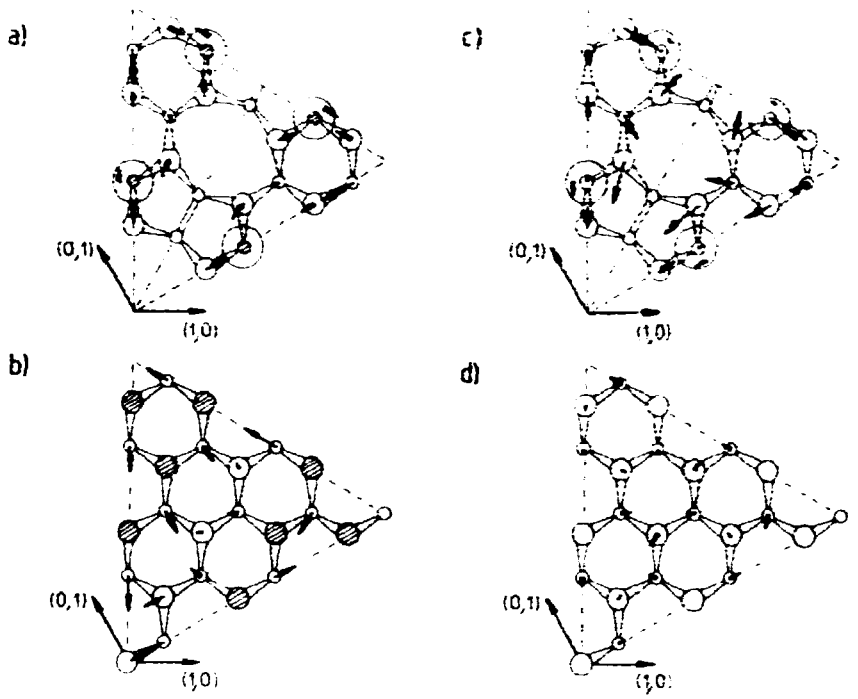

Figure 3.7: The displacements of the atoms in the first two bilayers of the DAS model for the Ge(111)7 × 7-Sn structure. The dimer atoms are at their actual positions and the displacements of the other atoms, multiplied by ten, are shown by arrows. Left-hand side: Experimental displacements. (a) Adatoms and first bilayer. (b): Second bilayer. The shaded atoms have been fixed in the least-squares fit. Right-hand side: Displacements from a minimization of the elastic strain energy calculated with a Keating model: (c) Adatoms and first bilayer, (d): Second bilayer.

The displacements of the adatoms and the atoms in the bilayer just below them are nearly the same as for the model without the second bilayer. The dominant feature in the displacement patterns is inwards displacements of the atoms bonded to the adatoms. For the 7 × 7 data the net inwards displacements have changed slightly to 0.025 ± 0.005 and 0.038 ± 0.005 around adatoms 1 and 2, respectively. For the 5 × 5 data the displacement is 0.021 ± 0.004. These values are close to the displacement of the Si(111)7 × 7 structure (Robinson et al. (1988)): 0.029 ± 0.005, but smaller than the value for the α-phase of the Ge(111)$\sqrt{3} \times \sqrt{3}$-Sn structure: 0.051 ± 0.004 (Chapter 2). The bond length of the dimers are nominally the same as for the previous models, which only included adatoms and first bilayer.

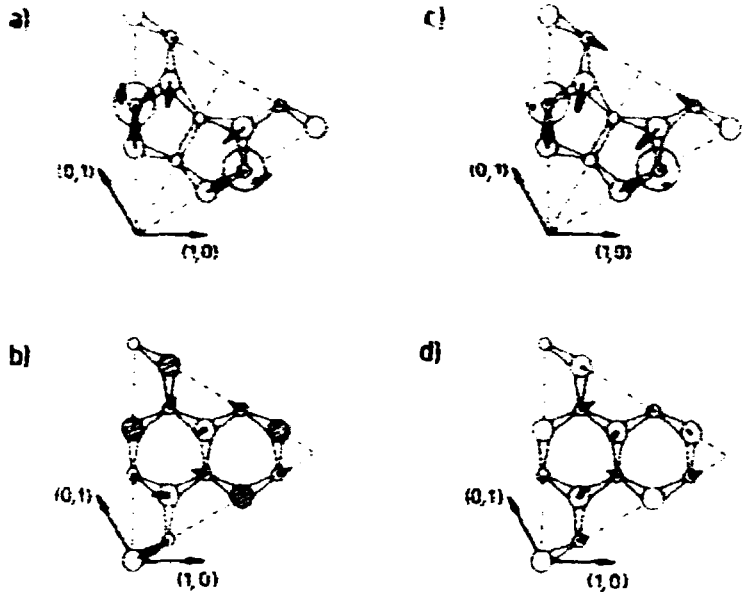

Figure 3.8: The displacements of the Ge(111)5 × 5-Sn structure. Left-hand side: Experiment. Right-hand side: From an elastic strain energy minimization. See Figure 3.7 for additional information.

The displacements of the second layer atoms are mainly outwards displacements of the fourth layer atoms relative to the projected positions of the adatoms. Hence, the displacement patterns around the adatoms in the 7 × 7 and 5 × 5 structures are similar to the displacement pattern of the Ge(111)$\sqrt{3} \times \sqrt{3}$-Sn surface (Chapter 2). The adatoms are bonded to the first layer atoms and pull these atoms inwards. The second and third layer atoms just below the adatoms are pushed downwards. This pushes the fourth layer atoms bonded to the third layer atoms outwards (see Figure 2.1). For the Ge(111)7 × 7-Sn structure the average outwards displacement of the fourth layer atoms is 0.038 ± 0.005 and for the Ge(111)5 × 5-Sn structure it is 0.027 ± 0.005. These values are similar to the value for the Ge(111)$\sqrt{3} \times \sqrt{3}$-Sn surface: 0.027 ± 0.003 (Chapter 2). However, it should be noted that the displacements in the second bilayer are as large as the displacements in the first bilayer.

An error synthesis was performed after the least-square fits. For the 7 × 7 data set a contour plot of the electron density difference was flat and noisy. In contrast the contour plot for the 5 × 5 structure showed additional electronic charge on the atom with the dangling bond, labelled 6 in Figure 3.6, on the dimer atom labelled 8 closest to the corner holes and in a position close to the dangling bond on atom 22 in the corner hole. In the next least-squares fit these electronic charges were allowed to vary. This model gave a $\chi^2 = 1.7$ for the following electronic charges: At the atom 6: 1.08 ± 0.07 and on the dimer atom 8: 1.21 ± 0.06, both in units of the electronic charge of a Ge atom. The electronic charge in the corner hole was described by including one atom in each corner hole. The atom is displaced away from the atom with a dangling bond in the center of the corner hole. It can

sit at three different symmetry-equivalent positions. However, the electronic density corresponds to a situation in which the three position are one third occupied by Sn atoms, i.e. for each unit cell only one of the three positions is occupied. The atom has a B-factor 5.4 ± 1.5 Å^2 and is situated at the position (0.18 ± 0.03, 0.35 ± 0.06) or at one of the two equivalent positions. This situation cannot be distinguished from an occupation of all three positions with atoms having a charge of 1/3 of an Sn atom. In this final model the adatom charge correspond to 0.90 ± 0.05 of the electron charge of a Sn atom.

The atom labelled 6 has only a marginally larger electronic charge than a Ge atom and so no further interpretation is possible. However, the additional charge on the dimer atom is significant and can be due to Sn substitution at this position. Assuming that the non-adatom positions are occupied by Ge atoms the Sn substitution of the dimer atom is 37% ± 11%. This corresponds to about two Sn atoms per 5 × 5 unit cell. The implication of this is discussed in Section 3.5 which contains estimates of the total energies of the structures.

3.4 Comparisons with Atomic Relaxations from Model Calculations

The previous section demonstrated similar atomic displacements for the Ge(111)7 × 7-Sn, Ge(111)5 × 5-Sn, Si(111)7 × 7 and Ge(111)$\sqrt{3} \times \sqrt{3}$-Sn structures. In order to obtain a good basis for a further discussion of these similarities, the atomic coordinates can be compared to the results of model calculations. The preferred technique for such calculations are ab-initio total-energy methods, but unfortunately, the large unit cell of the DAS structures makes such calculations impossible. However, semiempirical tight-binding calculations have been performed for the Si(111)5 × 5 and Si(111)7 × 7 DAS structures (Qian and Chadi (1987a,b,c)). In this work the positions of the adatoms and the atoms in the next three layers of the crystal have been optimized to give the lowest value for the total energy. The in-plane projection of the displacements are close to having 6 mm symmetry. The displacements in the two halves of the unit cell typically agree within 10%. The average displacements of the two halves of the unit cells are displayed in Tables 3.4 and 3.5.

The atomic relaxations can also be obtained by calculating and minimizing the elastic strain in the reconstructions. Section 2.6 and Appendix A and B demonstrate that the Keating model for the elastic energy is able to give relaxations that agree quite well with more advanced calculations and with experiment. In the Keating calculations (present work) for the 5 × 5 and 7 × 7 DAS models the positions of the adatoms and of the atoms in the first three bilayers (i.e. six layers) were optimized. The calculations involve the optimization of 171 and 89 parameters for the 7 × 7 and 5 × 5 structure, respectively. Section 2.6 and Appendix A contain details of the calculations. As for the tight-binding calculations the displacements of the adatoms and of the atoms in the first bilayer are found to have nearly 6 mm symmetry. The results for the Si(111)7 × 7, Ge(111)7 × 7-Sn, Si(111)5 × 5 and Ge(111)5 × 5-Sn are shown in Tables 3.4 and 3.5. The agreement between the results from tight-binding calculations and the Keating calculations is astonishing, considering the very different approaches. The largest differences are for the atoms

bonded to the adatoms (atom 4 and 5 for the Si(111)7 × 7 structure and atom 4 for the Si(111)5 × 5 structure). The bonds of the adatoms are heavily distorted and in the Keating calculations they are treated as bulk bonds. This is probably a too simplistic approach to account for the large deviations from the tetrahedral configuration.

The experimental displacements determined by x-ray diffraction for the Si(111)7 × 7 (Robinson et al. (1988)) and Ge(111)7 × 7-Sn (present work) structures are also displayed in Table 3.4. The results are from the least-squares fits of the models with 6 mm symmetry, that includes the adatoms and the atoms in the first bilayer. The experimental results for the Si(111)7 × 7 and the Ge(111)7 × 7-Sn surface agree quite well with the tight-binding calculations as well as with the Keating calculations. The displacement of atoms bonded to the adatoms are closest to the results of the tight-binding calculations. This is reasonable, due to the more realistic treatment of electronic properties in this type of calculations. Figures 3.9 and 3.10 show a graphical presentation of the displacements. The displacements are multiplied by ten except for dimer atoms. Figure 3.9 shows the results

Table 3.4. Atomic relaxations for the Si(111)7 × 7 and Ge(111)7 × 7-Sn surfaces.
a) X-ray diffraction experiment by Robinson et al. (1988). The structural model has 6 mm symmetry and includes only the adatoms and first bilayer.
b) Tight-binding calculation by Qian and Chadi (1987a).
c) Elastic strain calculations by the Keating model (present work).
d) X-ray diffraction experiment (present work). The same model as a), except that the Ge atoms below the adatoms were fixed.

		Si(111)7×7			Ge(111)7×7-Sn	
Atom #	Displacement Vector	a) Experiment χ^2=1.9	b) Tight-binding calc.	c) Keating calculation β/α=0.10	c) Keating calculation β/α=0.10	d) Experiment χ^2=3.6
1	1/√3(2,1)	}	-0.093	-0.012	-0.014	0.020(4)
11	"	} -0.007(3)	0.005	0.006	0.003	0.0*
2	1/√3(1,$\bar{1}$)	}	0.007	-0.006	0.005	0.018(4)
13	"	} -0.005(3)	0.005	0.006	0.004	0.0*
3	1/√3(2,1)	0.031(9)	0.031	0.034	0.024	0.041(6)
4	(1,1),1/√3(1,$\bar{1}$)	-0.029(8), 0.007(12)	-0.038,-0.005	-0.054,-0.011	-0.049,-0.016	-0.025(4),-0.012(4)
5	" "	0.030(7),-0.003(12)	0.034, 0.004	0.046,-0.004	0.040,-0.009	0.028(4),-0.002(4)
6	1/√3(2,1)	-0.016(9)	-0.024	-0.033	-0.033	-0.006(6)
7	1/√3(1,$\bar{1}$)	-0.033(9)	-0.021	-0.039	-0.032	0.000(5)
8	(1,1)	0.151(8)	0.163	0.158	0.156	0.147(5)
9	"	-0.195(8)	-0.206	-0.212	-0.213	-0.172(5)
10	"	0.178(8)	0.186	0.187	0.187	0.175(5)
12	(1,1),1/√3(1,$\bar{1}$)	-0.015(6),-0.014(10)	-0.007,-0.001	-0.007,-0.038	-0.008,-0.036	-0.011(4), 0.004(4)
14	1/√3(2,1)	-0.007(7)	-0.036	-0.017	-0.019	-0.043(6)

Table 3.5. Atomic displacements for the Si(111)5×5 and Ge(111)5×5-Sn-surfaces.
a) Tight-binding calculation by Qian and Chadi (1987c).
b) Elastic strain calculations by the Keating model (present work).
c) X-ray diffraction experiment (present work). The model has 6 mm symmetry and includes only the adatoms and the first bilayer.

		Si(111)5×5		Ge(111)5×5-Sn	
Atom #	Displacement Vector	a) tight-binding calc.	b) Keating calculation	b) Keating calculation	c) Experiment $\chi^2 = 5.1$
1	$1/\sqrt{3}(2,1)$	-0.001	-0.006	-0.009	0.031(6)
11	"	0.007	0.011	0.007	-0.018(10)
3	"	0.032	0.038	0.028	0.028(4)
4	$(1,1),1/\sqrt{3}(1,\bar{1})$	-0.034,-0.004	-0.048,-0.008	-0.042,-0.012	-0.023(3),-0.001(3)
6	-	-	-	-	-
8	$(1,1)$	0.166	0.162	0.161	0.163(4)
9	"	-0.202	-0.206	-0.207	-0.180(4)
12	$1/\sqrt{3}(1,\bar{1})$	0.004	-0.029	-0.027	-0.004(5)

from experiment for Ge(111)7×7-Sn, the tight-binding results for Si(111)7×7 (Qian and Chadi (1987a)) and the results from the Keating calculation for the Ge(111)7×7-Sn surface. The experimental results have a good qualitative agreement with both types of calculations. However, none of them are able to predict the experimentally observed displacements of the adatoms. The adatoms are found to be relaxed away from the dimers and the corner hole, while the calculations give the opposite direction.

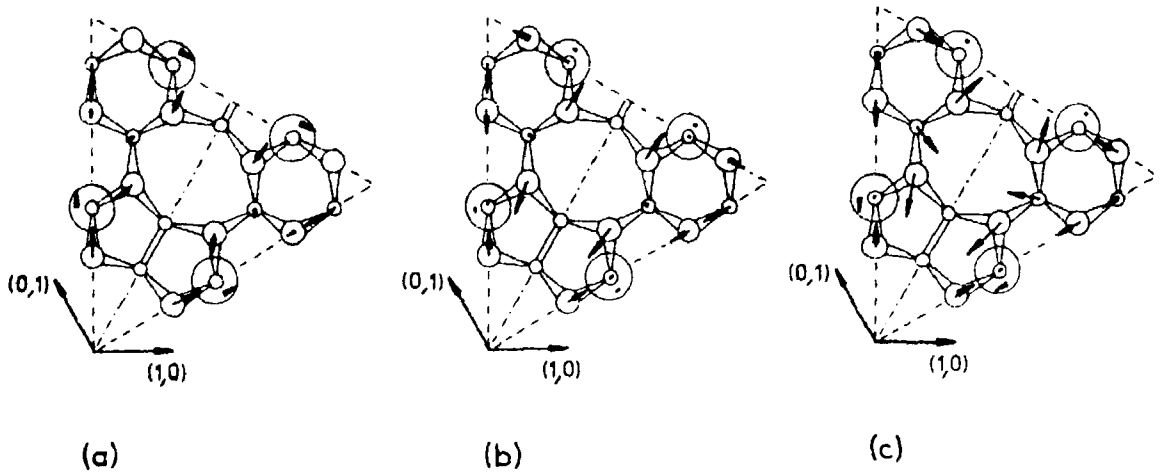

Figure 3.9: The atomic displacements of the Ge(111)7×7-Sn structure. The arrows show the displacement multiplied by ten. (a): The result of the x-ray scattering experiment as shown in Table 3.4 (present work). (b): From tight-binding calculations for Si(111)7×7 (Qian and Chadi (1987a)). (c): From a Keating calculation for Ge(111)7×7-Sn (present work).

The experimental results for the Ge(111)5 × 5-Sn structure are in very good agreement with the tight-binding results for the Si(111)5 × 5 structure (Qian and Chadi (1987c)) and the results from Keating calculation, as shown by Table 3.5 and Figure 3.10. Also for this structure both types of calculation fail to predict the observed displacement of the adatom.

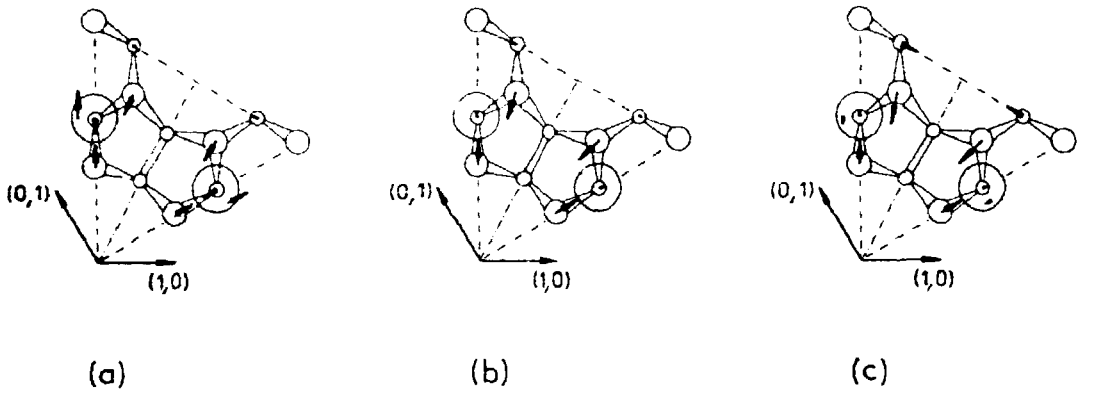

Figure 3.10: The atomic displacements for the Ge(111)5 × 5-Sn structure. The arrows show the displacements multiplied by ten. (a): The results of the x-ray scattering experiment as shown in Table 3.5 (present work). (b): From the tight-binding calculations for the Si(111)5 × 5 structure (Qian and Chadi (1987c)). (c): From the Keating calculation for the Ge(111)5 × 5-Sn surface (present work).

The projected dimer bond lengths are found to be about 3% longer than the bulk bond length by both tight-binding and Keating calculations. This value is somewhat small compared to the experimental values. For the Si(111)7 × 7 structure the dimer bonds are 6 ± 2% longer (Robinson et al. (1988)) for the Ge(111)7 × 7-Sn structure they are 11 ± 1% and 6 ± 1% longer and the dimer bond for the Ge(111)5 × 5-Sn surface is 7 ± 1% longer than the bulk value.

The Keating calculations also give the displacements of the atoms in the deeper layers. They can be compared to the experimental results for the models that include the adatoms, the atoms in the first bilayer with 6 mm symmetry and the atoms in the second bilayer with 3 m symmetry. The results from experiment and from Keating calculations for the Ge(111)7 × 7-Sn and Ge(111)5 × 5-Sn structures are displayed in Table 3.3 and shown in the Figures 3.7 and 3.8. The displacement have a good agreement except for the second layer atoms bonded to the "rest atom" in the corner hole, which has a dangling bond. A close inspection of the displacements in the upper layers (Table 3.3 and Figures 3.7 and 3.8) also shows that the displacements of the atoms bonded to the atom labelled 6 with a dangling bond, are not in good agreement with the results from the Keating calculation. The changes in coordination of these "rest atoms" are not taken into account in the Keating model, which assumes tetrahedral equilibrium bond configurations. The tight-binding calculations of Qian and Chadi (1987a,c) are more realistic on this point and a comparison with Table 3.4 and 3.5 shows as expected that the results of these calculations are in better agreement with experiment.

In some cases the atomic relaxations at the surface can be understood in terms of chemical arguments developed for simple molecules (Goddard and Harding (1978) and Swarts et al. (1980,1981)). In other cases these arguments have to be combined with total-energy calculations for the surface. However, even for simple molecules the bond configuration is a result of competing interactions and the behaviour is not easily understood (Goddard and Harding (1978)): The bond configuration has to minimize the electrostatic interactions and at the same time the valence electrons have to obey the Pauli principle. In the rest of this section the atomic relaxations around the rest atoms are discussed by combining chemical arguments for the local changes with results from total-energy and band structure calculations.

The ideal unrelaxed 1×1 surface has an sp^3 -orbital directed into the vacuum containing only one electron. The energy of the surface atom can be lowered by a rehybridization which transfers some of the s-character of the dangling bond into the double occupied bonds of the atom. This leads to an sp^2-like configuration for these bonds with p_z-character of the dangling bond. The ideal sp^2-configuration is planar with 120° between the bonds and the surface atom is relaxed inwards. The deformation of the bonds of the atoms bonded to the surface atom (sp^3-configuration) costs energy and this limits the inwards relaxation of the surface atoms. When the atomic positions are optimized in a total-energy calculation this inwards relaxation is found (Northrup et al. (1981), Vanderbilt and Louie (1984), Vanderbilt (1987a)). It leads to an increase in the bandwidth of the dangling bond states, which are present in the band gap (Schlüter et al. (1975)). A contour plot of the electron density of the occupied states shows as expected the strong p-character of the dangling bond states.

Haneman (1961,1982) suggested a "buckling" model with two inequivalent surface atoms for the 2×1 structure which is observed on the cleaved surfaces of Si and Ge. In this model one of the surface atoms is moved outwards and the other inwards in such a way that the bond lengths are approximately preserved. The doubling of the unit cell gives rise to two bands of surface states and the occupied lowest band corresponds to electronic states which are almost entirely on the upper atom (Schlüter et al. (1975)). This means that the electron in the dangling bond on the lower atom is transferred to the upper atom. The bonds to the substrate of the atom in the outer position are mainly p-like and the dangling bond is mainly s-like. A small hybridization of the s- and p-states leads to a spatial separation of the two dangling bond states (Goddard and Harding (1978)). This minimizes the electrostatic interactions for two electrons in this state and therefore it is favourable to transfer the electron from the inwards to the outwards relaxed atom. The configuration of the upper atom is quite similar to ammonia NH_3, which has a "lone pair" in an s-like state and angles between the three H-bonds that are smaller than the tetrahedral value (Swarts et al. (1980)).

The DAS structures have the adatoms and rest atoms in a local 2×2 arrangement. Total-energy calculations for the Si(111)2×2-Si (T_4) adatom surface shows that the rest atoms in the structure are similar to the outwards relaxed atoms in the buckling model (Northrup (1987) and Vanderbilt (1987a)). The bonding of the adatom to the dangling bonds of the substrate gives one band that corresponds to the dangling bond of the adatom and two

bands, that are about 2 eV lower in energy and are derived from the p_x and p_y-orbitals of the adatoms (Northrup (1986,1987)). A fourth band, which arises from the "rest atoms", is situated between these two sets of adatom-derived bands. The fact that the "rest-atom" derived band is situated at an energy lower than the adatom dangling bond state leads to a charge transfer of one electron from the adatom to the "rest atom". This leaves the upper bond empty and "rest-atom" derived band completely full. The total-energy calculations of Vanderbilt (1987d) (Appendix A) show that the "rest atom" is relaxed outwards as expected. The Keating calculations described in Appendix A do not take the rehybridization of the "rest atom" into account and hence do not give the outwards relaxation of the "rest atom". Figure 3.11 demonstrates the influence of the electronic effect on the projected relaxations. The figure shows the difference between the relaxations from the total-energy calculation (Vanderbilt (1987d)) and the Keating calculations (present work). A significant relaxation, towards the "rest atom" is seen for the atoms bonded to the "rest atom".

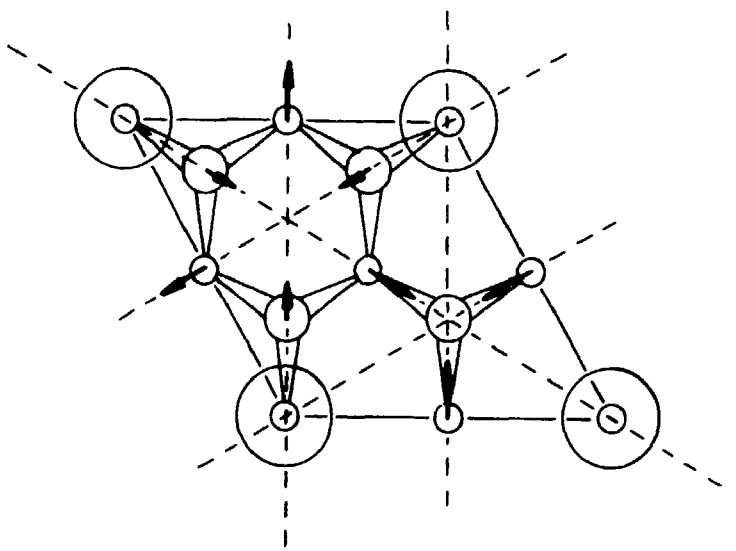

Figure 3.11: The relaxations due to electronic effects for the Si(111)2×2-Si adatom structure. The differences between the total-energy calculations (Vanderbilt (1987d)) and the Keating calculations (present work) multiplied by 15 are shown by arrows.

Tight-binding calculations for the 5×5 and 7×7 DAS structure also gave an outward relaxation of the "rest atoms" in these structure. (Qian and Chadi (1987a,c)). The number of "rest atoms" for the 5×5 and 7×7 structure is respectively 3 and 7 per unit cell compared to the number of adatoms, which is 6 and 12. The calculation shows, as expected, that the "rest atom" states are lower in energy than the adatom dangling bond states and therefore the "rest atom" states are completely filled. The influence on the in-plane relaxations of the rehybridization of the "rest atoms" is shown in Figure 3.12. The

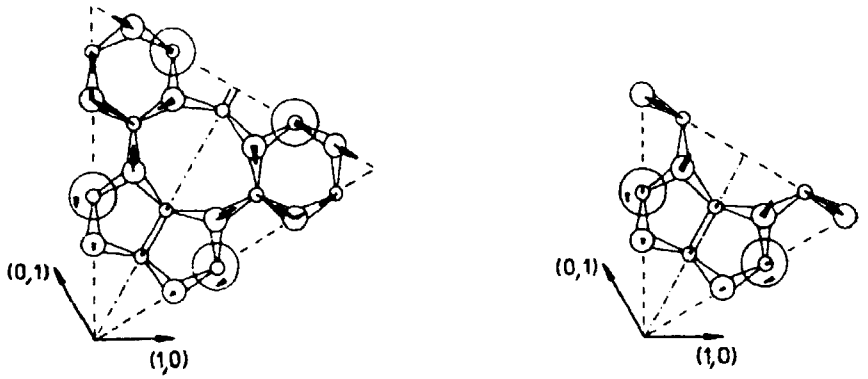

Figure 3.12: The influence of electronic effects on the relaxation in the top layers of the 7×7 (left-hand side) and the 5×5 (right-hand side) DAS structure. The arrows show the difference, multiplied by 15, between the tight-binding (Qian and Chadi (1987a,c)) and Keating calculations (present work).

differences between the tight-binding and Keating calculations multiplied by 15 are indicated by arrows. As expected a large relaxation of the atoms bonded to the "rest atoms" towards them is observed. The significant influence of the electronic effects on the relaxations accounts for the better agreement between experiment and the tight-binding calculations compared to the Keating calculations.

In summary, the observed atomic displacements of the Ge(111)7×7-Sn and Ge(111)5×5-Sn structures are well described by both Keating and tight-binding calculations. The tight-binding calculations give the best description of the relaxations in the upper layers, due to the more realistic treatment of the atoms which have changes in electronic configurations. For the deeper atoms, which have positions that are only slightly different from the bulk positions, the results from the Keating calculations are in good agreement with experiment.

3.5 Surface Stress and Total Energy

Attempts to understand surface reconstructions on semiconductor surfaces are mainly based on two different principles. One suggestion is that the reconstruction takes place because it is energetically favourable for the surface to reduce the number of dangling bonds. The other approach is to consider the reconstructions to be due to relief of stress in the surface region of the unreconstructed surface. These two ideas are not distinguishable and the only way to determine which of different proposed structural models for a surface is the most favourable is to calculate and compare the total energies.

The discussion of the surface stress was renewed by the calculations for the Si(111) surface performed by Pearson et al. in 1986. The stress calculations were based on an empirical expression for the energy including two- and three-body interactions. This energy expression has been shown to give a good description of structural properties of Si (Takai et al. (1985)). The calculation on the ideal Si(111)1×1 surface gave displacements for the relaxed surface which are similar to those found by ab-initio total-energy calculations. The surface stress was also calculated for the empirical potential and the surface was found to have a large compressive stress: -2.7 eV per 1×1 surface cell area. With this in mind, it is obvious to suggest that the dimer rows in the DAS structure are formed in order to relieve the stress. An optimization of the length of the six bonds of a dimer with ideal unrelaxed surroundings shows that the dimer bonds are stretched by about 6% relative to the bulk value. Therefore, the idea is that the dimers are topological defects that relieve compressive stress in the surface.

Vanderbilt (1987a) has recently performed ab-initio stress calculations for different structures on the Si(111) surface and found results quite different from Pearson et al.. The relaxed 1×1 surface with regular stacking and with a stacking fault in the surface layer were found to have a stress of -0.5 eV and 0.0 eV per 1×1 area, respectively. (A negative stress is compressive and positive is tensile). The calculation also showed that the π-bonded chain for the cleaved surfaces (Section 1.2.b) is under a large tensile stress along the chain (1.4 eV/"1×1" and a smaller tensile stress (0.4 eV/"1×1" perpendicular to the chain. These calculations show that it is not compressive stress that makes the 1×1 and the π-bonded 2×1 structures unfavourable.

To elucidate the stress in the DAS structure Vanderbilt (1987a) has also performed calculations for the Si(111)2×2-Si (T_4) surface with and without stacking fault in the surface layers. These adatom arrangements are similar to the adatoms in the DAS models. Both structures have a large tensile stress: 1.8 eV/" 1×1" for the regular stacking and 2.2 eV/" 1×1" for the faulted stacking. These stresses are caused by the bonding of the adatoms to the surface atoms. Finally, the stress of the adatom-free n×n DAS structures were calculated by a combination of ab-initio and Keating calculations. As expected the pull of the dimers results in a tensile stress for the 5×5, 7×7 and 9×9 structure. The values are, respectively, 1.22, 0.83 and 0.61 eV/" 1×1". These results and the results for the 2×2 adatom structured clearly demonstrates that the dimers and the adatoms both contribute to an increase in the surface tensile stress relative to the relaxed ideal 1×1 surface. Finally, the discussion in the previous section showed that the "rest atoms" also give rise to tensile stress.

In contrast to the calculations of Pearson et al. the calculations by Vanderbilt are based on a more reasonable and realistic energy expression, so his results should be reliable. It must be concluded from Vanderbilt's work that surface stress is not the decisive factor for surface reconstruction. The rest of this section is a discussion of the total-energy of the surface reconstructions in terms of dangling bond reduction.

Total-energy calculations are much more numerous for the Si(111) surface than for Ge(111). In the introduction (Chapter 1) it was argued from experimental and theoretical results that the physics and chemistry of the Si and Ge surfaces are quite similar. So, the following discussion of the Ge(111) and Si(111) surfaces is mainly based on the results available for Si.

The ideally terminated, unrelaxed Si(111)1×1 surface has an energy which is 1.63 eV/"1×1" higher than the bulk crystal. (Northrup (1987)). Relaxing the 1×1 surface gives an energy, which is -0.13 to -0.18 eV/" 1×1" relative to the unrelaxed surface. (Northrup et al. (1981), Pandey (1982), Nielsen et al. (1983) and Vanderbilt (1987a)). Therefore, a realistic structural model for a surface reconstruction has to have an energy lower than this value.

In Section 1.2.b the π-bonded chain model for the cleaved surfaces was described and discussed. For Si a relaxation of the outer double layer in the model gives an energy of ÷0.30 eV/"1×1" (Pandey (1982)). The calculations have been performed on repeated slab geometries. Each slab contains 5 double layers and have inversion symmetry. The surface reconstructions which are present at both sides of the slab, are separated by vacuum. When the position of all atoms in the slab are relaxed the energy of the π-bonded chain model is found to be between -0.36 and -0.47 eV/" 1×1" for Si and about -0.34 eV/" 1×1" for Ge (Northrup and Cohen (1982a,1983), Nielsen et al. (1983) and Vanderbilt (1987a)). The energy for Ge is estimated from the energy relative to an ideal unrelaxed antiferromagnetic ordered (2×1) geometry (-0.32 eV) and the energy gain (~ 0.02 eV) found for magnetic ordering on the Si(111) surface (Northrup and Cohen (1982b,1983)). The small extent of the geometry in the direction normal to the surface causes some problems. The subsurface relaxations of the reconstructions on different sides of a slab interact. Due to the inversion symmetry of the slab the reconstruction on both sides of the slab benefit from the relaxations of the atoms in the middle. Therefore, the energy of the relaxed geometries are underestimated and the correct value for the energy gain is probably slightly smaller.

The total energies of the 5×5 and 7×7 DAS structures on a Si(111) surface have been calculated by the tight-binding method. (Qian and Chadi (1987a,c)). The adatoms and the outer three layers were relaxed. This gave the energies -0.403 eV/" 1×1" (7×7) and -0.395 eV/" 1×1" (5×5) which both are close to the energy of the π-bonded chain model. A further decrease in the energy can be expected from a relaxation of deeper lying atoms. The energy difference between the 5×5 and 7×7 structure is only 8 meV, which seems reasonable considering that both structures are observed on the Ge(111)-Sn surface with only a small change in Sn coverage.

In order to estimate the elastic and electronic contribution to the total energy the results from ab-initio and Keating calculations can be combined (Qian and Chadi (1986) and Vanderbilt (1987b,c)). The presentation given below differs on some points from these works.

First the elastic contributions are discussed. The Keating model with the parameters for Si, α = 0.201 eV/Å^4 and β/α = 0.10, are applied on the 5×5 and 7×7 DAS structure. In contrast to Qian and Chadi (1986) and Vanderbilt (1987b,c) the adatoms are included. The

total strain energy is 18.95 eV and 34.93 eV for the 5×5 and 7×7 unit cell when the atoms are allowed to relax down to the sixth layer of the substrate. The strain induced by the adatoms are later included in the net electronic energy of the adatoms and it is therefore subtracted from the strain energy. The Keating calculation for a 2×2 adatom structure gives a strain energy $E^{Ad}_{Strain} = 2.41$ eV per adatom. Subtracting the strain energy of the adatoms gives:

$$E^{5\times5}_{strain}/(5\times5) = 3.80/25 \text{ eV} = 0.152 \text{ eV}/1\times1$$
$$E^{7\times7}_{strain}/(7\times7) = 5.07/49 \text{ eV} = 0.103 \text{ eV}/1\times1 \qquad (3\text{-}1)$$

These values are in good agreement with results for the adatom-free structures (Qian and Chadi (1986) and Vanderbilt (1987b,c). The density of the strain energy for the 5×5 structure is considerably higher than for the 7×7 structure due to the higher density of dimers in the 5×5 structure: 0.240 for the 5×5 and 0.184 for the 7×7 structure.

The $(2n+1)\times(2n+1)$ DAS structures have two kinds of dimers. Those that are part of the corner holes and those that are not. Therefore, the strain energy can be divided into an average energy for a dimer E_{dim} and an extra strain energy of a corner hole E_{CH} (Qian and Chadi (1986)):

$$E^{(2n+1)\times(2n+1)}_{strain} = 3n\, E_{dim} + E_{CH} \qquad (3\text{-}2)$$

The energies in (3-1) give two equations to determine E_{dim} and E_{CH}. The values are:

$$E_{dim} = 0.423 \text{ eV}$$
$$E_{CH} = 1.260 \text{ eV} \qquad (3\text{-}3)$$

The strain energy of any $(2n+1)\times(2n+1)$ DAS structure can be calculated from (3-2) and (3-3).

Next the electronic contributions to the total energy is considered. In order to make consistent estimates all values are taken from Vanderbilt (1987a), except the value for the ideal terminated unrelaxed 1×1 surface which is taken from Northrup (1987). The total energy of a 2×2 adatom arrangement is:

$$E^{2\times 2}_{reg} = 5.36\ \text{eV}/2\times 2 \qquad \text{(regular surface stacking)}$$

$$E^{2\times 2}_{flt} = 5.44\ \text{eV}/2\times 2 \qquad \text{(faulted surface stacking)} \qquad (3\text{-}4)$$

The 2×2 unit cell consists of one adatom and one "rest atom". The energy of the "rest atom" is estimated to be equal to the energy of a rest atom on the relaxed 1×1 surface:

$$E^{rest} = 1.45\ \text{eV/atom} \qquad (3\text{-}5)$$

This value is assigned to the "rest atom" in both the regular and faulted parts of the unit cells. The stacking-fault energy is then only present in the adatom energies:

$$E^{Ad}_{reg} = 3.91\ \text{eV/adatom}$$
$$E^{Ad}_{flt} = 3.99\ \text{eV/adatom} \qquad (3\text{-}6)$$

In the DAS structures these two kinds of adatoms are both present in equal numbers. Hence, an average value can be used:

$$E^{Ad} = 3.95\ \text{eV/adatom} \qquad (3.7)$$

The total energy is the sum of the elastic and electronic contributions:

$$E^{Tot} = \frac{1}{(2n+1)^2}\left(E_{CH} + 3n\,E_{dim} + n(n+1)E^{Ad} + (n(n-1)+1)E^{rest}\right) \qquad (3\text{-}8)$$

The energies calculated by this expression are displayed in Table 3.6 together with the energies for other relevant structures and the energies for the 5×5 and 7×7 structures calculated by the tight-binding method (Qian and Chadi (1987a,b)). The energies calculated by (3-8) are lowest for the 5×5 structure, but only 5 meV lower than the energy of the 7×7 structure. The tight-binding calculations give an energy difference of 8 meV in favour of the 7×7 structure. This is a reasonable agreement considering the very different methods of calculation.

Table 3.6. The total energy for different surface structures.
a) Northrup (1987)
b) Vanderbilt (1987a)
c) According to equation (3-8)
d) Northrup (1986)
e) Qian and Chadi (1987a)

	E	ΔE
Structure	eV/1×1	eV/1×1
1×1 unrelaxed [a]	1.63	0.0
1×1 relaxed [b]	1.45	-0.18
3×3 DAS [c]	1.320	-0.311
5×5 " [c]	1.274	-0.356
7×7 " [c]	1.278	-0.351
9×9 " [c]	1.286	-0.343
2×2 (T_4) [b]	1.34	-0.29
$\sqrt{3}\times\sqrt{3}$ (T_4) [d]	1.35	-0.28
2×1 π-bonded chain	1.27/1.16	-0.36/-0.47
5×5 DAS [e]	1.235	-0.395
7×7 DAS [e]	1.243	-0.403

From Table 3.6 it is also clear that for slightly different parameters it is possible to obtain the π-bonded chain model, the 5×5 or 7×7 DAS structures, the 2×2 adatom structure or the c(2×8) simple adatom model which is obtained by a small modification of the 2×2 adatom structure (Figure 1.7). The energy calculations combined with the experimental results for the Ge(111)-Sn surfaces offer a possible explanation for the observed structural transition: c(2×8) 7×7 DAS 5×5 DAS. For the pure Ge(111) surface it is energetically more favourable to eliminate dangling bonds by adatoms in the c(2×8) simple adatom model rather than incur the high elastic energy of the DAS model. Substitution of the adatoms in the DAS structure by Sn atoms lowers the energy of this structure below the energy of the simple adatom model. This is probably due to the smaller substrate relaxation around the larger Sn atoms compared to Ge adatoms. The main difference

between the 7×7 and 5×5 DAS structure is the density of dimers or equivalently the elastic energy density (Equation 3-1). The analysis of the experimental results for the Ge(111)5×5-Sn sample suggested that approximately every third dimer atom closest to the corner holes is substituted by Sn. The elastic energy reduction due to this substitution has been calculated with the Keating model. It was found to be 23 meV/1×1 for the elastic parameters of Si which is enough to account for the change from the 7×7 to the 5×5 DAS structure.

3.6 Summary and Conclusions

The analysis of the x-ray diffraction experiments have shown that the Ge(111)7×7-Sn and Ge(111)5×5-Sn structures are described by the DAS model with Sn as adatoms. The refined atomic positions of the reconstructions are in good agreement with tight-binding calculations for the Si DAS structures. The agreement with elastic energy minimization by the Keating model is slightly worse due to the inability of this model to treat atoms which undergo modification of their electronic structure. The displacements in the second bilayer are in good qualitative agreement with the predictions of the Keating model.

For the 5×5 structure the analysis gave indications of a Sn atom in the corner hole close to the atom with a dangling bond and of more charge on the dimer atom closest to the corner hole. About every third dimer atom was estimated to be substituted by Sn. An elastic energy calculation using the Keating model shows that Sn substitution gives a decrease in elastic energy, which explains the formation of the 5×5 structure instead of the 7×7 structure.

For the DAS structures the density of adatoms is 0.245 for the 7×7 and 0.240 for the 5×5 structure. As the 7×7 structure is observed after deposition of 0.3-0.5 monolayers of Sn (Ichikawa and Ino (1981)), the adatoms account for practically all of the Sn in this reconstruction. The Sn coverage of the 5×5 structure, estimated from the analysis, is 0.37 monolayers. Ichikawa and Ino determined that a minimum coverage of about 0.7 monolayers is required to obtain the 5×5 structure with no admixture of the 7×7 structure. The Sn atoms which are not located in the analysis can be either randomly substituted in the surface layers or be in disordered regions on the surface. The more physically appealing situation is a random distribution in the surface layers. The larger covalent radius of Sn compared to Ge, means that Sn substitution reduces the elastic energy cost of dimer formation.

ACKNOWLEDGEMENTS

I would like to thank my two supervisors Kim Carneiro, Copenhagen University and Danish Institute of Fundamental Metrology and Mourits Nielsen, Risø National Laboratory, for their encouraging support during the course of this work.

Making measurements at a synchrotron is very much a teamwork and I have been fortunate to work together with Mourits Nielsen, Robert Feidenhans'l, Robert L. Johnson, Francois Grey, and Kristian Kjær. The collaboration with these people is gratefully acknowledged.

I have benefitted from stimulating discussions with Jens Als-Nielsen, Jakob Bohr, Céleste Reiss, Hartmut Zabel, Ian Robinson, David Vanderbilt, Guo-Xin Qian, Ole Holm Nielsen, Hans Skriver and many others. In particular I would like to thank all those that have made unpublished results available to me.

The measurements would not have been possible without the efforts of the technical and scientific staff at HASYLAB and the technical staff at Risø National Laboratory. Their help is gratefully acknowledged.

For the preparation of this thesis I would like to thank Nanna Faure, Agnete Gjerløv and Karna Hansen for typing it and Robert Feidenhans'l and Robert L. Johnson for their critical reading of the manuscript and the many improvements they have suggested.

Finally, the financial support from the Danish Natural Science Foundation is acknowledged.

REFERENCES

AARTS, J., HOEVEN, A.J. and LARSEN, P.K. (1987) to be published.

APPELBAUM, J.A. and HAMAN, D.R. (1978). Surf. Sci. **74**, 21.

BARAFF, G.A., KANE, E.O. and SCHLÜTER, M. (1980). Phys. Rev. B **21**, 5662.

BATRA, I.P., HIMPSEL, F.J., MARCUS, P.M., TROMP, R.M., COOK, M.R., JONA, F. and LIU, H. (1985). The Structure of surfaces. Ed.: M.A. van Hove and S.Y. Tong (Springler Verlag, New York) p. 285.

BATTERMAN, B.W. and CHIPMAN, D.R. (1962). Phys. Rev. **127**, 690.

BECKER, R.S., GOLOVCHENKO, J.A. and SWARTZENTRUBER, B.S. (1985). Phys. Rev. Lett. **54**, 2678.

BENNETT, P.A., FELDMAN, L.C., KUK, Y., McRAE, E.G. and ROWE, J.E. (1983). Phys. Rev. B**28**, 3656.

BEVINGTON, P.R. (1969). Data Reduction and Error Analysis for the Physical Sciences. (McGraw-Hill).

BINNIG, G., ROHRER, H., GERBER, C. and WEIBEL, E. (1983). Phys. Rev. Lett. **50**, 120.

BOHR, J., FEIDENHANS'L, R., NIELSEN, M., TONEY, M., JOHNSON, R.L. and ROBINSON, I.K. (1985). Phys. Rev. Lett. **54**, 1275.

BOHR, J., FEIDENHANS'L, R., NIELSEN, M., TONEY, M., JOHNSON, R.L. and ROBINSON, I.K. (1986). Phys. Rev. Lett. **56**, 2878.

BRINGANS, R.D. AND HÖCHST, H. (1982). Phys. Rev. B**25**, 1081.

BRINGANS, R.D., UHRBERG, R.I.G.,BACHRACH, R.Z. and NORTHRUP, J.E. (1986). J. Vac. Sci. Technol. A**4**, 1380.

CHADI, D.J. and CHIANG, C. (1981). Phys. Rev. B**23**, 1843.

CHEN, P., BOLMONT, D. and SÉBENNE (1982). Solid State Commun. **44**, 1191.

CHIPMAN, D.R. (1960). J. of Appl. Phys. **31**, 2012.

CHOU, M.Y., COHEN, M.L., and LOUIE, S.G. (1985). Phys. Rev. B**32**,7979.

CULBERTSON, R.J., FELDMAN, L.C. and SILVERMAN, P.J. (1980). Phys. Rev. Lett. **45**, 2043.

CULBERTSON, R.J., KUK, Y. and FELDMAN, L.C. (1986). Surf. Sci. **167**, 127.

DiCENZO, S.B., BENNETT, P.A., TRIBULA, D., THIRY, P., WERTHEIM, G.K. and ROWE, J.E. (1985). Phys. Rev. B**31**, 2330.

DOSCH, H. (1987). Phys. Rev. B**35**, 2137.

DOSCH, H., BATTERMAN, B.W. and WACK, D.C. (1986). Phys. Rev. Lett. **56**, 1144.

EISENBERGER, P. and MARRA, W.C. (1981). Phys. Rev. Lett. **46**, 1081.

ESTRUP, P.J. and MORRISON, J. (1964). Surf. Sci. **2**, 465.

FARNSWORTH, H.E., SCHLIER, R.E. and DILLON, J.A. (1959). J. Phys. Chem. Solids **8**, 116.

FEIDENHANS'L, R. (1986). Ph. D. Thesis (Aarhus University) (Available as Report Risø-M-2569 on request to Risø Library, DK-4000 Roskilde, Denmark).

FEIDENHANS'L, R., SKOV PEDERSEN, J., NIELSEN, M., GREY, F. and JOHNSON, R.L. (1986). Surf. Sci. **178**, 927.

FUOSS, P.H., LIANG, K.S. and EISENBERGER, P. (1986). Synchrotron Radiation Research: Advances in Surfaces and Low-Dimensional Science. Ed.: R.Z. Bachrach (Plenum).

GODDARD, W.A. III and HARDING, L.B. (1978). Ann. Rev. Phys. Chem. **29**, 363.

GOSSMANN, H.-J., BEAN, J.C., FELDMAN, L.C., McRAE, E.G. and ROBINSON, I.K. (1985). Phys. Rev. Lett. **55**, 1106.

GREY, F. (1986). Thesis, University of Copenhagen, unpublished.

GREY, F., JOHNSON, R.L., SKOV PEDERSEN, J., FEIDENHANS'L, R., and NIELSEN, M. (1987). The Structure of Surfaces II, Ed.: J.F. van der Veen and M.A. van Hove (Springer Verlag, Berlin) p. 292.

HAMERS, R.J., TROMP, R.M. and DEMUTH, J.E. (1987). Surf. Sci. **181**, 346.

HANEMAN, D. (1961). Phys. Rev. **121**, 1093.

HANEMAN, D. (1982). Adv. in Phys. **31**, 165.

HANEMAN, D. (1987). Rep. Progr. Phys. **50**, 1045.

HANSSON, G.V., BACHRACH, R.Z., BAUER, R.S. and CHIARADIA, P. (1981). Phys. Rev. Lett. **46**, 1033.

HANSSON, G.V., NICHOLLS, J.M., MÅRTENSSON, P. and UHRBERG, R.I.G. (1986). Surf. Sci. **168**, 105.

HARRISON, W.A. (1980). Electronic Structure (W.H. Freeman and Co., San Francisco).

HECHT, E. (1975). Optics (McGrae-Hill, New York) p. 40.

HIGASHIYAMA, K., KONO, S., SAKURAI, H. and SAGAWA, T. (1986). Surf. Sci. **175**, L794.

HIGASHIYAMA, K., PARK, C.Y. and KONO, S. (1987). The Structure of Surfaces II, E.: J.F. van der Veen and M.A. van Hove (Springer Verlag, Berlin) p. 346.

HIMPSEL, F.J., MARCUS, P.M., TROMP, R., BATRA, I.P., COOK, M.R., JONA, F. and LIU, H. (1984). Phys. Rev. **B30**, 2257.

HOLLAND, B.W., DUKE, C.B. and PATON, A. (1984). Surf. Sci. **140**, L269.

ICHIKAWA, T. (1983). Solid State Comm. **46**, 827.

ICHIKAWA, T. and INO, S. (1978). Solid State Comm. **27**, 483.

ICHIKAWA, T. and INO, S. (1981). Surf. Sci. **105**, 395.

JONES, R. (1987). J. Phys. **C20**, L271.

KAHN, A. (1983). Surf. Sci. Rep. **3**, 193.

KEATING, P.N. (1966). Phys. Rev. **145**, 637.

KINOSHITA, T., KONO, S. and SAGAWA, T. (1985). Phys. Rev. **B32**, 2714.

KINOSHITA, T., KONO, S. and SAGAWA, T. (1986). Phys. Rev. **B34**, 3011.

LANDER, J.J., GOBELI, G.W. and MORRISON, J. (1963). J. Appl. Phys. **34**, 2298.

de LAUNAY, J. (1956). Solid State Physics Vol.2, p. 223. Ed.: F. Seitz and D. Turnbull (Acad. Press).

Le LAY, G. and MÉTOIS, J.J. (1983). Appl. of Surf. Sci. **17**, 131.

Le LAY, G. and MÉTOIS, J.J. (1984). J. de Physique (Paris) Colloque **45**, C5-427.

LONSDALE, K. (Editor) (1962). International Tables for X-ray Crystallography Vol.III (Kynoch Press, England).

MARÉE, P.M.J., NAKAGAWA, K. and van der VEEN, J.F. (1987) to be published.

MARRA, W.C., EISENBERGER, P. and CHO, A.Y. (1979). J. Appl. Phys. **50**, 6927.

MARTIN, R.M. (1970). Phys. Rev. **B1**, 4005.

McKINLEY, A., WILLIAM, R.H., PARKE, A., and SRIVASTAVA, G.P. (1981) Vacuum **31**, 549.

McRAE, E.G. (1983). Phys. Rev. B28, 2305.

MÉTOIS, J.J. and Le LAY, G. (1983). Surf. Sci. **133**, 422.

NICHOLLS, J.M., MÅRTENSSON, P. and HANSSON, G.V. (1985a). Phys. Rev. Lett. **54**, 2363.

NICHOLLS, J.M., MÅRTENSSON, P., HANSSON, G.V. and NORTHRUP, J.E. (1985b). Phys. Rev. B32, 1333.

NICHOLLS, J.M., HANSSON, G.V., UHRBERG, R.I.G. and FLODSTRÖM, S.A. (1986). Phys. Rev. B33, 5555.

NICHOLLS, J.M., REIHL, B. and NORTHRUP, J.E. (1987). Phys. Rev. Lett. B35, 4137.

NIELSEN, O.H., MARTIN, R.M., CHADI, D.J. and KUNC, K. (1983). J. Vac. Sci. Technol. **B1**, 714.

NORTHRUP, J.E. (1984). Phys. Rev. Lett. 53, 683.

NORTHRUP, J.E. (1986). Phys. Rev. Lett. 57, 154.

NORTHRUP, J.E. (1987). Proc. of the 18'th Intern. Conf. on the Physics of Semiconductors. Ed.: O. Engström (World Scientific, Singapore) p. 61.

NORTHRUP, J.E. and COHEN, M.L. (1982a). Phys. Rev. Lett. 49, 1349.

NORTHRUP, J.E. and COHEN, M.L. (1982b). J. Vac. Sci. Technol. 21, 333.

NORTHRUP, J.E. and COHEN, M.L. (1983). Phys. Rev. B27, 6553.

NORTHRUP, J.E., IHM, J. and COHEN, M.L. (1981). Phys. Rev. Lett. **47**, 1910.

OLMSTEAD, M.A. (1987). Surf. Sci. Rep. **6**, 159.

PALMBERG, P.W. and PERIA, W.T. (1967). Surf. Sci. **6**, 57.

PANDEY, K.C. (1981). Phys. Rev. Lett. **47**, 1913.

PANDEY, K.C. (1982). Phys. Rev. Lett. **49**, 223.

PAULING, L. (1948). The Nature of the Chemical Bond (Cornell Univ. Press) p. 179.

PEARSON, E., HALICIOGLU, T. and TILLER, W.A. (1986). Surf. Sci. **168**, 46.

PERFETTI, P., NICHOLLS, J.M. and REIHL, B. (1987). Phys. Rev. B **36**, 6160.

POLLMANN, J., KRÜGER, P. and MAZUR, A. (1987). Vac. Sci. Technol. B5, 945.

QIAN, G.-X. and CHADI, D.J. (1986) J. Vac. Sci. Technol. B4, 1079.

QIAN, G.-X. and CHADI, D.J. (1987a). Phys. Rev. B35, 1288.

QIAN, G.-X. and CHADI, D.J. (1987b). J. Vac. Sci. Technol. A5, 906.

QIAN, G.-X. and CHADI, D.J. (1987c) unpublished.

ROBINSON, I.K. (1983). Phys. Rev. Lett. 50, 1145.

ROBINSON, I.K. (1986a). J. Vac. Sci. Technol. A4, 1309.

ROBINSON, I.K. (1986b). Handbook of Synchrotron Radiation, Vol.3. Ed.: D.E. Moncton and G.S. Brown (North-Holland, Amsterdam).

ROBINSON, I.K. (1986c). Phys. Rev. B33, 3830.

ROBINSON, I.K., WASKIEWICZ, W.K., FUOSS, P.H., STARK, J.B. and BENNETT, P.A. (1986). Phys. Rev. B33, 7013.

ROBINSON, I.K., WASKIEWICZ, W.K., FUOSS, P.H. and NORTON, L.J. (1988) Phys. Rev. B37, 4325.

SAITOH, M., OURA, K., ASANO, K., SHOJI, F. and HANAWA, T. (1985). Surf. Sci. 154, 394.

SAKAMA, H., KAWAZU, A. and UEDA, K. (1986). Phys. Rev. B34, 1367.

SAKURAI, H., HIGASHIYAMA, K., KONO, S. and SAGAWA, T. (1983). Surf. Sci. **134**, L550.

SATO, K., KONO, S., TERUYAMA, T., HIGASHIYAMA, K. and SAGAWA, T. (1985). Surf. Sci. **158**, 644.

SCHIFF, L.I. (1968). Quantum Mechanics (McGraw-Hill, New York).

SCHLÜTER, M., CHELIKOWSKY, J.R., LOUIE, S.G. and COHEN, M.L. (1975). Phys. Rev. **B12**, 4200.

SPENCE, J.C.H. (1983). Ultramicroscopy **11**, 117.

STEIF, A., TIERSTEN, S.C. and YING, S.C. (1987). Phys. Rev. **B35**, 857.

SWARTS, C.A., GODDARD, W.A.III and McGILL, T.C. (1980). J. Vac. Sci. Technol. **17**, 982.

SWARTS, C.A., McGILL, T.C. and GODDARD, W.A.III (1981) Surf. Sci. **110**, 400.

TAKAI, T., HALICIOGLU, T. and TILLER, W.A. (1985). Phys. Status Solidi **130b**, 475.

TAKAYANAGI, K. (1984). J. Microscopy **136**, 287.

TAKAYANAGI, K., TANISHIRO, Y., TAKAHASHI, M. and TAKAHASHI, S. (1985a). J. Vac. Sci. Technol. **A3**, 1502.

TAKAYANAGI, K., TANISHIRO, Y., TAKAHASHI, S. and TAKAHASHI, M. (1985b). Surf. Sci. **164**, 367.

TONNER, B.P., LI, H., ROBRECHT, M.J., ONELLION, M. and ERSKINE, J.L. (1987). Phys. Rev. B[illegible], 989.

TROMP, R.M. and van LEONEN, E.J. (1985). Surf. Sci. **155**, 441.

TROMP, R.M., van LEONEN, E.J., IWAMI, M. and SARIS, F.W. (1982). Solid State Comm. **44**, 971.

TROMP, R.M., SMIT, L. and van der VEEN, J.F. (1983). Phys. Rev. Lett. **51**, 1672.

UHRBERG, R.I.G., HANSSON, G.V., NICHOLLS, J.M. and FLODSTRÖM, S.A. (1982). Phys. Rev. Lett. **48**, 1032.

UHRBERG, R.I.G., HANSSON, G.V., NICHOLLS, J.M., PERSSON, P.E.S. and FLODSTRÖM, S.A. (1985). Phys. Rev. **B31**, 3805.

VANDERBILT, D. (1987a). Phys. Rev. Lett. **59**, 1456.

VANDERBILT, D. (1987b). Phys. Rev. **B36**, 6209.

VANDERBILT, D. (1987c). The structure of Surfaces II. Ed.: J.F. van der Veen and M.A. van Hove (Springer Verlag, Berlin) p. 276.

VANDERBILT, D. (1987d) unpublished results.

VANDERBILT, D. and LOUIE, S.G. (1984). Phys. Rev. **B29**, 7099.

van der VEEN, J.F. (1985). Surf. Sci. Rep. **5**, 199.

VINEYARD, G.H. (1982). Phys. Rev. **B26**, 4146.

WARREN, B.E. (1969). X-ray diffraction (Addison-Wesley, Reading, Mass.).

YANG, W.S. and JONA, F. (1984). Phys. Rev. **B29**, 899.

YOKOTSUKA, T., KONO, S., SUZUKI, S. and SAGAWA, T. (1983) Solid State Comm. **46**, 401.

YOKOTSUKA, T., KONO, S., SUZUKI, S. and SAGAWA, T. (1984). J. Phys. Soc. Jap. **53**, 696.

YIN, M.T. and COHEN, M.L. (1981). Phys. Rev. **B24**, 2303.

YIN, M.T. and COHEN, M.L. (1982). Phys. Rev. **B26**, 5668.

ZHANG, S.B., COHEN, M.L. and NORTHRUP, J.E. (1985). Surf. Sci. **157**, L303.

APPENDIX A: The Keating Model

The theories that existed in 1966 could not in a simple way give an explanation of the bulk elastic properties of covalent materials with zinc-blende structure. Keating (1966) proposed a new simple two parameter model which has a form that is in agreement with the crystal symmetry. In this model the elastic energy is given by:

$$E = \alpha \sum_{\substack{\text{all} \\ \text{bonds}}} (\vec{x}_{ij}^{\,2} - r_o)^2 + \beta \sum_{\substack{\text{all} \\ \text{bond} \\ \text{angles}}} (\vec{x}_{ij} \cdot \vec{x}_{ik} + \tfrac{1}{3} r_o^2)^2 \qquad \text{(A-1)}$$

where $\vec{x}_{ij}$ is the vector from atom i to atom j and r_o is the equilibrium bond length. The parameters α and β describe the energy cost of bond length and bond-angle deformation, respectively. The factor 1/3 in the last term gives an equilibrium bond configuration which is tetrahedral (Figure A-1).

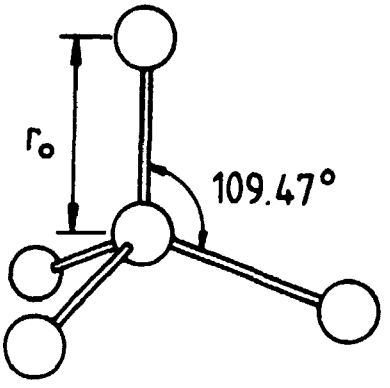

Figure A-1: The tetrahedral bond configuration.

The Keating model predicts a relation for the elastic constants which is found to be very well fulfilled for crystals with zinc-blende structure (Keating (1966) and Martin (1970)). The values of α and β given by Keating and Martin (Table A-1) were chosen to reproduce the experimental long-wavelength elastic constants. However, when investigating relaxations in surface reconstructions it is the behaviour at finite wave vector which is of importance. If the phonon spectrum is calculated by the Keating model and the long-wavelength values of α and β are used one sees that the transverse acoustic branch is inadequately described at the zone boundary. (Baraff et al. (1980)). The experimentally

Table A-1. Keating parameters from the long-wavelength (LW) limit and "short" wavelength (SW) limit. The unit of α and β is eV/Å^4.

	α	β	β/α	
Si(LW)	0.2053	0.0585	0.285	a)
Si(SW)	0.2009	0.0183	0.0912	b)
Ge(LW)	0.1508	0.0443	0.294	a)
Ge(SW)	0.1614	0.0132	0.0819	c)

a) Martin (1970)
b) Baraff et al. (1980)
c) Steif et al. (1987)

determined branch is much lower in energy at the zone boundary than the Keating model predicts. A better overall agreement, throughout the Brillouin zone, is obtained when using a value for the β-parameter which is about 3 times smaller than the long-wavelength value (Baraff et al. (1980) and Steif et al. (1987)). Table A-1 contains the parameters α and β for Si and Ge. A representative value of the ratio β/α for both Si and Ge is 0.10 which has been used in the calculations described in this thesis. This value is also in accordance with the value $\beta/\alpha = 0.098$ used by Qian and Chadi (1986) and the value $\beta/\alpha = 0.131$ estimated from ab-initio calculations of the phonon frequencies of Si (Jones (1987)).

In order to perform calculations on surface structures with more than one kind of atom a generalized form of (A-1) is introduced:

$$E = \alpha \sum_{\substack{\text{all}\\ \text{bonds}}} \left[\vec{x}_{ij}^{\,2} - (b_i+b_j)^2 \right]^2 + \beta \sum_{\substack{\text{all}\\ \text{bond}\\ \text{angles}}} \left[\vec{x}_{ij} \cdot \vec{x}_{ik} + \tfrac{1}{3}(b_i+b_j)(b_i+b_k) \right]^2 \qquad \text{(A-2)}$$

where b_i is the covalent radius of atom i. At this stage two points have to be considered: (1) α and β depend on atom type. (2) Some atoms are only bonded to three other atoms. The expression for the elastic energy in the Keating model is very simple and in order not to destroy the simplicity by speculative choices of parameters it was decided to try the most simple solutions to (1) and (2). Since, generally α and β are not known for bonds between different kind of atoms, they were chosen to have the same value as for the substrate bonds. Furthermore, the atoms with reduced coordination were also chosen to have tetrahedral equilibrium bond configurations. As shown below these choices gave relaxations that are in good agreement with the results from total-energy calculations.

The Keating calculation employs periodic boundary conditions parallel to the surface. At the interface between the surface reconstruction and the bulk a double layer fixed at ideal positions is used as the boundary condition. In the calculations it has to be specified which atoms are bonded to each other. The atomic positions are then determined by minimizing the elastic strain energy with respect to the atomic position. The form of the potential ensures that the minimum is well-defined.

The structure of the Si(111)$\sqrt{3} \times \sqrt{3}$-Si surface with adatoms at threefold coordinated sites above the second layer of substrate atoms (T_4 site) has been obtained by ab-initio total-energy calculations (Northrup (1986)). The calculations employ a repeated slab geometry with eight layers of atoms, with inversion symmetry, in each slab. The positions of the adatoms and the atoms in the outer three layer have been optimized (Figure A-2).

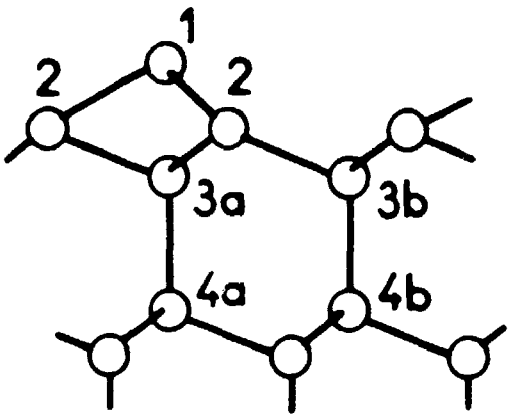

Figure A-2: The atom labelling of the $\sqrt{3} \times \sqrt{3}$-structure with adatoms at T_4 sites (side view).

The displacements are given in Table A-2 in units of a = 3.840 Å, the length of the basis vector in the 1×1 surface unit cell. The distances d_1 from the adatom to the first layer atoms and d_2 from the adatom to the atom just below are also displayed in Table A-2. The atomic positions have also been obtained by minimizing the Keating energy (present work). The same atoms have been relaxed, as in the total-energy calculations, and the displacements are given in Table A-2. There is an excellent agreement between the results of the two calculations. The main discrepancy is for the distances from the adatom to its nearest neighbours. This reflects that the Keating model is too simple to give a good description of the heavily distorted bonds of the adatoms.

Figure A-3 shows the Si(111)2 × 2-Si (T_4) surface and a labelling of the independent atoms is indicated. The atomic geometry has been determined by Vanderbilt (1987c) by ab-initio total-energy calculations. A slab geometry with eight layers of atoms in each slab was used and all atomic positions were optimized. The results are displayed in Table A-3 together

Table A-2. Atomic displacements of the Si(111)$\sqrt{3}\times\sqrt{3}$-Si (T_4) surface from total-energy calculations (Northrup (1986)) and Keating calculations. δr_i and δz_i are the radial and normal displacement of atom i, respectively. d_1 and d_2 are the distances from the adatom to the atoms in the first and second layer of the substrate, respectively. Distances are in units of a = 3.840 Å.

	Total Energy calc.	Keating Energy calc.
δr_2	-0.039	-0.038
δz_2	-0.021	-0.004
δz_{3a}	-0.102	-0.073
δz_{4a}	-0.066	-0.050
δz_{3b}	0.025	0.028
δz_{4b}	0.015	0.018
d_1	0.648	0.615
d_2	0.649	0.568

Sum of covalent radii: 0.612

with the results from a Keating calculations (present work) in which the atoms in the outer six layers have been relaxed. As for the Si(111)$\sqrt{3}\times\sqrt{3}$-Si surface good agreement is observed, but again some discrepancy is seen for the distances from the adatoms to the nearest neighbours. The most significant deviation for the relaxations is for the in-plane

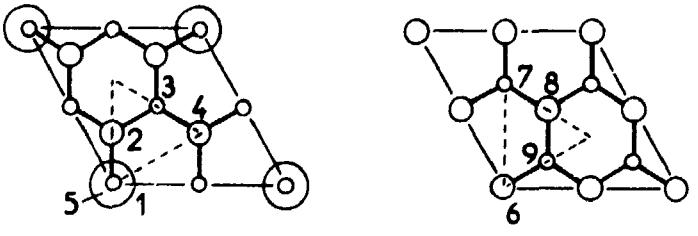

Figure A-3: Atom labelling in the irreducible unit of the 2×2 (T_4) adatom structure. Left-hand side: Adatoms and first bilayer. Right-hand side: Second bilayer.

Table A-3. The same as Table A-2, but for the Si(111) 2×2-Si (T_4) surface. The atom labelling is shown in Figure A-3.

	i	disp. vector	Total Energy calc.	Keating Energy calc.
δr_i:	2	$1/\sqrt{3}(1,2)$	-0.027	-0.041
	3	$1/\sqrt{3}(\bar{1},1)$	-0.022	-0.002
	8	$1/\sqrt{3}(\bar{1},1)$	0.004	0.000
	9	$1/\sqrt{3}(2,1)$	0.012	0.014
δz_i:	1		0.109	0.088
	2		-0.018	-0.007
	3		0.036	0.023
	4		0.067	0.025
	5		-0.102	-0.087
	6		-0.076	-0.069
	7		0.003	0.010
	8		0.020	0.018
d_1			0.642	0.614
d_2			0.619	0.583

Sum of covalent radii: 0.612

displacement of atom 3 and the displacement in the direction normal to the surface of atom 4. This is due to the lower coordination of atom 4 which has a dangling bond. This leads to an equilibrium bond configuration differing from tetrahedral. The Keating calculation does not take this into account. This point is discussed in detail in Section 3.4.

The conclusion of the above comparisons of atomic relaxations from total-energy and Keating calculations, is that it is possible to obtain reliable predictions of the atomic displacements from Keating calculations. It is a great advantage that these very simple calculations can be used instead of total-energy calculations. The computer time required to optimize the Keating energy of a structure is orders of magnitude smaller than the time required in a total-energy calculation. Therefore, structures with much larger unit cells can be handled. However, it should not be forgotten that the electronic contributions to the energy in the Keating model are only included in a global approximation. For properties other than the geometric structure more advanced calculations have to be performed.

APPENDIX B: Subsurface Relaxation in the Ge(001) 2 × 1 Structure by the Keating Model

The ideally terminated Ge(001) surface has a high density of dangling bonds (Figure B-1). The reconstruction of the surface consists of a dimerization of the surface atoms and it gives rise to a 2 × 1 structure (Figure B-1). The atomic geometry of this surface has been determined by grazing-incidence x-ray diffraction (Eisenberger and Marra (1981), Grey (1986) and Grey et al. (1987)). The best data set contains the in-plane intensity of 27 fractional-order reflections (Grey et al. (1987)). The intensity profiles in the direction

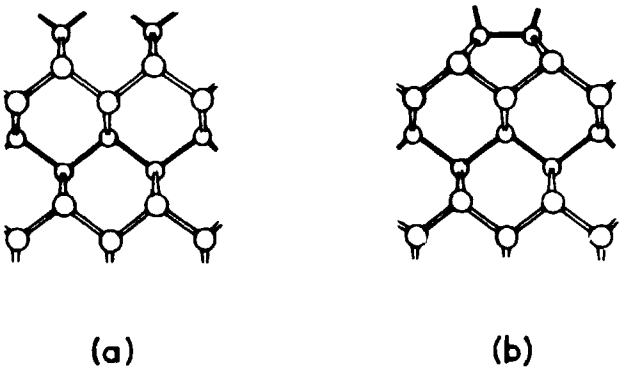

Figure B-1. Side view of the ideally terminated Ge(001) surface (a) and the Ge(001) 2 × 1 surface with a symmetric dimer (b).

normal to the surface of four fractional-order Bragg rods were also measured. The analysis of the in-plane structure factor intensities showed that a non-buckled, non-twisted dimer model with displacements of the second layer atoms is in agreement with experimental data (Figure B-2). The displacement of the dimer atoms is 0.206 ± 0.003 and the displacement of the second layer atoms is 0.019 ± 0.003. (In this appendix the displacements parallel to the surface are in unit of the surface lattice constant, a = 4.000 Å for Ge and a = 3.840 Å for Si. Displacements in the direction normal to the surface are in units of the bulk lattice constant a_0 = 5.658 Å for Ge and a_0 = 5.431 Å for Si).

The measured intensity variation along the fractional-order Bragg rods is shown as points in Figure B-3. The momentum transfer in the direction normal to the surface *l* is in units of the bulk reciprocal (001) lattice vector. The dramatic variation is due to the extent of the surface reconstruction in the direction normal to the surface. The analysis showed that significant relaxations are present down to the eighth layer of the substrate. The displacements of the final model are displayed in Table B-1.

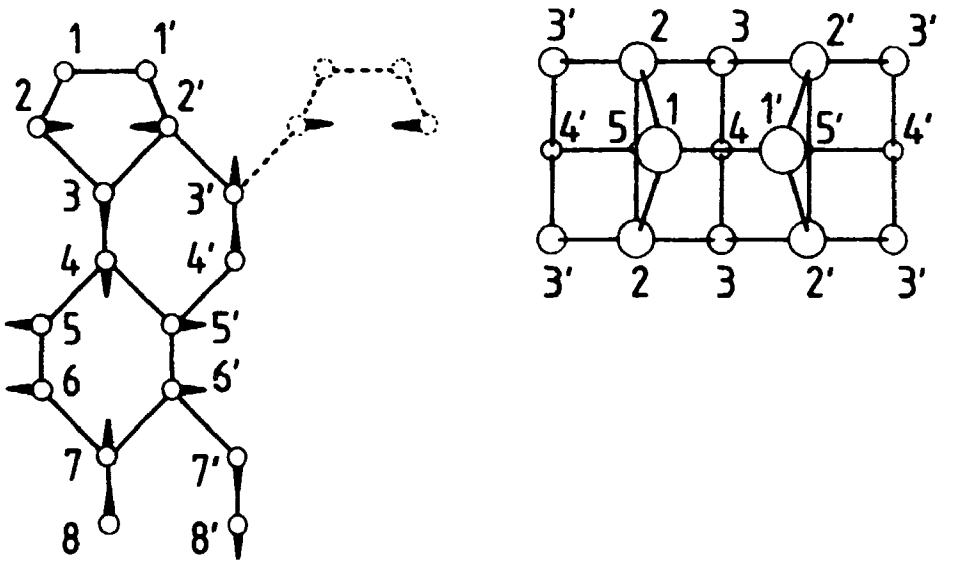

Figure B-2. Left-hand side: Side view of the dimer model. The atom labelling is shown and the directions of the displacements are indicated by arrows. Right-hand side: Top view of the model.

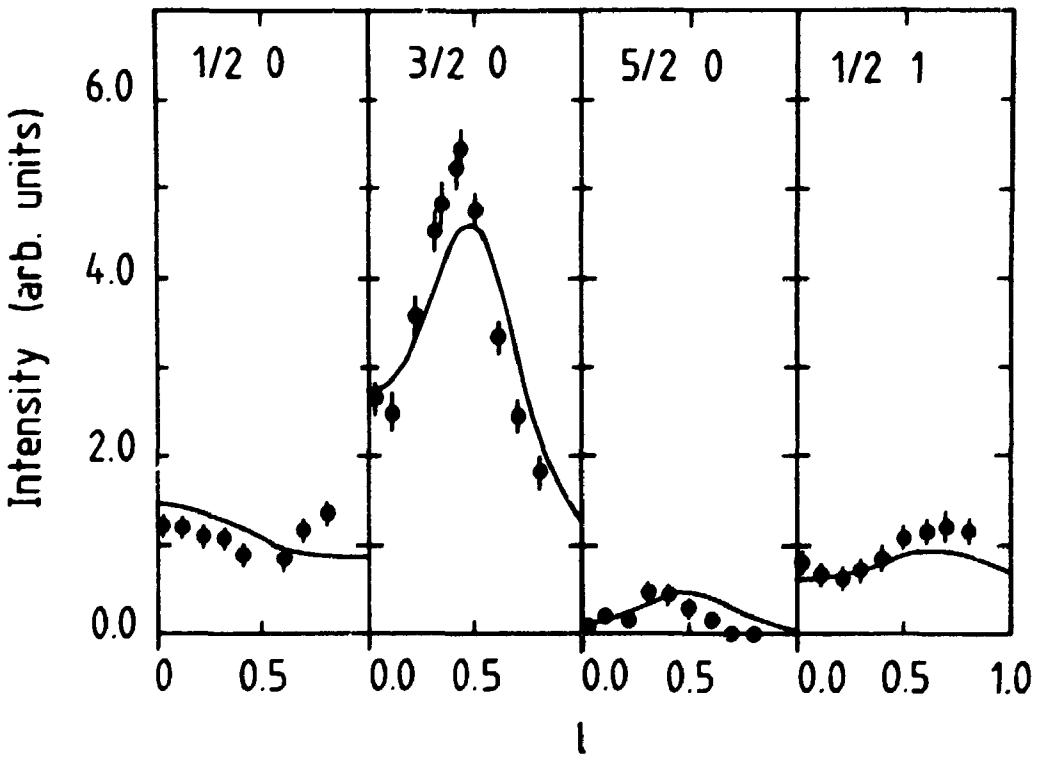

Figure B-3. The intensity variation along four of the fractional-order Bragg rods. The momentum transfer l in the direction normal to the surface is in units of the bulk reciprocal (00l) lattice vector. Experimental results are shown as points. The full curve is calculated from the structure determined by the Keating calculation.

Table B-1. Atomic displacements (Δx,Δz) for the dimer model. Δx is in units of $a = 4.000$ Å for Ge and $a = 3.840$ Å for Si. Δz is in units of $a_0 = 5.658$ Å for Ge and $a_0 = 5.431$ Å for Si.

* : a fixed parameter

**: a parameter fixed due to the symmetry

1): a parameter fixed and estimated from tight-binding and ab-initio total-energy calculations

a) X-ray diffraction experiment (Grey (1986)), Grey et al. (1987))

b) Keating calculation (present work)

c) Tight-binding calculation (Pollman et al. (1987))

d) Keating calculation for the long-wavelength parameters (Appelbaum and Hamann (1978))

e) Ab-initio total-energy calculation (Yin and Cohen (1981))

f) LEED experiment (Holland et al. (1984)).

	Ge(001)2×1				Si(001)2×1	
	Experiment [a]	Keating calculation[b] $\beta/\alpha = 0.10$	T.B. calculation[c]	Keating calculation[d] $\beta/\alpha = 0.32$	Ab-initio calculation[e]	LEED Experiment[f]
1	0.200(3), 0.0*	0.189,-0.028	0.115, 0.020	0.181,-0.027	0.149,-0.029	0.130, -0.046
1'	-0.200(3), 0.0*	-0.189,-0.028	-0.281,-0.092	-0.181,-0.027	-0.270,-0.086	-0.234, -0.113
2	0.020(3), 0.0*	0.026,-0.002	0.014, 0.015	0.031,-0.001	0.024,-0.009	0.024, -0.004
2'	-0.020(3), 0.0*	-0,026,-0.002	0.014,-0.005	-0.031,-0.001	-0.030, 0.004	-0.027, 0.010
3	0.0** ,-0.027(4)	0.0**,-0.024	-0.010,-0.006	0.0**,-0.024	-0.002,-0.034	-0.004[1], 0.027[1]
3'	0.0** , 0.027(4)	0.0**, 0.022	-	0.0**, 0.024	-0.009, 0.024	-0.001[1], 0.024[1]
4	0.0** ,-0.027(4)	0.0**,-0.017	0.010, 0.008	0.0**,-0.013	0.016,-0.025	0.007[1],-0.021[1]
4'	0.0** , 0.027(4)	0.0**, 0.016	-	0.0**, 0.013	-0.016, 0.019	0.003[1] 0.018[1]
5	-0.012(2), 0.0*	-0.013, 0.000	-	-0.007 0.0*	-	-
5'	0.012(2), 0.0*	0.013, 0.000	-	0.007 0.0*	-	-
6	-0.012(2), 0.0*	-0.004, 0.000	-	-	-	-
6'	0.012(2), 0.0*	0.004, 0.000	-	-	-	-
7	0.0** , 0.010(5)	0.0**, 0.003	-	-	-	-
7'	0.0** ,-0.010(5)	0.0**,-0.002	-	-	-	-
8	0.0** , 0.010(5)	0.0**, 0.002	-	-	-	-
8'	0.0** ,-0.010(5)	0.0**,-0.002	-	-	-	-

The brackets indicate the atoms which have been restricted to move together in the model, in order to reduce the number of parameters. The direction of the displacements are shown by arrows in Figure B-2, and they can be interpreted as elastic relaxations due to the formation of the dimer bond. These aspects have been further elucidated by a calculation and minimization of the elastic strain described by the Keating model (Keating (1966)). The details of the calculations and the choice of parameters are discussed in Appendix A. In the minimization of the strain energy the position of 12 layers of atoms were optimized. The displacements in the two deepest layers were negligible which shows that the structure is fully relaxed. The displacements of the upper eight layers are shown in Table B-1, and they are in good agreement with the experimentally determined displacements. The table also contains the structure determined by a tight-binding calculation (Pollmann et al. (1987)), by a previous Keating calculation for the value of the elastic parameters from the long-wavelength limit (Appelbaum and Hamann (1978)). The displacements for the similar Si(001)2 × 1 surface, determined by ab-initio total-energy calculations (Yin and Cohen (1981)) and by a LEED experiment (Holland et al. (1984)), are also shown. In contrast to the x-ray diffraction experiment, the total-energy calculations and the LEED experiment are in favour of a buckled dimer model.

The structure determined by the Keating calculation have been used to calculate the intensity variation shown as a full curve in Figure B-3. Only a scale factor and a common Debye-Waller factor for the Ge atoms has been least-square fitted and the agreement $\chi^2 = 5.0$ was obtained compared to the value $\chi^2 = 2.7$ for the model by Grey et al. (1987). The agreement between the experimental data and the curves is quite good and it can be concluded that the Keating model also for this structure give atomic relaxations which are in agreement with experiment.

APPENDIX C: Data: Rodscans of the α-Phase of the Ge(111) $\sqrt{3}\times\sqrt{3}$-Sn and Ge(111) $\sqrt{3}\times\sqrt{3}$-Pb Surfaces

Measured structure factor intensities $|F_{hkl}^{exp}|^2$, experimental uncertainties σ_{hk} and model structure factor intensities $|F_{hkl}^{mod}|^2$ for the best model. See Chapter 2 for more information.

Ge(111)$\sqrt{3}\times\sqrt{3}$-Sn

h	k	l	$\lvert F_{hkl}^{exp}\rvert^2 +/- \sigma_{hk}$	$\lvert F_{hkl}^{mod}\rvert^2$
1/3	1/3	0.108	24.96+/-1.05	22.60
"	"	0.164	20.68+/-1.05	20.77
"	"	0.220	17.59+/-1.05	18.86
"	"	0.274	18.15+/-1.05	17.39
"	"	0.330	15.62+/-1.05	16.57
"	"	0.384	17.27+/-1.05	16.49
"	"	0.440	17.91+/-1.05	16.87
"	"	0.494	16.95+/-1.05	17.20
2/3	2/3	0.108	8.17+/-1.05	6.96
"	"	0.164	6.06+/-1.05	3.38
"	"	0.220	4.23+/-1.05	1.74
"	"	0.274	4.52+/-1.05	3.45
"	"	0.330	9.93+/-1.05	8.84
"	"	0.384	18.73+/-1.05	16.27
"	"	0.440	23.77+/-1.05	23.91
"	"	0.494	27.60+/-1.05	28.82
4/3	1/3	0.128	20.03+/-1.05	18.56
"	"	0.192	13.46+/-1.05	15.80
"	"	0.240	10.50+/-1.05	13.44
"	"	0.294	11.55+/-1.05	12.09
"	"	0.348	13.38+/-1.05	13.33
"	"	0.404	17.19+/-1.05	17.62
"	"	0.458	24.41+/-1.05	23.71
"	"	0.494	24.12+/-1.05	27.94
1/3	4/3	0.128	3.83+/-1.05	4.43
"	"	0.182	1.95+/-1.05	1.35
"	"	0.240	0.37+/-1.05	0.49
"	"	0.294	2.11+/-1.05	1.73
"	"	0.348	2.64+/-1.05	3.98
"	"	0.404	4.42+/-1.05	6.12
"	"	0.458	7.30+/-1.05	7.06
"	"	0.494	6.77+/-1.05	6.88
5/3	2/3	0.108	5.62+/-1.05	7.52
"	"	0.164	4.21+/-1.05	6.63
"	"	0.220	7.90+/-1.05	7.30
"	"	0.274	9.24+/-1.05	8.59
"	"	0.330	7.63+/-1.05	9.58
"	"	0.384	5.82+/-1.05	9.45
"	"	0.440	5.96+/-1.05	7.99
"	"	0.494	3.15+/-1.05	5.69
2/3	5/3	0.108	23.37+/-1.05	21.16
"	"	0.164	23.30+/-1.05	22.28
"	"	0.220	23.10+/-1.05	20.89
"	"	0.274	15.73+/-1.05	17.67
"	"	0.330	12.45+/-1.05	13.57
"	"	0.384	14.06+/-1.05	10.20
"	"	0.440	13.72+/-1.05	8.37
"	"	0.494	12.52+/-1.05	8.50

Ge(111)$\sqrt{3}\times\sqrt{3}$-Pb

h	k	l	$\lvert F^{exp}_{hkl}\rvert^2 +/- \sigma_{hk}$	$\lvert F^{mod}_{hkl}\rvert^2$
1/3	1/3	0.080	44.82+/-3.24	43.84
"	"	0.142	41.90+/-3.24	44.13
"	"	0.208	41.68+/-3.24	43.74
"	"	0.272	40.66+/-3.24	42.19
"	"	0.340	38.71+/-3.24	39.40
"	"	0.404	37.55+/-3.24	36.39
"	"	0.476	35.44+/-3.24	33.49
"	"	0.538	33.12+/-3.24	31.74
2/3	2/3	0.080	23.81+/-3.24	19.99
"	"	0.142	21.53+/-3.24	16.76
"	"	0.208	20.38+/-3.24	14.46
"	"	0.272	18.48+/-3.24	15.34
"	"	0.340	20.38+/-3.24	19.91
"	"	0.404	28.58+/-3.24	25.86
"	"	0.476	31.43+/-3.24	31.09
"	"	0.538	30.10+/-3.24	32.28
4/2	1/3	0.080	31.01+/-3.24	24.71
"	"	0.142	27.04+/-3.24	25.57
"	"	0.208	22.74+/-3.24	24.02
"	"	0.272	19.86+/-3.24	21.95
"	"	0.340	20.98+/-3.24	21.54
"	"	0.404	26.78+/-3.24	23.93
"	"	0.476	28.47+/-3.24	28.88
"	"	0.536	26.28+/-3.24	32.68
1/3	4/3	0.080	8.30+/-3.24	13.04
"	"	0.142	5.06+/-3.24	9.17
"	"	0.208	4.77+/-3.24	7.78
"	"	0.272	6.21+/-3.24	8.87
"	"	0.340	6.98+/-3.24	10.98
"	"	0.404	9.19+/-3.24	12.10
"	"	0.476	9.10+/-3.24	11.40
"	"	0.536	7.21+/-3.24	9.79
5/3	2/3	0.080	12.71+/-3.24	11.31
"	"	0.142	11.84+/-3.24	10.56
"	"	0.208	12.33+/-3.24	11.49
"	"	0.272	13.75+/-3.24	12.63
"	"	0.340	12.82+/-3.24	12.48
"	"	0.404	10.15+/-3.24	10.47
"	"	0.476	7.97+/-3.24	6.85
"	"	0.536	6.66+/-3.24	4.07
2/3	5/3	0.080	24.67+/-3.24	20.36
"	"	0.142	23.57+/-3.24	23.02
"	"	0.208	21.61+/-3.24	23.02
"	"	0.272	18.01+/-3.24	20.27
"	"	0.340	14.52+/-3.24	15.95
"	"	0.404	13.04+/-3.24	12.59
"	"	0.476	12.82+/-3.24	11.24
"	"	0.536	12.39+/-3.24	12.00

APPENDIX D: Data: In-plane Intensities for the Ge(111) 5 × 5-Sn Reconstruction

In the figure the stars indicate the positions of the integer-order reflections. The filled circles are the fractional-order reflections and the area is proportional to the measured structure factor intensity $|F_{hk}^{exp}|^2$. The table contains the measured structure factor intensity $|F_{hk}^{exp}|^2$, experimental uncertainties σ_{hk} and model structure factor intensities $|F_{hk}^{mod}|^2$ for the best model. See Chapter 3 for more information.

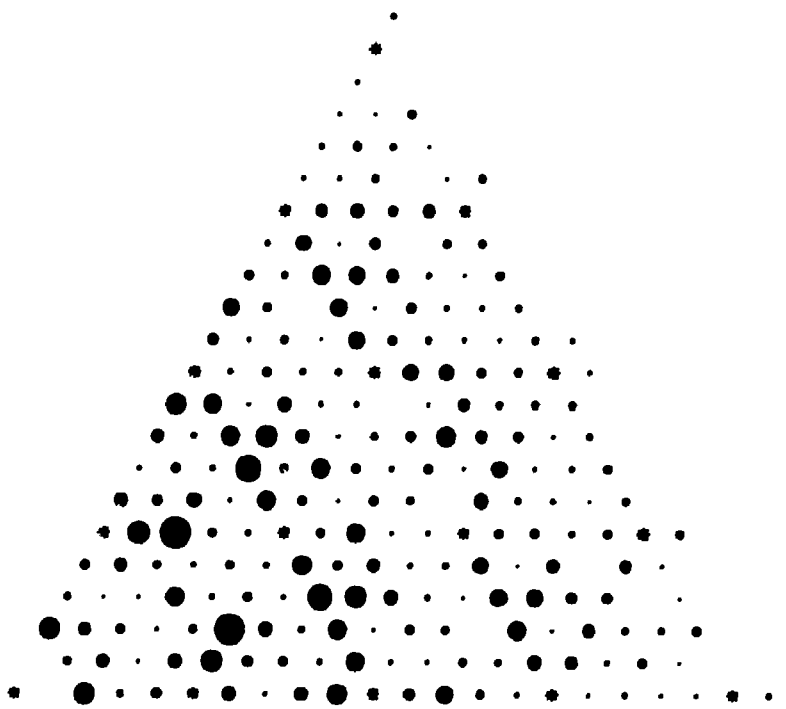

5·h	5·k	$\lvert F_{hk}^{exp}\rvert^2 +/- \sigma_{hk}$	$\lvert F_{hk}^{mod}\rvert^2$
2	0	21.25+/-4.31	28.04
3	0	2.10+/-0.48	2.51
4	0	4.93+/-0.94	8.49
6	0	9.56+/-0.98	10.65
7	0	0.60+/-0.14	0.66
8	0	6.83+/-0.73	5.78
9	0	20.18+/-2.06	21.30
11	0	5.60+/-0.66	5.68
12	0	12.57+/-1.36	11.42
13	0	3.11+/-0.46	0.68
14	0	0.83+/-0.42	0.90
16	0	0.38+/-0.47	0.40
17	0	1.08+/-0.49	0.34
18	0	0.30+/-0.50	0.88
19	0	0.40+/-0.50	0.40
21	0	1.07+/-0.45	1.51
1	1	2.64+/-0.72	5.98
2	1	7.01+/-1.42	7.25
3	1	0.15+/-0.23	0.06
4	1	8.15+/-0.83	7.20
5	1	23.86+/-2.49	24.01
6	1	4.65+/-0.51	3.60
7	1	4.24+/-0.47	4.06
8	1	1.06+/-0.20	1.17
9	1	17.88+/-1.85	16.79
10	1	0.67+/-0.28	0.11
11	1	0.51+/-0.32	0.27
12	1	2.60+/-0.36	1.96
13	1	1.51+/-0.40	1.27
14	1	9.28+/-1.13	6.76
15	1	6.66+/-0.92	6.25
16	1	0.48+/-0.48	0.30
17	1	2.98+/-0.50	2.55
18	1	0.10+/-0.50	0.22
19	1	0.00+/-0.49	0.07
2	2	3.80+/-0.85	1.28
3	2	0.30+/-0.09	0.23
4	2	2.65+/-0.31	1.93
5	2	48.21+/-4.87	45.97
6	2	9.24+/-0.87	10.58
7	2	1.23+/-0.33	0.07
8	2	16.62+/-1.68	14.53
9	2	0.26+/-0.26	0.02
10	2	3.28+/-0.43	2.10
11	2	2.62+/-0.41	3.10
12	2	0.00+/-0.38	0.10
13	2	16.79+/-1.85	11.86
14	2	0.09+/-0.45	0.09
15	2	8.37+/-0.95	6.38
16	2	1.87+/-0.49	2.95
17	2	1.40+/-0.50	2.51
18	2	2.97+/-0.50	2.34
3	3	17.63+/-1.72	14.68
4	3	0.76+/-0.13	1.10
5	3	3.39+/-0.41	2.04
6	3	0.62+/-0.17	0.78
7	3	34.13+/-3.44	26.00
8	3	22.56+/-2.30	26.25
9	3	9.06+/-0.99	8.44
10	3	1.26+/-0.26	1.52
11	3	0.11+/-0.37	0.46
12	3	12.71+/-1.30	13.43
13	3	12.67+/-1.41	10.02
14	3	4.30+/-0.56	3.48
15	3	4.19+/-0.58	4.24
16	3	0.00+/-0.50	0.36
17	3	0.20+/-0.50	0.37
4	4	2.84+/-0.59	2.73
5	4	1.30+/-0.27	1.21
6	4	16.79+/-1.74	12.55
7	4	2.94+/-0.39	1.67
8	4	7.63+/-0.79	7.76
9	4	0.83+/-0.32	1.14
10	4	1.65+/-0.36	1.52
11	4	12.61+/-1.27	13.76
12	4	0.17+/-0.43	0.13
13	4	7.35+/-0.83	5.57
14	4	0.00+/-0.48	0.30
15	4	7.04+/-0.79	5.82
16	4	0.30+/-0.50	0.18
6	5	2.93+/-0.38	2.00
7	5	17.67+/-1.81	14.71
8	5	0.31+/-0.31	0.79
9	5	0.84+/-0.35	1.06
11	5	3.21+/-0.51	3.13
12	5	3.71+/-0.45	3.39
13	5	1.05+/-0.48	1.07
14	5	2.56+/-0.49	2.92
16	5	2.38+/-0.50	2.66
6	6	0.16+/-0.27	0.44
7	6	4.15+/-0.50	4.92
8	6	1.87+/-0.35	2.39
9	6	0.00+/-0.38	0.09
10	6	10.82+/-1.17	12.73
11	6	1.52+/-0.45	1.40
12	6	0.94+/-0.47	0.45
13	6	0.20+/-0.49	0.22
14	6	2.79+/-0.50	2.64
15	6	0.00+/-0.50	0.02
7	7	0.90+/-0.34	0.65
8	7	3.79+/-0.46	2.92
9	7	0.33+/-0.41	0.08
10	7	10.70+/-1.15	14.45
11	7	0.65+/-0.47	0.38
12	7	0.78+/-0.49	0.81
13	7	2.69+/-0.50	3.74
8	8	17.27+/-1.81	12.14
9	8	6.07+/-0.70	5.82
10	8	3.81+/-0.46	5.07
11	8	0.39+/-0.19	0.58
12	8	1.79+/-0.40	1.82
9	9	1.49+/-0.28	1.24
10	9	2.61+/-0.39	2.43
11	9	2.08+/-0.40	2.14
11	10	0.60+/-0.50	1.44

APPENDIX E: Data: In-plane Intensities for the Ge(111) 7 × 7-Sn Reconstruction

In the figures the stars indicate the positions of the integer-order reflections. The filled circles are the fractional-order reflections and the area is proportional to the measured structure factor intensity $|F_{hk}^{exp}|^2$. The data for Si(111) 7×7 (Robinson et al. (1988)) is displayed in a figure for comparison. The table contains the measured structure factor intensity $|F_{hk}^{exp}|^2$, experimental uncertainties σ_{hk} and model structure factor intensities $|F_{hk}^{mod}|^2$ for the best model. See Chapter 3 for more information.

Data set Ge(111) 7 × 7-Sn no. 1:

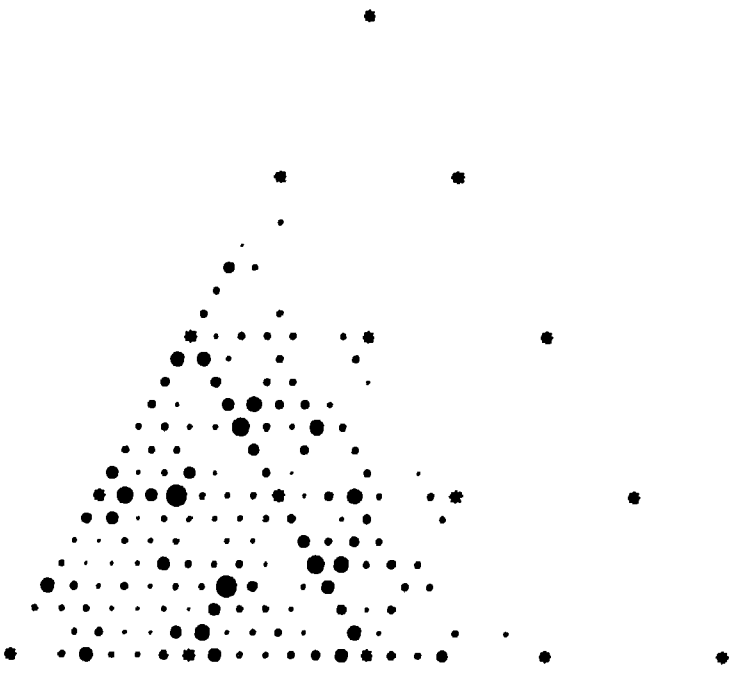

Data set Ge(111) 7 × 7-Sn no. 2:

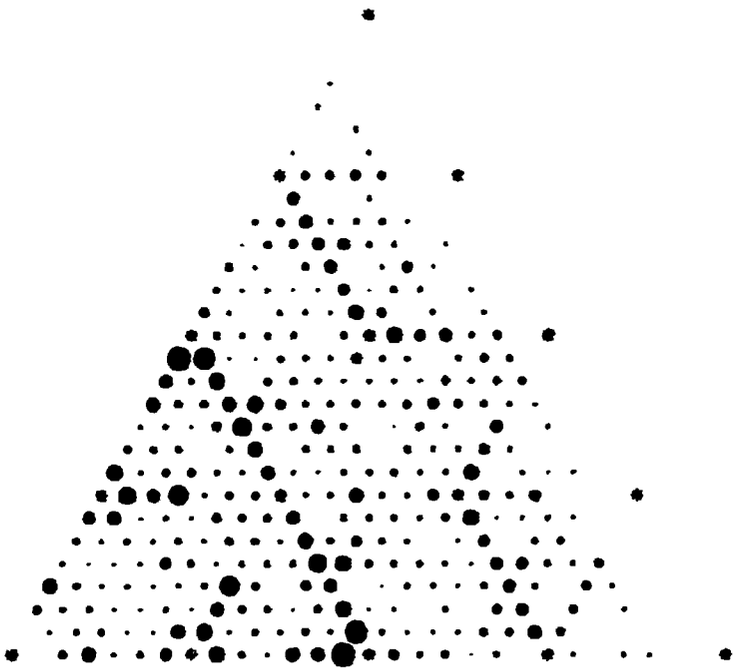

Data set Ge(111) 7 × 7-Sn no. 3:

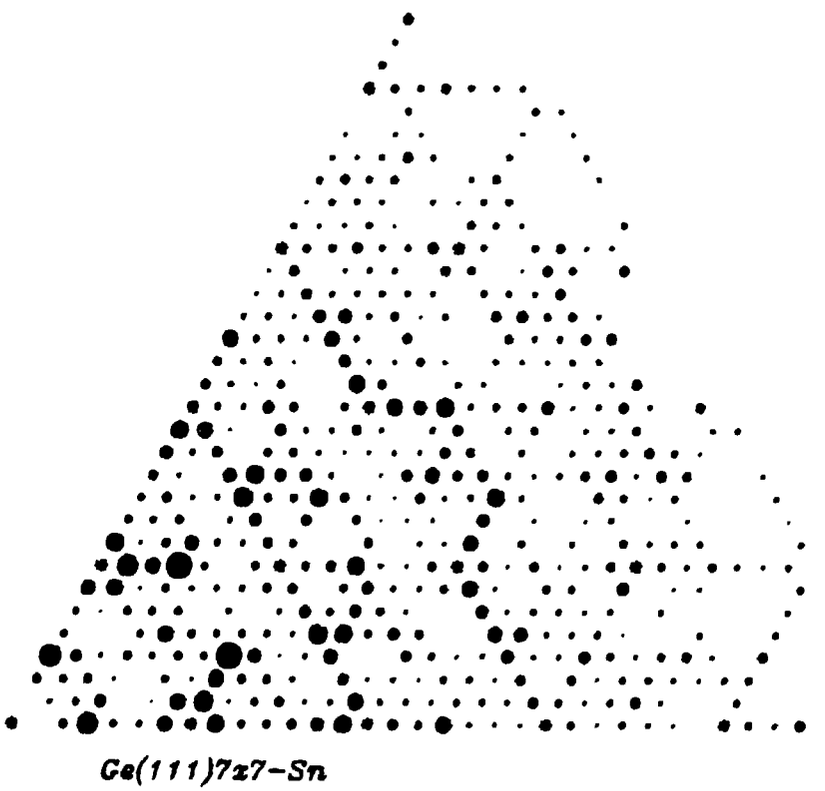

Data set Si(111) 7×7:

(Robinson et al. (1987))

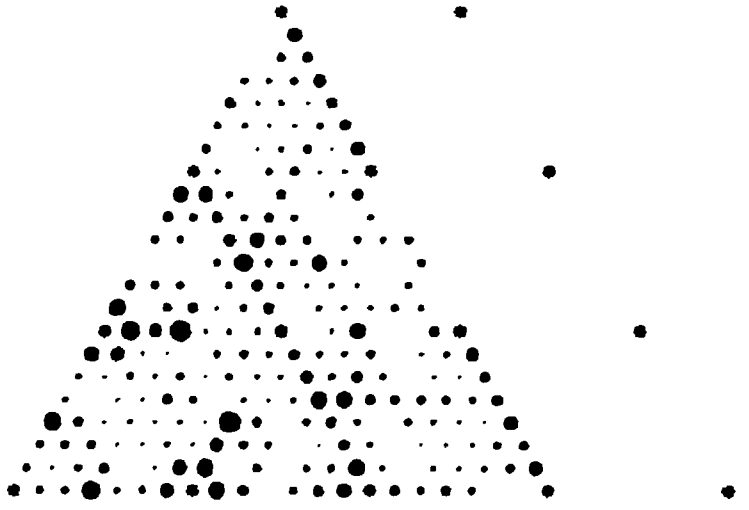

Si(111)7x7

Data set Ge(111) 7×7-Sn no. 1:

7·h	7·k	$\lvert F_{hk}^{exp}\rvert^2 +/- \sigma_{hk}$	$\lvert F_{hk}^{mod}\rvert^2$
2	0	3.26+/-1.00	4.48
3	0	23.60+/-5.00	29.08
4	0	2.50+/-0.40	3.36
5	0	1.50+/-0.24	2.04
6	0	10.72+/-1.72	16.01
8	0	16.48+/-1.70	13.24
9	0	2.69+/-0.28	2.87
10	0	2.39+/-0.40	2.46
11	0	5.27+/-0.52	4.68
12	0	8.00+/-0.88	7.35
13	0	22.54+/-2.30	21.76
15	0	4.69+/-0.46	5.40
17	0	13.13+/-1.70	7.95
18	0	0.05+0-0.30	0.20
16	0	3.22+/-0.40	3.64
3	1	5.90+/-0.88	7.19
4	1	0.12+/-0.20	0.00
6	1	14.87+/-1.50	13.13
7	1	26.80+/-2.70	26.15
8	1	0.65+/-0.18	0.52
9	1	2.94+/-0.44	1.39
10	1	4.88+/-0.62	5.12
13	1	21.42+0-2.30	21.20
14	1	0.72+/-0.34	0.40
17	1	2.72+/-0.40	2.92
19	1	1.18+/-0.70	0.58
2	2	3.00+/-0.60	3.48
3	2	0.84+/-0.18	0.44
4	2	0.20+/-0.20	0.03
5	2	1.94+/-0.26	1.78
6	2	0.16+/-0.20	0.02
7	2	14.74+/-1.50	15.28
8	2	2.01+/-0.50	2.55
9	2	3.18+/-0.40	3.11
12	2	9.28+/-1.74	9.99
13	2	1.06+/-0.54	0.15
14	2	4.02+/-1.80	0.35
3	3	2.53+/-0.56	1.41
5	3	1.88+/-0.70	2.04
6	3	2.39+/-0.20	1.93
7	3	55.85+/-5.54	37.75
8	3	12.65+/-1.36	11.20
11	3	18.44+/-1.96	17.75
14	3	4.41+/-0.50	5.14
15	3	3.31+/-0.42	3.66
4	4	17.76+/-1.80	13.93
5	4	3.16+/-0.34	3.30
6	4	1.86+/-0.40	1.76
7	4	3.60+/-0.80	1.52
10	4	37.26+/-3.80	26.98
11	4	27.60+/-2.80	24.22
12	4	3.63+/-0.50	3.46
13	4	4.76+/-0.54	5.98
14	4	3.62+/-0.64	1.87
6	5	1.18+/-0.40	1.25
7	5	1.02+/-0.36	0.12
9	5	13.82+/-1.44	10.43
10	5	3.63+/-0.52	3.34
11	5	7.93+/-0.96	6.72
12	5	3.92+/-0.72	3.50
6	6	1.76+/-0.30	1.67
7	6	2.60+/-0.40	2.17
8	6	5.63+/-1.40	8.93
10	6	1.32+/-0.42	0.24
11	6	7.33+/-1.10	7.59
14	6	2.20+/-0.50	2.58
9	7	6.01+/-0.94	5.81
10	7	25.90+/-4.80	18.30
11	7	1.88+/-0.88	1.34
13	7	3.99+/-0.60	5.04
10	8	4.24+/-0.74	4.79
9	9	2.98+/-0.50	2.73
4	3	0.94+/-0.20	0.94
2	1	2.62+/-0.52	4.43
5	1	0.50+/-0.20	0.04
11	1	0.46+/-0.40	0.01
12	1	0.00+/-0.50	0.50
10	2	0.78+/-0.50	0.65
11	2	0.00+/-0.50	0.12
9	3	0.00+/-0.40	0.44
10	3	1.48+/-1.48	0.02
12	3	0.00+/-1.02	0.03
13	3	0.00+/-0.60	0.01
8	4	0.32+/-0.40	0.11
9	4	0.00+/-0.50	0.89
5	5	0.00+/-0.30	0.13
8	5	0.00+/-0.74	0.24
9	6	0.00+/-0.60	0.16
8	7	0.18+/-0.74	0.53
12	8	0.58+/-0.56	0.02

Data set Ge(111) 7×7-Sn no. 2:

7·h	7·k	$\lvert F_{hk}^{exp}\rvert^2 +/- \sigma_{hk}$	$\lvert F_{hk}^{mod}\rvert^2$
1	1	0.23+/-0.41	0.56
2	0	2.79+/-0.55	2.48
2	1	1.15+/-0.28	2.18
3	0	8.98+/-1.50	10.01
2	2	1.33+/-0.27	1.69
3	1	1.69+/-0.28	1.12
4	0	0.74+/-0.19	0.69
3	2	0.44+/-0.13	0.07
4	1	0.07+/-0.06	0.11
5	0	1.20+/-0.19	2.15
3	3	0.53+/-0.16	0.11
4	2	0.11+/-0.08	0.04
5	1	0.22+/-0.09	0.01
6	0	6.31+/-0.86	10.05
4	3	0.28+/-0.05	0.01
5	2	0.89+/-0.12	1.22
6	1	7.90+/-0.90	10.09
4	4	4.77+/-0.55	4.32
5	3	0.54+/-0.08	0.52
6	2	0.15+/-0.06	0.06
7	1	11.99+/-1.36	15.08
5	4	1.50+/-0.19	1.57
6	3	0.99+/-0.13	0.70
0	8	11.20+/-1.27	11.07
7	2	7.71+/-0.88	8.53
1	8	0.37+/-0.08	0.32
5	5	0.30+/-0.10	0.09
4	6	0.26+/-0.09	0.13
3	7	18.69+/-2.11	14.84
0	9	1.83+/-0.23	2.13
2	8	2.10+/-0.27	1.57
1	9	1.80+/-0.23	1.14
6	5	2.84+/-0.35	3.02
7	4	0.74+/-0.16	0.23
8	3	2.46+/-0.32	2.91
0	10	0.24+/-0.11	0.16
9	2	1.44+/-0.20	1.27
6	6	2.39+/-0.36	1.43
5	7	2.06+/-0.29	0.92
10	1	0.84+/-0.16	0.47
4	8	1.01+/-0.19	0.38
3	9	0.00+/-0.17	0.07
0	11	8.43+/-0.99	3.59
2	10	0.17+/-0.15	0.07
7	6	2.17+/-0.40	0.75
8	5	0.60+/-0.20	0.43
1	11	1.72+/-0.27	0.65
9	4	1.14+/-0.24	0.96
10	3	3.44+/-0.44	1.71
0	12	7.97+/-0.95	6.70
11	2	2.05+/-0.29	0.81
6	8	7.91+/-1.01	5.74
5	9	10.01+/-1.18	7.42
4	10	15.66+/-1.81	11.87
12	1	0.86+/-0.18	0.74
3	11	7.79+/-0.91	7.48
0	13	25.85+/-2.96	16.66
8	7	0.65+/-0.25	0.60
9	6	0.00+/-0.18	0.12
2	12	10.88+/-1.26	8.56
10	5	2.05+/-0.31	1.82
11	4	11.08+/-1.27	10.57
1	13	22.55+/-2.59	16.89
12	3	0.00+/-0.14	0.01

7·h	7·k	$\lvert F_{hk}^{exp}\rvert^2 +/- \sigma_{hk}$	$\lvert F_{hk}^{mod}\rvert^2$
8	8	0.29+/-0.25	0.25
7	9	1.38+/-0.36	1.33
6	10	1.55+/-0.37	0.94
13	2	0.11+/-0.14	0.01
5	11	4.20+/-0.63	4.29
4	12	2.01+/-0.33	1.78
1	14	1.37+/-0.32	0.94
3	13	0.03+/-0.17	0.03
8	9	1.03+/-0.33	1.30
7	10	7.74+/-0.96	6.13
6	11	1.19+/-0.37	1.25
0	15	4.12+/-0.57	3.78
2	14	0.47+/-0.22	0.09
5	12	1.63+/-0.34	1.10
4	13	1.46+/-0.29	0.97
1	15	0.31+/-0.26	0.00
9	9	1.41+/-0.30	1.53
8	10	1.29+/-0.32	0.83
3	14	1.21+/-0.28	0.24
7	11	1.16+/-0.37	0.03
6	12	1.17+/-0.26	0.48
0	16	1.37+/-0.27	1.03
2	15	0.00+/-0.18	0.00
5	13	0.92+/-0.35	0.38
4	14	1.14+/-0.31	0.74
9	10	0.00+/-0.17	0.01
1	16	0.32+/-0.16	0.01
8	11	1.88+/-0.39	0.84
7	12	0.72+/-0.27	0.98
3	15	0.89+/-0.30	0.43
6	13	1.03+/-0.32	0.84
0	17	2.07+/-0.32	1.38
5	14	0.00+/-0.19	0.01
2	16	0.66+/-0.27	0.29
10	10	0.01+/-0.16	0.32
4	15	0.72+/-0.23	0.14
9	11	1.34+/-0.31	1.14
8	12	0.68+/-0.22	0.61
1	17	0.46+/-0.28	0.06
7	13	4.68+/-0.64	5.89
3	16	0.25+/-0.25	0.33
6	14	1.83+/-0.35	2.55
0	18	0.07+/-0.28	0.05
5	15	0.34+/-0.37	0.49
2	17	0.00+/-0.20	0.01
10	11	2.52+/-0.47	1.36
9	12	0.67+/-0.30	0.32
4	16	0.21+/-0.31	0.42
8	13	1.11+/-0.46	0.70
1	18	1.78+/-0.39	1.07
3	17	1.53+/-0.34	1.03
6	15	9.14+/-1.11	12.14
0	19	0.94+/-0.37	0.03
5	16	4.95+/-0.73	6.71
11	11	4.85+/-0.62	4.67
2	18	2.96+/-0.52	2.25
10	12	0.37+/-0.25	0.03
9	13	0.68+/-0.31	0.09
8	14	9.83+/-1.28	9.21
4	17	6.14+/-0.87	6.67
7	15	3.21+/-0.73	3.22
1	19	2.08+/-0.58	1.72
3	18	6.50+/-0.85	6.02
6	16	0.03+/-0.37	0.00
11	12	2.69+/-0.48	2.56
5	17	0.00+/-0.40	0.01
10	13	0.00+/-0.30	0.03
2	19	6.68+/-1.04	5.63
9	14	4.46+/-0.72	4.86
8	15	0.00+/-0.34	0.01
4	18	6.27+/-0.95	4.84
7	16	1.73+/-0.40	1.77
1	20	6.79+/-1.04	4.43
3	19	0.70+/-0.48	0.29
6	17	0.31+/-0.37	0.22
12	12	0.87+/-0.25	0.98
11	13	1.36+/-0.37	0.78
10	14	6.34+/-0.95	4.51
5	18	1.13+/-0.39	0.62
9	15	0.51+/-0.38	0.35
2	20	0.00+/-0.55	0.11
8	16	0.74+/-0.37	0.95
4	19	1.10+/-0.54	1.49
7	17	4.24+/-0.76	5.85
1	21	2.74+/-0.84	3.25
6	18	0.79+/-0.43	1.48
3	20	0.00+/-0.41	0.00
12	13	2.12+/-0.45	1.34
11	14	0.86+/-0.48	1.91
10	15	0.00+/-0.35	0.02
5	19	1.91+/-0.58	2.29
9	16	0.00+/-0.33	0.16
0	22	0.15+/-0.53	0.22
2	21	2.48+/-0.65	3.39

Data set Ge(111) 7 × 7-Sn no. 3:

7·h	7·k	$\lvert F_{hk}^{exp}\rvert^2 +/- \sigma_{hk}$	$\lvert F_{hk}^{mod}\rvert^2$
1	1	0.47+/-1.10	0.62
2	0	2.59+/-0.73	2.26
2	1	1.67+/-0.36	2.44
3	0	21.48+/-1.64	20.61
2	2	2.57+/-0.47	2.86
1	3	5.83+/-0.55	6.19
0	4	1.81+/-0.32	1.96
2	3	0.22+/-0.23	0.45
1	4	0.00+/-0.25	0.15
0	5	1.19+/-0.23	1.34
3	3	2.52+/-0.32	1.56
4	2	0.00+/-0.25	0.06
5	1	0.06+/-0.28	0.13
6	0	9.36+/-0.75	9.27
3	4	1.31+/-0.33	1.20
2	5	1.64+/-0.35	1.28
1	6	10.51+/-0.70	7.65
4	4	11.16+/-0.78	11.32
5	3	2.00+/-0.25	1.56
6	2	0.18+/-0.19	0.11
7	1	18.88+/-0.93	15.78
4	5	2.03+/-0.24	2.35
3	6	1.70+/-0.27	0.93
8	0	13.72+/-0.72	11.86
2	7	10.70+/-0.59	9.30
1	8	0.13+/-0.24	0.20
5	5	0.00+/-0.34	0.03
6	4	0.94+/-0.25	1.26
3	7	33.52+/-1.50	32.53
0	9	2.02+/-0.31	1.74
8	2	2.48+/-0.31	1.63
9	1	1.88+/-0.28	1.77
5	6	0.63+/-0.31	0.07
4	7	1.83+/-0.34	1.61
3	8	7.87+/-0.50	8.03
10	0	1.78+/-0.30	1.95
2	9	1.85+/-0.30	2.10
6	6	1.02+/-0.51	0.74
7	5	0.00+/-0.33	0.69
1	10	3.37+/-0.35	2.78
8	4	0.90+/-0.36	0.17
9	3	0.01+/-0.28	0.41
0	11	3.55+/-0.39	1.46
10	2	0.47+/-0.36	0.40
6	7	2.53+/-0.62	1.97
5	8	0.49+/-0.43	0.28
11	1	0.20+/-0.30	0.35
4	9	0.39+/-0.45	0.49
3	10	0.31+/-0.29	0.01
12	0	6.90+/-0.48	6.28
2	11	0.00+/-0.29	0.11
8	6	3.32+/-9.47	5.08
9	5	5.48+/-0.49	6.62
10	4	17.15+/-0.90	18.45
1	12	0.90+/-0.33	0.57
11	3	8.17+/-0.60	9.02
0	13	14.33+/-0.88	13.38
8	7	1.81+/-0.54	0.05
9	6	0.00+/-0.41	0.21
12	2	4.66+/-0.44	5.77
10	5	1.80+/-0.35	1.70
4	11	15.51+/-0.92	16.37
13	1	10.99+/-0.67	13.13
12	3	0.00+/-0.25	0.09
8	8	0.00+/-0.45	0.06
7	9	4.03+/-0.72	2.60
6	10	2.41+/-0.71	0.08
13	2	0.17+/-0.32	0.35

7·h	7·k	$\lvert F_{hk}^{exp}\rvert^2 +/- \sigma_{hk}$	$\lvert F_{hk}^{mod}\rvert^2$
5	11	5.31+/-0.64	3.82
4	12	2.18+/-0.40	1.9?
14	1	1.01+/-0.27	0.89
3	13	0.00+/-0.24	0.11
7	10	14.53+/-0.97	13.73
6	11	5.66+/-0.65	4.11
0	15	3.35+/-0.61	4.64
2	14	0.52+/-0.41	0.19
5	12	2.15+/-0.56	1.86
4	13	4.86+/-0.52	4.00
1	15	0.80+/-0.36	0.17
9	9	1.87+/-0.46	2.28
8	10	2.63+/-0.47	3.85
3	14	4.44+/-0.62	3.06
7	11	0.55+/-0.37	0.19
6	12	0.57+/-0.50	0.03
0	16	2.64+/-0.37	3.11
2	15	0.05+/-0.34	0.25
5	13	0.31+/-0.35	0.19
4	14	2.89+/-0.48	2.65
9	10	0.09+/-0.35	0.14
1	16	0.56+/-0.46	0.00
8	11	0.01+/-0.35	0.22
7	12	0.17+/-0.34	0.01
3	15	1.74+/-0.52	2.22
6	13	0.50+/-0.36	0.06
0	17	11.28+/-0.76	13.55
5	14	0.01+/-0.37	0.42
2	16	1.38+/-0.54	0.79
10	10	0.01+/-0.32	0.45
4	15	0.00+/-0.40	0.23
9	11	0.04+/-0.33	0.35
8	12	0.38+/-0.36	0.09
1	17	1.36+/-0.44	1.63
7	13	2.98+/-0.56	3.07
3	16	0.07+/-0.40	0.55
6	14	1.84+/-0.62	1.79
0	18	0.74+/-0.48	0.86
5	15	0.00+/-0.46	1.16
2	17	1.13+/-0.39	0.32
10	11	3.51+/-0.48	3.70
9	12	0.25+/-0.37	0.11
4	16	0.00+/-0.47	0.30
8	13	0.32+/-0.44	0.36
1	18	1.00+/-0.52	0.18
3	17	0.42+/-0.49	0.17
6	15	12.12+/-1.12	10.18
0	19	0.20+/-0.44	0.11
5	16	5.84+/-0.87	6.57
11	11	9.57+/-0.84	7.66
2	18	0.18+/-0.52	0.10
10	12	0.24+/-0.52	0.54
9	13	0.00+/-0.69	0.67
8	14	9.71+/-0.99	8.99
4	17	9.25+/-1.32	11.58
7	15	2.72+/-0.76	3.71
1	19	0.65+/-0.57	0.74
3	18	6.32+/-1.04	7.09
6	16	0.23+/-0.48	0.23
11	12	3.28+/-0.53	2.44
5	17	0.35+/-0.50	0.01
10	13	0.89+/-0.42	0.01
0	20	0.13+/-0.69	0.33
2	19	3.51+/-0.96	3.29
9	14	6.17+/-0.68	6.26
8	15	0.00+/-0.43	0.08
4	18	8.07+/-1.03	6.30
7	16	0.10+/-0.49	0.64
1	20	4.08+/-1.08	4.52
3	19	0.53+/-0.56	0.77
6	17	0.00+/-0.59	0.54
12	12	2.06+/-0.47	2.27
11	13	3.61+/-0.46	3.64
10	14	13.62+/-1.01	14.30
5	18	0.93+/-0.61	0.69
2	20	0.00+/-0.65	0.28
8	16	2.03+/-0.58	1.02
4	19	0.59+/-0.67	1.04
7	17	2.46+/-0.71	2.15
1	21	1.90+/-0.91	1.81
6	18	1.95+/-0.50	2.30
3	20	0.48+/-0.72	0.54
12	13	0.00+/-0.43	0.08
11	14	0.98+/-0.62	2.02
10	15	0.73+/-0.72	0.43
5	19	0.93+/-0.62	2.85
9	16	0.12+/-0.54	0.05

7·h	7·k	$\lvert F_{hk}^{exp}\rvert^2 +/- \sigma_{hk}$	$\lvert F_{hk}^{mod}\rvert^2$
0	22	1.25+/-0.96	0.93
2	21	2.29+/-0.72	3.56
8	17	0.00+/-0.42	0.20
4	20	0.75+/-0.47	1.53
7	18	0.08+/-0.47	2.14
1	22	0.21+/-0.49	0.05
13	13	1.03+/-0.55	1.14
12	14	1.46+/-0.53	1.30
6	19	0.90+/-0.41	0.88
11	15	0.21+/-0.68	0.06
3	21	4.73+/-0.63	6.15
10	16	0.00+/-0.46	0.27
9	17	0.00+/-0.61	0.34
5	20	0.32+/-0.41	0.28
0	23	0.13+/-0.44	0.32
2	22	0.30+/-0.44	0.09
8	18	0.73+/-0.58	0.59
4	21	1.06+/-0.50	1.95
7	19	0.54+/-0.56	1.41
13	14	1.65+/-0.79	3.02
12	15	0.00+/-0.61	0.20
1	23	1.40+/-0.60	1.40
11	16	0.89+/-0.74	0.61
6	20	0.00+/-0.41	0.10
3	22	1.57+/-0.45	2.30
10	17	0.00+/-0.50	0.45
9	18	0.02+/-0.46	0.06
5	21	0.79+/-0.63	1.49
0	24	1.50+/-0.66	0.64
8	19	0.00+/-0.44	0.28
2	23	1.01+/-0.46	0.71
4	22	0.03+/-0.41	0.06
7	20	3.02+/-0.53	2.91
12	16	0.48+/-0.73	1.00
11	17	2.35+/-0.68	2.15
1	24	3.68+/-0.62	2.27
6	21	5.36+/-0.67	4.93
10	18	3.55+/-0.63	2.95
3	23	0.30+/-0.60	0.09
9	19	1.01+/-0.66	1.06
5	22	0.00+/-0.39	0.53
8	20	2.12+/-0.66	2.44
0	25	0.48+/-0.50	0.14
2	24	1.20+/-0.55	1.09
14	15	0.13+/-0.73	0.11
13	16	0.36+/-0.57	0.22
4	23	0.00+/-0.37	0.19
12	17	0.56+/-0.51	0.28
11	18	5.30+/-0.76	5.35
1	25	0.32+/-0.34	0.42
10	19	0.91+/-0.48	0.05
6	22	0.00+/-0.41	0.22
3	24	1.65+/-0.50	1.72
5	23	0.61+/-0.33	0.06
8	21	0.72+/-0.50	0.03
15	15	0.81+/-0.49	0.02
0	26	0.14+/-0.42	0.18
14	16	0.63+/-0.47	1.68
2	25	0.52+/-0.45	0.46
13	17	0.77+/-0.66	0.97
12	18	1.65+/-0.41	1.03
7	22	1.96+/-0.47	2.35
4	24	0.00+/-0.31	0.25
11	19	0.33+/-0.37	0.93
10	20	0.05+/-0.34	0.17
1	26	0.00+/-0.33	0.32
6	23	0.06+/-0.31	0.19
3	25	3.57+/-0.50	2.59
9	21	0.00+/-0.35	0.09
5	24	0.00+/-0.32	0.09
15	16	0.48+/-0.36	0.80
14	17	3.33+/-0.46	2.39
8	22	0.80+/-0.48	0.12
13	18	2.13+/-0.47	2.19
2	26	0.21+/-0.33	0.12
12	19	3.10+/-0.53	2.37
7	23	0.67+/-0.33	1.03
4	25	0.94+/-0.42	0.72
11	20	3.43+/-0.34	3.07
10	21	0.95+/-0.27	0.67
6	24	0.41+/-0.33	0.84
1	27	0.00+/-0.35	0.31
3	26	0.17+/-0.31	0.39
9	22	0.30+/-0.26	0.45
15	17	3.48+/-0.27	1.39
14	18	0.27+/-0.19	0.31
5	25	0.00+/-0.31	0.16

2·h	2·k	$\|F_{hk}^{exp}\|^2 +/- \sigma_{hk}$	$\|F_{hk}^{mod}\|^2$
0	23	1.10+/-0.22	0.85
13	19	0.00+/-0.14	0.22
12	20	0.97+/-0.26	0.38
2	27	1.10+/-0.36	0.19
7	24	1.84+/-0.30	2.37
11	21	2.95+/-0.31	2.57
1	28	1.85+/-0.51	2.63
13	20	0.00+/-0.18	0.10
12	21	0.25+/-0.14	0.39
0	29	1.20+/-0.43	1.78
2	28	1.31+/-0.27	1.29
7	25	0.97+/-0.19	0.81
14	20	3.10+/-0.29	2.36
3	28	3.29+/-0.31	2.84
13	21	0.30+/-0.16	0.17
0	30	0.60+/-0.22	0.67
7	26	0.30+/-0.19	0.29
4	28	1.14+/-0.24	0.92
13	22	0.94+/-0.22	0.38
5	28	0.81+/-0.24	0.80
11	24	0.23+/-0.21	0.11
0	31	3.91+/-0.33	3.52
7	27	1.37+/-0.25	1.14
10	25	0.64+/-0.23	0.96
6	28	1.12+/-0.37	1.62
9	26	0.09+/-0.26	0.15
8	27	0.70+/-0.33	0.33

Riso National Laboratory

Riso - M - 2713

Title and author(s)

An X-ray Diffraction Study of the Reconstructions Induced by Sn and Pb on the Ge(111) Surfaces

Jan Skov Pedersen

Date February 1988

Department or group Physics

Groups own registration number(s)

Project/contract no.

Pages 104 Tables 24 Illustrations 40 References 127

ISBN 87-550-1425-9

Abstract (Max. 2000 char.)

Abstract: This report describes surface x-ray diffraction studies of Ge(111) surfaces covered by submonolayers of Sn and Pb. The report is divided into three parts: The first part is a brief review of the properties of the "clean" Si(111) and Ge(111) surfaces, of the properties of the Sn- and Pb-covered Ge(111) surfaces, and of the surface x-ray scattering technique. Part two of the report concerns x-ray scattering measurements on the α-phase of the Ge(111)$\sqrt{3}\times\sqrt{3}$-Sn and the Ge(111)$\sqrt{3}\times\sqrt{3}$-Pb reconstructions. The structure factor analysis shows a significant relaxation in the Ge substrate induced by the Sn/Pb adatoms. The registry of the adatoms is determined from the analysis of the integer-order reflections. The intensity profiles of the fractional-order Bragg rods display a pronounced variation, which is explained by subsurface relaxation extending four atomic layers into the bulk. Part three of the report describes the structure of the 7×7 and 5×5 reconstructions that are observed after deposition of submonolayers of Sn on the Ge(111) surface and subsequent annealing. The diffraction patterns for both structures show considerable similarity with the pattern for Si(111)7×7, and the analysis shows that the Dimer-Adatom-Stacking-fault (DAS) model also is applicable to the Sn-induced Ge(111)7×7 and Ge(111)5×5 structures. The adatoms are identified to be Sn. The results of the refinement of the atomic coordinates show that the atoms in the upper five atomic layers are displaced from their ideal positions. The displacements around the adatoms are similar to the displacements of the Ge(111)$\sqrt{3}\times\sqrt{3}$-Sn surface. Furthermore, the observed relaxations are in good agreement with the predictions of total-energy calculations. In order to perform a detailed comparison between the experimentally and theoretically determined atomic positions, a series of elastic strain calculations by the Keating model have been carried out. It is demonstrated that this model gives a good description of the atomic relaxations of the Ge(111)$\sqrt{3}\times\sqrt{3}$-Sn (Pb), Ge(111)7×7-Sn, and Ge(111)5×5-Sn surfaces.

Descriptors - INIS

ATOMIC DISPLACEMENTS; GERMANIUM; LAYERS; LEAD; RELAXATION; SURFACES; TIN; X-RAY DIFFRACTION

Available on request from Riso Library, Riso National Laboratory, (Riso Bibliotek, Forskningscenter Riso), P.O. Box 49, DK-4000 Roskilde, Denmark.
Telephone 02 37 12 12, ext. 2262. Telex: 43116, Telefax: 02 36 06 09

Available on request from
Risø Library,
Risø National Laboratory, P.O. Box 49,
DK-4000 Roskilde, Denmark
Phone (02) 37 12 12 ext. 2262

ISBN 87-550-1425-9
ISSN 0418-6435